

Copyright Warning & Restrictions

The copyright law of the United States (Title 17, United States Code) governs the making of photocopies or other reproductions of copyrighted material.

Under certain conditions specified in the law, libraries and archives are authorized to furnish a photocopy or other reproduction. One of these specified conditions is that the photocopy or reproduction is not to be “used for any purpose other than private study, scholarship, or research.” If a user makes a request for, or later uses, a photocopy or reproduction for purposes in excess of “fair use” that user may be liable for copyright infringement,

This institution reserves the right to refuse to accept a copying order if, in its judgment, fulfillment of the order would involve violation of copyright law.

Please Note: The author retains the copyright while the New Jersey Institute of Technology reserves the right to distribute this thesis or dissertation

Printing note: If you do not wish to print this page, then select “Pages from: first page # to: last page #” on the print dialog screen

The Van Houten library has removed some of the personal information and all signatures from the approval page and biographical sketches of theses and dissertations in order to protect the identity of NJIT graduates and faculty.

2)

The Design and Testing of a Personal Computer Controlled Scanning Acoustic Microscope for Orthopaedic Surgical Applications

1) Hubert Heinrich Berndt

Thesis submitted to the Faculty of the Graduate School of
the New Jersey Institute of Technology in partial fulfillment of
the requirements for the degree of
Master of Science in Electrical Engineering
Spring 1991

Approval Sheet

Title of Thesis: The Design and Testing of a Personal Computer Controlled Scanning Acoustic Microscope for Orthopaedic Surgical Applications

Name of Candidate: Hubert H. Berndt

Master of Science in Electrical Engineering, 1991

Thesis and Abstract Approval:

Mark C. Zimmerman, Ph.D.

Date

J. Russell Parsons, Ph.D.

Date

John D. Carpinelli, Ph.D.

Date

Stanley S. Reisman, Ph.D.

Date

BIOGRAPHICAL SKETCH

Author : Hubert Berndt
Degree : Master of Science in Electrical Engineering
Date : May, 1991
Date of Birth :
Place of Birth :

Education :

- BACHELOR OF SCIENCE in Telecommunications and Electronics, Fachhochschule Regensburg, Regensburg, Bavaria, Germany, 1989
- MASTER OF SCIENCE in Electrical Engineering, New Jersey Institute of Technology, Newark, New Jersey, 1991

Presentations and Publications :

Berndt, Hubert "Scanning Acoustic Microscopy and Human Femoral Bone Remodelling," Presented in Hartford, Connecticut, April, 1991, at the IEEE Seventeenth Annual Northeast Bioengineering Conference. IEEE 91CH2997-5: New York, 1991.

Awards:

- Research fellowship at George L. Schultz Laboratories for Orthopaedic research, 1990
- Fulbright Scholarship for a study in the United States, 1989

To Ursula,

It was worth the effort.

Acknowledgements

I would like to extend special thanks to the following people. Dr. Mark C. Zimmerman for his advice, patience and continuing support. It was through his ideas that I was able to realize this thesis. Dr. J. Russell Parsons, for allowing me to make extensive use of his laboratory at UMDNJ. Dr. Maurizio Cibischino, for preparing the human bone specimens presented in this thesis, and Mrs. Alecia Marcantonio for teaching me the techniques of specimen preparation.

In addition, this work would not have been possible without the help of the staff of the George L. Schulz Laboratories for Orthopaedic Research and many other individuals, whom are too numerous to thank individually.

I would also like to acknowledge the Whitaker Foundation for funding this project, and the Fulbright Commission for academic support.

TABLE OF CONTENTS

ACKNOWLEDGEMENTS	i
TABLE OF CONTENTS	ii
LIST OF TABLES AND FIGURES	iii
ABSTRACT	1
1. INTRODUCTION	2
1.1 General Introduction to Ultrasound Microscopy	3
1.1.1 Methods of Ultrasonic Microscopy	5
1.1.1.1 C - SAM.....	8
1.1.1.2 Scanning Laser Acoustic Microscopy SLAM.....	12
1.1.1.3 Scanning Acoustic Microscopy SAM.....	14
1.1.2 Amplitude and Phase Acoustic Microscope	16
1.2 Ultrasound, SAM and Orthopaedic Applications.....	18
1.3 Rationale for Study.....	22
2. MATERIAL & METHODOLOGY	24
2.1 System Configuration & Improvements.....	25
2.1.1 The Mechanical Scanning System.....	27
2.1.2 Data Acquisition.....	27
2.1.3 Data Processing and Presentation.....	33
2.1.4 System Improvements.....	39
2.1.4.1 Software Solution Averaging.....	42
2.1.4.2 Software Solution Interpolation.....	43
2.1.4.3 Hardware Triggering Solution	45
2.2 Data Acquisition and Triggering experiment.....	48
2.3 Experiment in scanning of four pairs of femoral specimens.....	50
2.4 Mechanical Testing of Human Cadaveric Bone	51
3. RESULTS AND DISCUSSION	56
3.1 Data Presentation and femoral section	56
3.2 System configuration and Improvements	57
3.3 Triggering Experiment (improving accuracy of device)	58
3.4 Results from scanning of four pairs of femurs	67
3.5 Mechanical Testing of Human Cadaveric Bone	70
4. CONCLUSIONS	85
REFERENCES	86
APPENDIX A	89
APPENDIX B	99
APPENDIX C	107
APPENDIX D	119

LIST OF TABLES AND FIGURES

Introduction

- Fig. 1.1:* Three different Ultrasound Scanning methods 5
- Fig. 1.2:* Ultrasound wave propagation 6
- Fig. 1.3:* Structural features that cause ultrasonic echo variations 7
- Fig. 1.4:* C-SAM principle 9
- Fig. 1.5:* A-B-C-scan modes of C-SAM 10
- Fig. 1.6:* Coin scanned using a subsurface ultrasonic technique (German IDM) 12
- Fig. 1.7:* Principle of SLAM 13
- Fig. 1.8:* SAM principle 14
- Fig. 1.9:* SAM transducer and excitation of surface (Rayleigh) waves 15
- Fig. 1.10:* Principle of ultrasonic transmission technique 19
- Fig. 1.11:* Reflection factor (r) and acoustic impedance (z) 19
- Fig. 1.12:* Correlation between ultrasonic transmission and reflecting technique 20

Material and Methodology

- Fig. 2.1:* PC based Ultrasonic Scanning Microscope (George L. Schultz Laboratories for Orthopaedic Research) 24
- Fig. 2.2:* System block diagram 25
- Fig. 2.3:* Scanning Acoustic Microscope - System configuration 26
- Fig. 2.4:* Ultrasonic transducers 28
- Fig. 2.5:* Block diagram for the Ultrasonic Analyzer 29
- Fig. 2.6:* Reflection signal (internal) 30
- Fig. 2.7:* The Peak Level output from the ultrasonic analyzer 31
- Fig. 2.8:* Grayscale distribution modification 33
- Fig. 2.9a:* Center of gravity and three regions 34

<i>Fig. 2.9b:</i>	<i>Creating the line $L(q)$</i>	35
<i>Fig. 2.10:</i>	<i>Circular averaging - image computations</i>	38
<i>Fig. 2.11:</i>	<i>Peak Level Output signal and external triggering</i>	40
<i>Fig. 2.12:</i>	<i>Image distortion due to acceleration or deceleration of table</i>	40
<i>Fig. 2.13:</i>	<i>Computer sampling with two data acquisition boards</i>	41
<i>Fig. 2.14:</i>	<i>Peak Level output signal before and after low pass filtration</i>	42
<i>Fig. 2.15:</i>	<i>Sampling of the peak level output signal with maximal and minimal amplitude</i>	43
<i>Fig. 2.16:</i>	<i>Image line shifting</i>	44
<i>Fig. 2.17:</i>	<i>Peak level output signal and internal strobe signal</i>	45
<i>Fig. 2.18:</i>	<i>Interfacing UA - device with data acquisition board</i>	45
<i>Fig. 2.19:</i>	<i>Distorted images without application of displacement algorithms</i>	46
<i>Fig. 2.20:</i>	<i>The same SAM image as Fig. 2.19 after applying displacement algorithms</i>	47
<i>Fig. 2.21a:</i>	<i>Color distribution modification</i>	52
<i>Fig. 2.21b:</i>	<i>Color and Gray scale presentation</i>	53
<i>Fig. 2.22:</i>	<i>Femoral Midshaft SAM Images of specimens imbedded in plastic</i>	54
<i>Fig. 2.23:</i>	<i>Femural specimen preparation</i>	55

Results and Discussion

<i>Fig. 3.1:</i>	<i>One US penny in grayscale</i>	62
<i>Fig. 3.2:</i>	<i>One US quarter in grayscale</i>	62
<i>Fig. 3.3:</i>	<i>Other coins with a flat surface in grayscale</i>	63
<i>Fig. 3.4:</i>	<i>SAM image of a NYC subway token</i>	64
<i>Fig. 3.5:</i>	<i>SAM image with different sampling increments</i>	64
<i>Fig. 3.6:</i>	<i>Block diagram demonstrating interfacing of the external trigger and counter</i>	65
<i>Fig. 3.7:</i>	<i>Electronic circuit of counter trigger</i>	66
<i>Fig. 3.8:</i>	<i>Femoral section position and anatomic orientation</i>	67
<i>Fig. 3.9:</i>	<i>Femoral Midshaft SAM Images of #2363 in color</i>	71

Fig. 3.10:	<i>Diagram with results of circular averaging of femur #2363 left</i>	72
Fig. 3.11:	<i>Diagram with results of circular averaging of femur #2363 right</i>	73
Fig. 3.12:	<i>Femoral Midshaft SAM Images of #2329 in color</i>	74
Fig. 3.13:	<i>Diagram with results of circular averaging of femur #2329 left</i>	75
Fig. 3.14:	<i>Diagram with results of circular averaging of femur #2329 right</i>	76
Fig. 3.15:	<i>Femoral Midshaft SAM Images of #2326 in color</i>	77
Fig. 3.16:	<i>Diagram with results of circular averaging of femur #2326 left</i>	78
Fig. 3.17:	<i>Diagram with results of circular averaging of femur #2326 right</i>	79
Fig. 3.18:	<i>Femoral Midshaft SAM Images of #2366 in color</i>	80
Fig. 3.19:	<i>Diagram with results of circular averaging of femur #2366 left</i>	81
Fig. 3.20:	<i>Diagram with results of circular averaging of femur #2366 right</i>	82
Fig. 3.21:	<i>3-D presentation of Femoral Midshaft SAM image #2366</i>	83
Fig. 3.22:	<i>Color SAM image of a NYC subway token</i>	84

Appendix A: Tables of acoustic impedance data from human femoral sections and data regarding X-Y table position 89

Tab. 1:	<i>Ranges of acoustic impedances</i>	90
Tab. 2:	<i>X-Y table positions with: $R = 250; S = 2; F = 20; N = 1000$</i>	91
Tab. 3:	<i>X-Y table positions with: $R = 252; S = 2; F = 20; N = 1000$</i>	91
Tab. 4:	<i>X-Y table positions with: $R = 254; S = 2; F = 20; N = 1000$</i>	92
Tab. 5:	<i>X-Y table positions with: $R = 254; S = 1; F = 20; N = 1000$</i>	92
Tab. 6:	<i>X-Y table positions with: $R = 252; S = 1; F = 30; N = 500$</i>	93
Tab. 7:	<i>X-Y table positions with: $R = 252; S = 2; F = 20; N = 500$</i>	93
Tab. 8:	<i>X-Y table positions with: $R = 254; S = 1; F = 30; N = 500$</i>	93
Tab. 9:	<i>Results of circular averaging of femur #2326 - left and right</i>	94
Tab. 10:	<i>Results of circular averaging of femur #2329 - left and right</i>	95

<i>Tab. 11:</i>	<i>Results of circular averaging of femur #2363 - left and right</i>	96
<i>Tab. 12:</i>	<i>Results of circular averaging of femur #2366 - left and right</i>	97
<i>Tab. 13:</i>	<i>Maximum load (N) and stroke load (mm) prior to fracture for #2366 femoral cross section</i>	98

Appendix B: Graphic presentation of data regarding X-Y table position 99

<i>Fig. D.1:</i>	<i>Velocity-Time (V-T) diagram with parameters: R 250; S 2; F 20; N 1000</i>	100
<i>Fig. D.2:</i>	<i>Position-Time (S-T) diagram with parameters: R 250; S 2; F 20; N 1000</i>	100
<i>Fig. D.3:</i>	<i>Velocity-Time (V-T) diagram with parameters: R 252; S 2; F 20; N 1000</i>	101
<i>Fig. D.4:</i>	<i>Position-Time (S-T) diagram with parameters: R 252; S 2; F 20; N 1000</i>	101
<i>Fig. D.5:</i>	<i>Velocity-Time (V-T) diagram with parameters: R 254; S 2; F 20; N 1000</i>	102
<i>Fig. D.6:</i>	<i>Position-Time (S-T) diagram with parameters: R 254; S 2; F 20; N 1000</i>	102
<i>Fig. D.7:</i>	<i>Velocity-Time (V-T) diagram with parameters: R 254; S 1; F 20; N 1000</i>	103
<i>Fig. D.8:</i>	<i>Position-Time (S-T) diagram with parameters: R 254; S 1; F 20; N 1000</i>	103
<i>Fig. D.9:</i>	<i>Velocity-Time (V-T) diagram with parameters: R 252; S 1; F 30; N 500</i>	104
<i>Fig. D.10:</i>	<i>Position-Time (S-T) diagram with parameters: R 252; S 1; F 30; N 500</i>	104
<i>Fig. D.11:</i>	<i>Velocity-Time (V-T) diagram with parameters: R 252; S 2; F 20; N 500</i>	105
<i>Fig. D.12:</i>	<i>Position-Time (S-T) diagram with parameters: R 252; S 2; F 20; N 500</i>	105
<i>Fig. D.13:</i>	<i>Velocity-Time (V-T) diagram with parameters: R 254; S 1; F 30; N 500</i>	106
<i>Fig. D.14:</i>	<i>Position-Time (S-T) diagram with parameters: R 254; S 1; F 30; N 500</i>	106

Appendix C: Computer programs 107

<i>Program 1:</i>	<i>Scanning program SCAN1.BAS, using data acquisition board from Data Translation®</i>	108
<i>Program 2:</i>	<i>Scanning program SCAN2.BAS, using data acquisition board from ADAC inc.</i>	113
<i>Program 3:</i>	<i>Scanning program SCAN3.BAS, using data acquisition board from ADAC inc.</i>	118

Appendix D: Description of stepper motor controller movement characteristics. 119

ABSTRACT

This thesis describes scanning acoustic microscopy and ultrasonic image processing to characterize and evaluate materials of known properties, as well as novel materials. This work describes the assembly and testing of a PC based device for nondestructive evaluation of bone materials for usage in orthopaedics research. It includes the identification of some hardware problems and their solution, and it also describes different image processing techniques that have been developed and applied in this work. In a growing number of disciplines it has been discovered that an acoustic microscope can provide new information, especially about the elastic properties of specimens and how acoustic waves interact with them. This work examines a PC based apparatus for scanning acoustic microscopy and the testing of this device by investigating different materials. In this thesis ultrasound has been used to evaluate the elastic or stiffness properties of human bone specimens, in particular those from femurs. Dependent on the location within the bone, the data obtained is an approximate value proportional to the local stiffness of bone on the surface of the investigated specimen. Such data can be used for studies of mechanical remodelling of the entire bone. In order to evaluate the physical/acoustic properties and to obtain detailed representations, the data from the scanned object is subjected to conversions and further ultrasonic image processing. Using different image processing techniques, it is also possible to compare the extracted data to that from other specimens that differ in size and shape. Further information about the physical properties of a material can be obtained by analyzing either reflected or transmitted ultrasound. Scanning acoustic microscopy (SAM) is a reflection technique where the amplitude of the reflected sound wave is measured. Using the transmission technique, it is possible to determine the velocity of an acoustic wave through the investigated material. In bone and only in bone materials, there exists a strict connection between the transmitted velocity, acoustic impedance or reflected wave amplitude and modulus of elasticity (Young's modulus).

1. INTRODUCTION

Acoustics, the science of sound, involves the production, control, and reception of mechanical vibrations in solids and fluids. Sound can be reflected, refracted, and scattered at a material interface. Acoustic microscopy has much in common with conventional optical microscopy with the difference being the use of ultrasound waves rather than light waves. In both approaches waves illuminate an object and the wave reflections are detected. In a light microscope, electromagnetic light waves pass through the lens; in an acoustic microscope a focused electroacoustic transducer is acoustically coupled to the sample through water or some other fluid. For an optical microscope the detector is the eye, camera or a single detector which is moved across the projection plane. Ultrasonic microscopy uses basically the latter concept; a sample is moved over an acoustic transducer. In optical microscopes the contrast of the examined object is due to changes in its optical properties, while in the acoustic microscope the contrast is due to changes in elastic properties. Thus, with ultrasound information about the material's physical properties can be obtained by analyzing either reflected or transmitted waves.

The devices used with ultrasound have changed significantly since they were introduced over 20 years ago. The first generation devices were very complex, highly sophisticated and expensive apparatus, that could only be used in special laboratories for non destructive evaluation (NDE) in investigations of metals. The data was presented in the form of images that could not be further enhanced or analyzed given the technology available. Using new microcomputer technology based on personal computer hardware and compatible peripheral boards for data acquisition, together with improved sampling devices and new imaging techniques, it is now possible to obtain and evaluate ultrasound images of objects according to defined aspects and criteria. These PC based devices can be built in smaller laboratories and used for special applications. Such a device has been designed and

configured for use in our orthopaedic research laboratory to investigate the properties of bone and the phenomenon of bone remodelling and characteristics of bone in different locations and comparisons of different bone specimens.

1.1 General Introduction to Ultrasound Microscopy

The first practical Scanning Acoustic Microscope (SAM) was developed and built in the early '70s by Lemons and Quate [1]. A few years later Jipson and Quate [2], obtained resolutions beyond optical resolutions using the same technique. Since then scanning acoustic microscopy has become a major non-destructive evaluation tool involving imaging, characterizing, and detecting defects in structural materials [3, 4]. Different SAM technique approaches can be also used for the evaluation of material properties. Besides the advantage of being a non-destructive technique, SAM can yield micromechanical information not attainable with other techniques. Further, acoustic waves can be used to image features inside an optically opaque material. Therefore, it can be used for sub-surface materials analysis, such as mineral content in bone tissues [5, 6], grain structure in titanium [4, 7, 8], or elastic properties and velocity in bone materials [9-13].

Depending on the technique, equipment, or data sampling methods, different ultrasound methods can provide data representing different physical properties of the tested materials. Using the reflective scanning method [3], an obtained signal is a function of amplitude and phase of the reflected energy from the investigated object [14]. Using the transmission technique, it is possible to obtain information about the velocity of sound within the material [15] and knowing the density of the investigated material we can obtain the acoustic impedance. With this information Yoon and Katz [24] and also other investigators [22, 26] have shown, that for bone material there is a relationship between the density of the material, the acoustic velocity, the acoustic impedance and the modulus of

elasticity (Young's modulus or C_{33}). Using different ultrasonic scanning techniques [4,8,16], the signal of the reflected energy can modulate a laser beam or it can be transformed into a voltage value. The voltage signal is then converted into a digital value, transformed into a gray or false color scale and represented as an ultrasound image on the CRT screen [14]. This image can be enhanced for further evaluations [17] by using different image enhancement techniques.

In a growing number of disciplines it is being discovered that the acoustic microscope can provide new information, specifically about the elastic properties of material specimens and how acoustic waves interact with them [18,19,20]. The variations in elastic properties are easily detected where there may be no corresponding changes in the optical properties, like detection of individual grains in a titanium sample that are visible acoustically but not optically [8]. This technique is routinely used in the aerospace industry for the imaging of heavily stressed parts for subsurface cracks, voids, and delimitations in materials where such features are undetectable optically or by any other means currently available [15]. Another common usage for this technology is in microelectronic components. It is possible to detect mechanical defects that are not detectable by electrical testing but can affect the electrical reliability [4]. While in the past the most attention has been paid to the investigation of solid materials, namely metals, application of ultrasonics in the fields of biology and medicine, where soft materials are prevalent, is still in its infancy. In a small number of preliminary experiments SAM has been used in the study of animal cells and tissues [9], of bone remodelling about orthopaedic implants [12-13], in dental research [5,21] and in the investigation of "old" and "new" materials like stones, minerals or plastics[6]. For hard tissue analysis, this technique offers the advantage of non-destructive testing of a sample which can then be processed, enhanced and further analyzed with other techniques. Secondly, it provides an analysis of material properties on a scale not possible with conventional mechanical testing techniques.

1.1.1 Methods of Ultrasonic Microscopy

There are three different microscopy techniques involving ultrasound: The scanning acoustic microscopy (SAM), scanning laser acoustic microscopy (SLAM), and C-SAM. Each of these three techniques has a specific utility and does not compete with the others in regard to its application. The principle of these three different ultrasound scanning methods are shown in Fig. 1.1

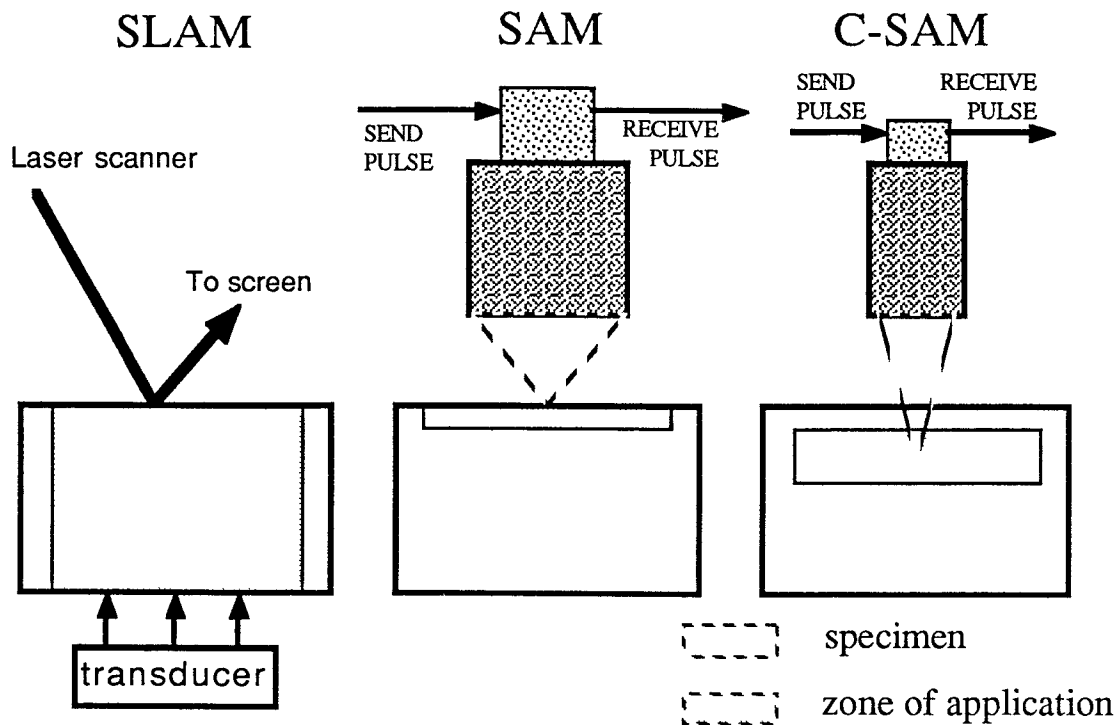


Fig. 1.1: Three different Ultrasound Scanning methods

These different techniques only have in common that they use electroacoustic impulses and have to follow the same physical limits. One of those limits is the resolution. The higher the frequency, the shorter the wavelengths, and therefore correspondingly higher resolution. Another factor that influences the resolution is the transport media

(couplers) for the wave transmission between the transducer and the specimen. Of course, the higher the frequency the greater the attenuation. The three methods are vastly different and each of these techniques utilizes different ultrasonic transducers and frequency range.

While the SLAM technique sends waves through the material and allows investigations of the entire thickness, C-SAM can investigate a specimen only at a specified depth, up to few millimeters below the surface. SAM is a method for a surface investigation only. The last two methods are basically reflection mode instruments. The basic operation of the reflection mode instruments is actually very simple and a stroboscopic image of the wave propagation is shown in Fig. 1.2.

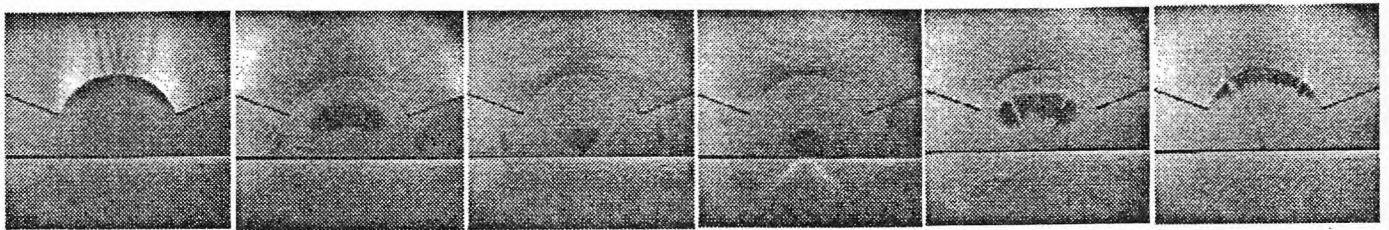


Fig. 1.2: Ultrasound wave propagation

A spherically formed acoustic transducer is excited with an electrical pulse [20] and generates an acoustic wave on the surface adjacent to the coupler medium. This acoustic wave converges to a small focal point inside the specimen or on its surface. The coupler medium usually is a liquid, instead of a gas, because of the higher acoustic coupling properties of a liquid. Other liquids like liquid helium or liquid nitrogen are used for applications with very high frequencies (beyond 2GHz) [2]. These liquids have a lower attenuation and an acoustic velocity that is only one sixth that of water. The acoustic wave is partially absorbed by the specimen and the remainder reflected. The reflected wave returns to the transducer and is converted into an electrical signal. The variations in the returned echo come from different effects see Fig. 1.3. First, changes in the surface

topography, voids, vertical cracks, or delimitations create differences in the amount of energy reflected (see images of coins presented in Fig. 3.1 to 3.4) and secondly, the amplitude of the return signal depends on the acoustic impedance or the reflectivity of the surface material.

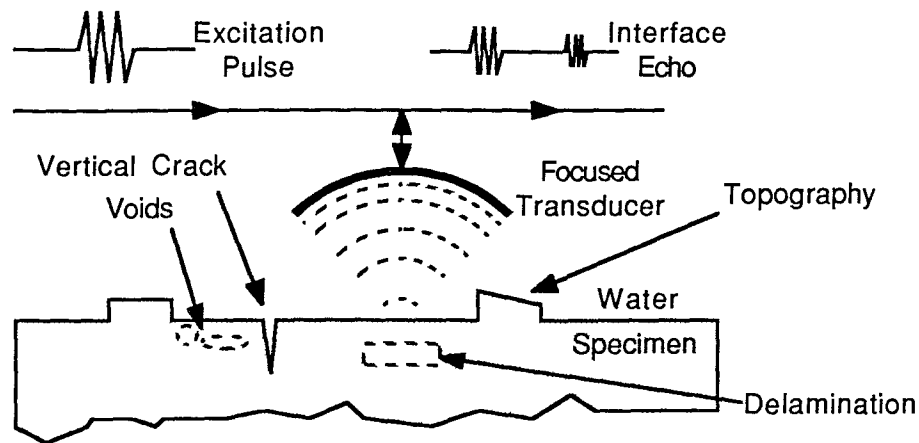


Fig. 1.3: Structural features that cause ultrasonic echo variations

The specimen is scanned across the sample area in a raster fashion by movement of the transducer or the specimen chamber with a mechanical stage moved by stepping motors. According to the mechanical stage position in a virtual X-Y plane and the intensity of the returned signal, an ultrasound image can be created and displayed on the CRT in gray levels or color map. Most of the instruments need a special hardware device interface or a computing algorithm to adjust the characteristic between the position of the mechanical stage (such as acceleration and deceleration movement) and the exact position of data pixels on the screen.

The transducers used in ultrasonic microscopy differ mainly in their frequency, focal length, size, and the ratio of the focal length to aperture (known as F number). For example, if a transducer has a focal length of 32 mm and diameter of 16mm, the characteristic of this transducer would be described as F2. A second important characteristic of a transducer is the acceptance angle, which is the maximum angle relative

to its axis at which acoustic waves are sent or received. The sine of the acceptance angle, θ_{\max} is one half the diameter divided by the radius of curvature or:

$$\sin(\theta_{\max}) = \frac{1}{2} F \quad \text{where } F \text{ is defined above.} \quad (1)$$

The maximal resolution, as mentioned before, depends on the operating frequency, coupler medium used, and the transducer properties. Therefore the resolution of a transducer with known characteristics depends mainly on the wavelengths in the transmitting coupler medium. This wavelength arise from the frequency and acoustic velocity of this coupler medium, leading to

$$\lambda = \frac{c}{f} \quad \text{where} \quad \begin{array}{l} f = \text{frequency} \\ c = \text{velocity} \\ \lambda = \text{wavelength} \end{array} \quad (2)$$

1.1.1.1 C - SAM

Acoustic C-SAM is a pulse-echo reflection type microscope. These systems can investigate subsurface materials properties but cannot image within a few millimeters or less of the surface because of interference with the reflection front. Using this technique, near surface investigations could only be possible by receiving and investigating the Rayleigh-waves [16-pp58, 8-pp97]. But in order to realize this a huge apparatus would be necessary. This method is ideal for analyzing at a specific depth. The frequency operating range is between 10 and 100 MHz and therefore it is not possible to obtain particularly high resolutions. Ultrasound waves are transmitted by a coupling medium like water or other inert fluids. The angle of the rays from the transducer lens is generally kept small so that the incident ultrasound does not exceed the critical cutoff angle of refraction between the

fluid coupling and the solid sample. The reflected echo contains amplitude and phase information that provide information about the sub-structure of the investigated specimen. As in SAM, the transducer or the specimen is mechanically translated in a raster form, and the collected data is the $V(z)$ function with respect to the x-y location. The transducer acts as sender and receiver, being electronically switched between the transmit and receive modes. Principles of C-SAM are illustrated in Figure 1.4.

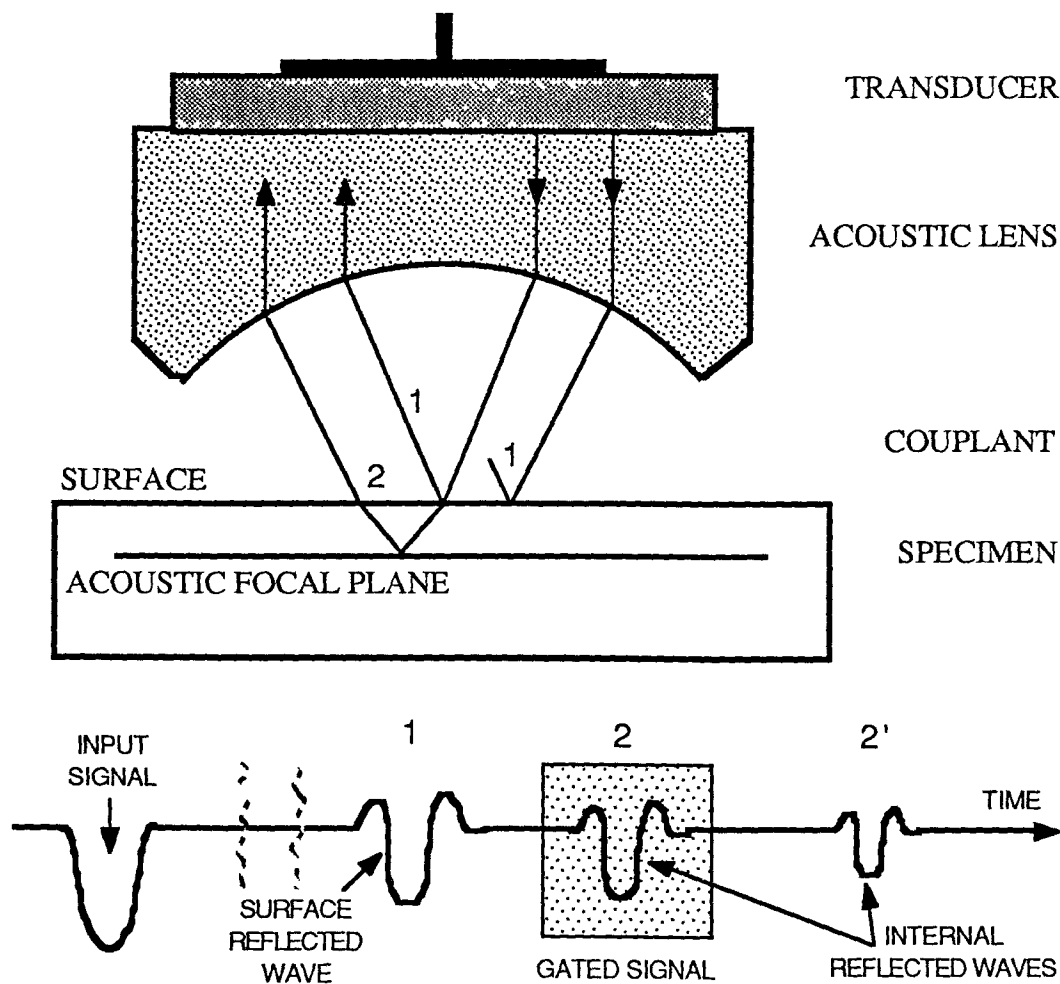


Fig. 1.4: C-SAM principle

The transducer used for this approach must generate waves that can penetrate deep into a specimen that has much higher acoustic properties. The acoustic properties of a material are defined with the acoustic impedance, reflection and the velocity. The wave radiation angle must be small enough and far under the critical angle to avoid total reflection and surface waves, called Pseudo-Rayleigh waves [16]. These waves are important in another ultrasonic technique, SAM, which will be discussed later.

The different echos that are generated by using the C-SAM method are shown in schematic in Figure 1.5. Depending on the area within the specimen in which we are interested, it is possible to gate one of those interface echos and evaluate the acoustic properties at this specific level.

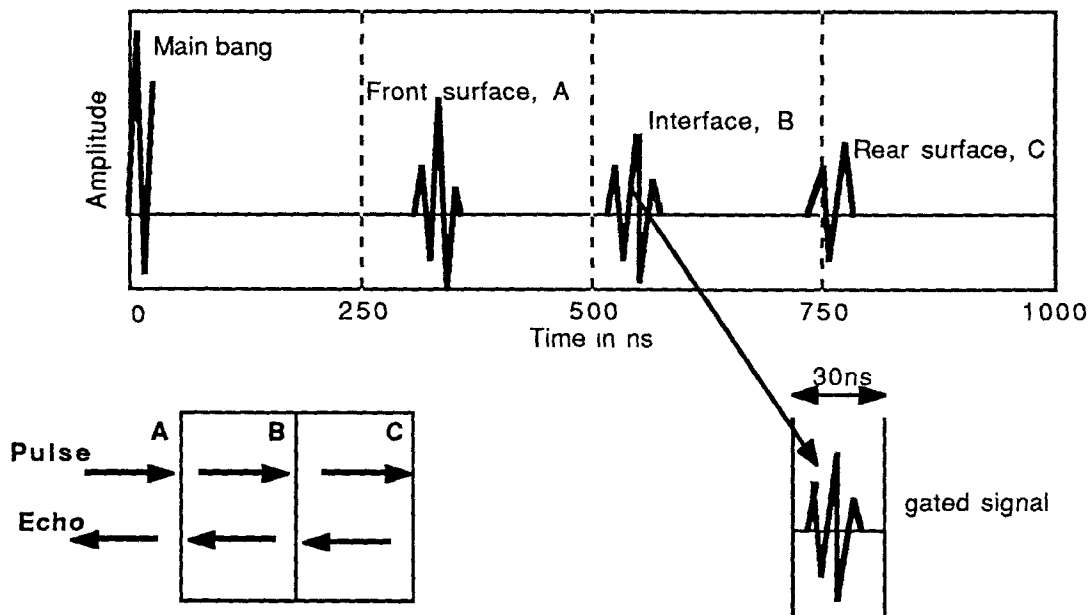


Fig. 1.5: A-B-C-scan modes of C-SAM

A very short pulse is sent from the transducer to the specimen. The ultrasonic wave is partially reflected from the surface. The remaining portion penetrates the specimen and is partially reflected again from some material features in the sub region of the specimen. The return time is a function of the distance between the interface and transducer. Ignoring the

first echo from the specimen's surface, it is possible to gate a following echo and so, to window a certain level within the evaluated specimen.

In "amplitude only" microscopy, this returned pulse is a function of the reflection; the generated signal is a voltage value that can be converted into gray scale or false color map.

In phase evaluation, which involves echo polarity encoding of the returned signal, it is possible to obtain more information about the characteristics of detected voids and delaminations. The phase is positive from higher impedance reflection and negative from lower impedance reflection. For example, while the echo amplitude of a plastic - ceramic boundary is very similar to a plastic - airgap boundary, the phase response between these two signals is 180° out of phase. The biggest advantages of this approach is the ability to image anomalies at a specific level. Connected with more complicated devices it is possible to "look" inside an optically opaque material. This technique is not useful in regions immediately below the surface and the maximum depth of penetration is determined and limited by the attenuation losses and geometric refraction within the sample. Besides this, denser materials require a transducer to have a longer focal length; therefore, a proper transducer and lens are necessary for good results in this type of application. In microelectronics, amplitude echo and phase investigations together give quite exact information about the mechanical structure inside of electronic components like integrated circuits or semiconductors. A highly reliable integrated circuit must, beside fulfilling electrical tests, also prove that internal metal connections will not be damaged by maximum current and temperature influence. For this requirement it must also be guaranteed that it is hermetically sealed from ionic contamination and moisture in the atmosphere. This can be proved by investigating the IC package by C-SAM - phase data. A C-SAM image of the backside of a coin appears on the next side in Figure 1.6.

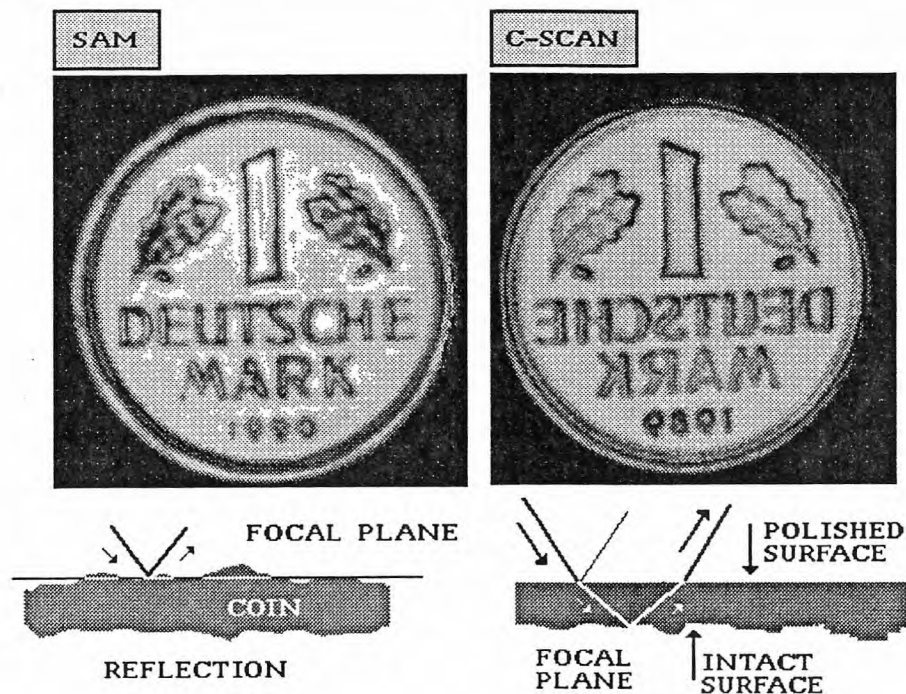


Fig. 1.6: Coin scanned using a subsurface ultrasonic technique (German IDM)

1.1.1.2 Scanning Laser Acoustic Microscopy SLAM

This technique is quite different than the aforementioned method. The general difference is that SLAM (see Fig. 1.7) is less a reflection technique than a transmission one. The technique entails the following: 1) an ultrasonic piezoelectric transducer sends waves to the bottom surface of the sample, 2) the transmitted waves go up to the top surface of the specimen, and 3) transmit to the surface of the coupling liquid. The surface of the coupling liquid is scanned by a quick laser beam and projected to a screen, creating up to 30 pictures per second. The ultrasound wave that travels through the sample material is affected by the homogeneity of the material. Wherever there are anomalies, like voids, cracks and air inclusions, the ultrasound is differentially attenuated and the resulting image

reveals characteristic light and dark features which correspond to the localized acoustic properties of the sample. Delaminations can be clearly detected by this technique and represented in real time. As mentioned, this method permits investigations in real-time and provides simultaneous viewing of the entire thickness of the sample, as in x-ray radiography.

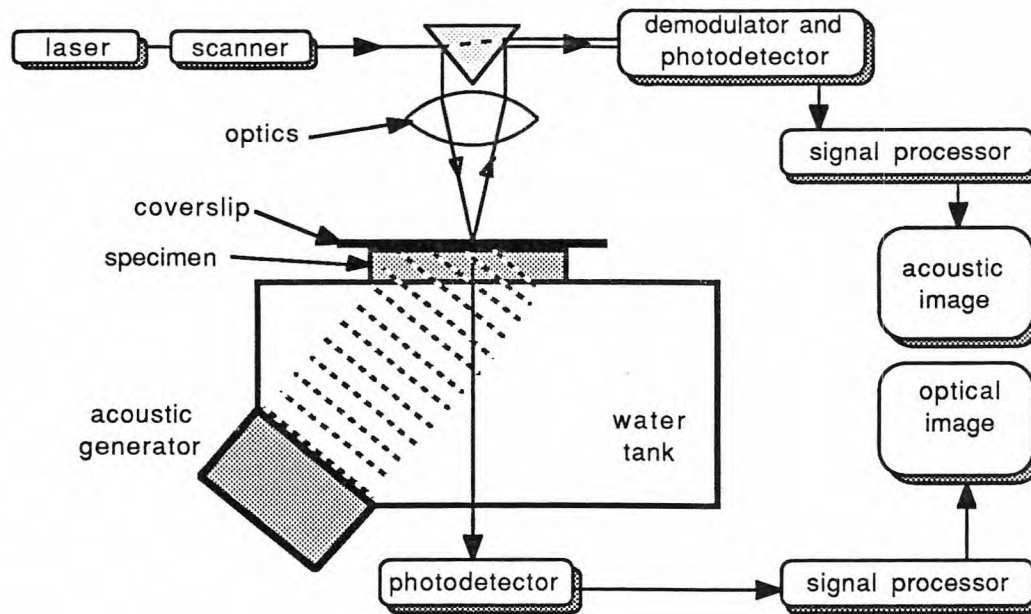


Fig. 1.7: Principle of SLAM

Therefore it is possible to observe structure changes while a specimen is being stressed. It is also possible to reconstruct holographic images. SLAM is therefore the most extensive technique in terms of complicated apparatus and computer analysis. This is an excellent technique for examining tiny hybrid electronic components, large metal plates, aircraft turbine blades, and ceramic engine cylinder liner tubes.

1.1.1.3 Scanning Acoustic Microscopy SAM

Scanning acoustic microscopy is a typical reflection type microscope where the amplitude or the phase of the reflected sound wave is measured (see Fig 1.8). Using this technique it is possible to investigate the surface and near-surface region of a material. The frequency range that a SAM microscope is usually operated is between 100 and 2000 MHz and it uses long pulse radio-frequency (RF), instead of short pulses like the C-SAM. The specimen penetration limit is only one wave length of sound. Using water as coupler and a transducer frequency of 30MHz the maximum penetration will be around 100 μ m. The transducer has a much shorter focal point and therefore a very wide angle of the sound waves, that is well beyond the critical cutoff angle, so that there is essentially no wave propagation into the material (and hence non-invasive).

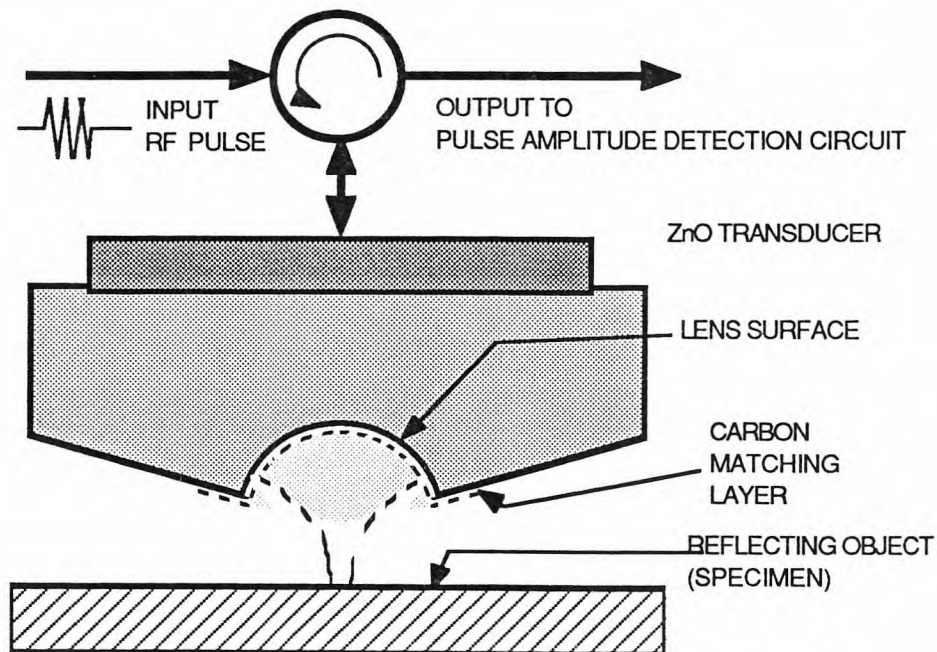


Fig. 1.8: SAM principle

The reflected acoustic signal level is determined by the elastic properties of the material at the near surface zone, known as the surface wave (see Figure 1.9). The surface wave is described in the $V(z)$ curve.

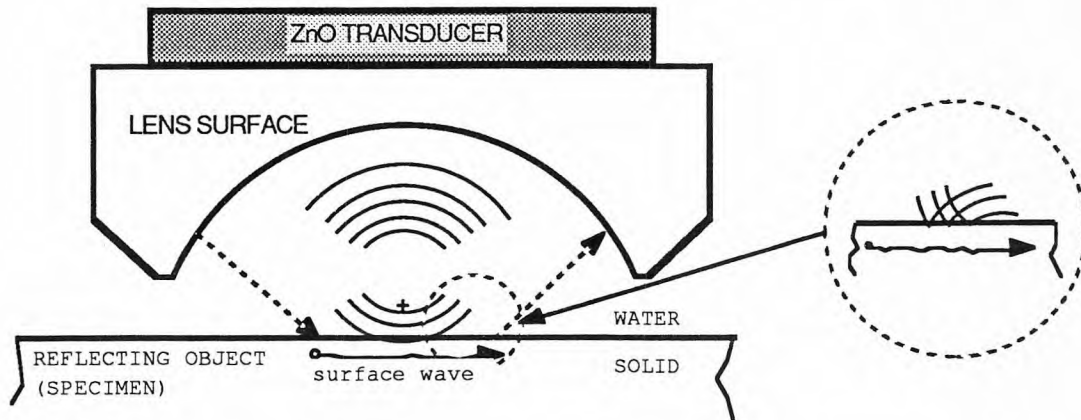


Fig. 1.9: SAM transducer and excitation of surface (Rayleigh) waves

This curve is an experimental obtained curve which characterizes the acoustic lense response expressed in form of an integral. In order to explain this definition, a liquid/solid interface for the surface wave propagation and a physical model for a acoustic lense can be used. The definition of this curve will be not explained further in this work, further informations about can be obtained in [16-pp15 and 20]. An image is usually generated as a function of transducer position and from echo amplitude data over the X-Y field of view. The transducer acts as sender and receiver and is mechanically translated in a raster form, to create a rectilinear image.

SAM technique can operate at very high frequencies and can obtain resolutions close to or better than optical microscopes. Therefore, SAM produces the highest resolution of all acoustic microscopy techniques. Because of the accuracy, it is necessary to make sure that the investigated surface is situated on a true horizontal plane and always placed in the focus level. Surface preparation of a specimen is a critical parameter. The

normal mode of SAM has a broad spectrum of applications, especially in non-destructive evaluation (NDE). For instance, high resolution images of titanium plate surfaces and different composite materials provide information about the material structure. This technique is widely used especially in microelectronics and aerospace industries. A micro-subsurface evaluation of silicon wafers can provide information regarding electrical reliability.

1.1.2 Amplitude and Phase Acoustic Microscope

The previously described acoustic microscopy techniques measure the amplitude of the reflected signal [27]. By measuring the amplitude and phase it is possible to obtain much more accurate data. Phase detection is very sensitive to variations in surface topography and impedance reflection at the material interface. The differences in the topography lead to changes in the time delay of the reflected signal, which changes the measured phase. Using a 3 MHz transducer, the acoustic wavelength is 0.5 mm, which gives a 360° phase for each 250 μm change in the height of the specimen in a given direction. If the angular resolution of the microscope is 0.1° , the detected height variation will be 0.1 μm . Therefore, very accurate profile measurements of the sample can be made. In most cases this precision is higher than the mechanical stage used for scanning movement. Coincident measurement of phase with amplitude makes it possible to acquire signals for images from subsurface defects by removing the effects from the surface features. In general, most acoustic transducers are excited with a narrow band, quasi-continuous burst (CW) consisting of just one frequency. For amplitude and phase detection a gated wave over a finite time extent is used. This signal is between a short pulse and a quasi-continuous tone burst. As it is easier to evaluate a signal for imaging at just one frequency, it is more convenient to use a short tone burst rather than a pulse of

length comparable to a half cycle of an RF signal. Further, it is easier to design narrow band transducers and detectors that respond to tone bursts and it is possible to put more energy into a tone burst rather than into a short pulse. The CW-signal can be specified by its amplitude and phase, using the simple equation:

$$A \cos(\omega t + \phi), \quad \text{where} \quad \begin{array}{l} A = \text{amplitude} \\ \omega = \text{frequency} \\ t = \text{time} \\ \phi = \text{phase} \end{array} \quad (3)$$

The amplitude and phase of a tone burst are those of the Fourier transform of the tone burst evaluated at the fundamental frequency. To a good approximation the phase is proportional to the round trip time delay of the tone burst. It follows from the Fourier shift theorem that:

$$F\{f(t+\Delta t)\} = F(\omega)e^{j\omega\Delta t} \quad (4)$$

where $F(\omega)$ is the Fourier transform of $f(t)$. The time delay is approximately $\Delta t = 2\frac{D}{c}$, where D is the distance from the transducer to the sample and c is the acoustic velocity of the coupling medium. Since the wave number is $k = 2\frac{\pi}{\lambda} = \frac{\omega}{c}$ the phase ϕ is proportional to the distance from the sample to the transducer: $\phi = 2\frac{\pi}{\lambda} = \frac{\omega}{c}$ and each change in the distance ΔD will cause a change in the phase $\Delta\phi$;

$$\text{therefore,} \quad \Delta\phi = 2k\Delta D. \quad (5)$$

1.2 Ultrasound, SAM and Orthopaedic Applications

As described before, most ultrasound microscopy applications are used in the evaluation of solid materials, such as metals, composite materials, ceramics and plastics. In recent years it has been shown that acoustic microscopy can also be used in investigations of biomaterials, like animal and human cells [6,9], and hard tissues such as fish scales, teeth, and bone. SAM has been successfully used in a study evaluating the elastic properties of dental materials for dental treatments and further changes of elastic properties of dental hard tissues associated with the progress of caries [5].

Ultrasonic techniques have been used in the recent past for the measurement of the elastic constants of bone. In orthopaedic research, ultrasonic techniques have been used extensively to measure the anisotropic elastic properties of calcified tissue. Abendschein and Hyatt [22] demonstrated that there was a good correlation between the longitudinal modulus (E_3) measured by using ultrasound and mechanical techniques. Later, Yoon and Katz [24] derived the equations relating the elastic constant with the experimentally obtained modulus.

Different investigators have used the transmission ultrasound technique for measuring the ultrasound velocity within the specimen. This was accomplished by placing the specimen between two transducers, one a transmitter and the other a receiver. Knowing the distance between these transducers, and the time for the ultrasound to travel through the specimen, it was possible to determine the velocity. Given the geometrical orientation of this specimen, it is possible to determine the elastic constants (Young's modulus) in all three space orientations [23]. Yoon and Katz [24], Sidney [25], and Van Buskirk and Ashman [26] have made significant contributions regarding the use of ultrasound to measure material properties, and in determining the properties of bone. The principles of transmission techniques are illustrated in Figure 1.10.

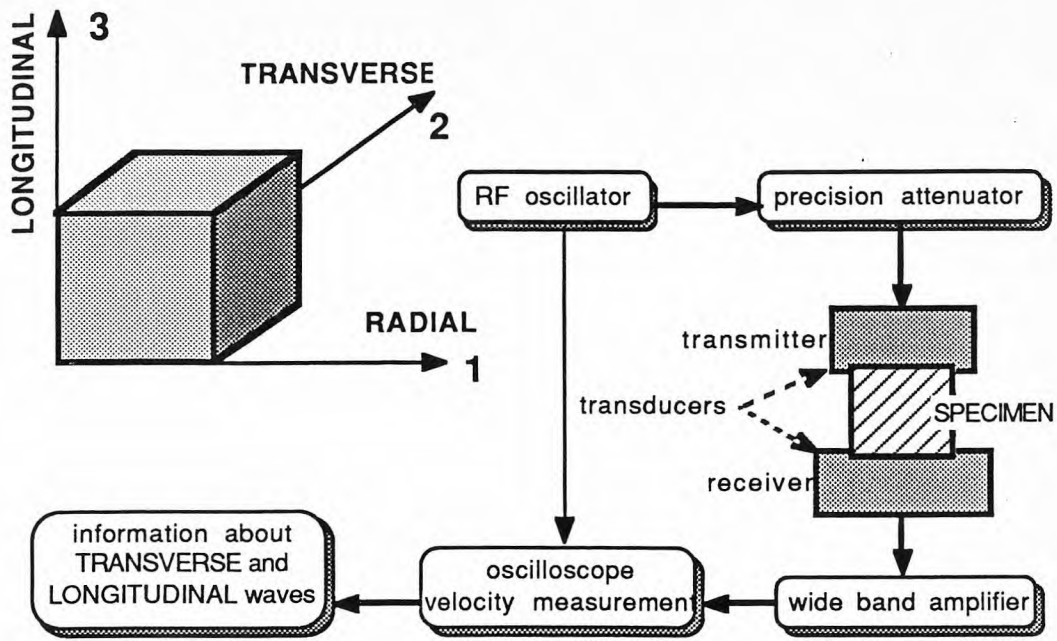


Fig. 1.10: Principle of ultrasonic transmission technique

Meunier et. al. [10] and Zimmerman et. al. [12, 13] have used the reflecting technique that is well known in material research and NDE testing for the study of bone remodelling. Because there is a strict connection between the acoustic impedance, velocity and the reflection coefficients for all materials according to formula (6) and (7), it is also possible to apply the reflecting technique (see Fig. 1.11).

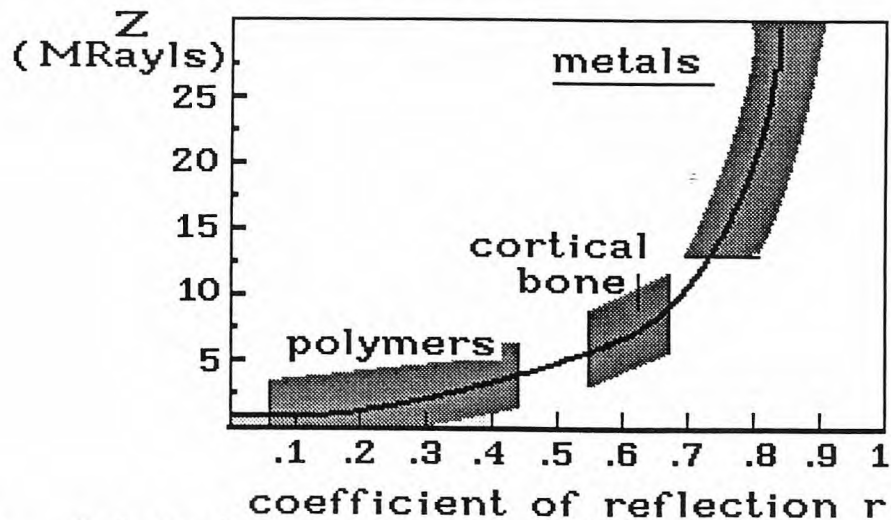


Fig. 1.11: Reflection factor (r) and acoustic impedance (z)

Meunier [10,29] has also shown that there is a high correlation between the data obtained using transmission and reflection techniques. Using the transmission technique, he measured the elastic stiffness in 30 different femur specimens. He also measured the acoustic reflection and impedance from the same specimens. He compared this obtained data and found a correlation factor of 0.99 as illustrated in Figure 1.12.

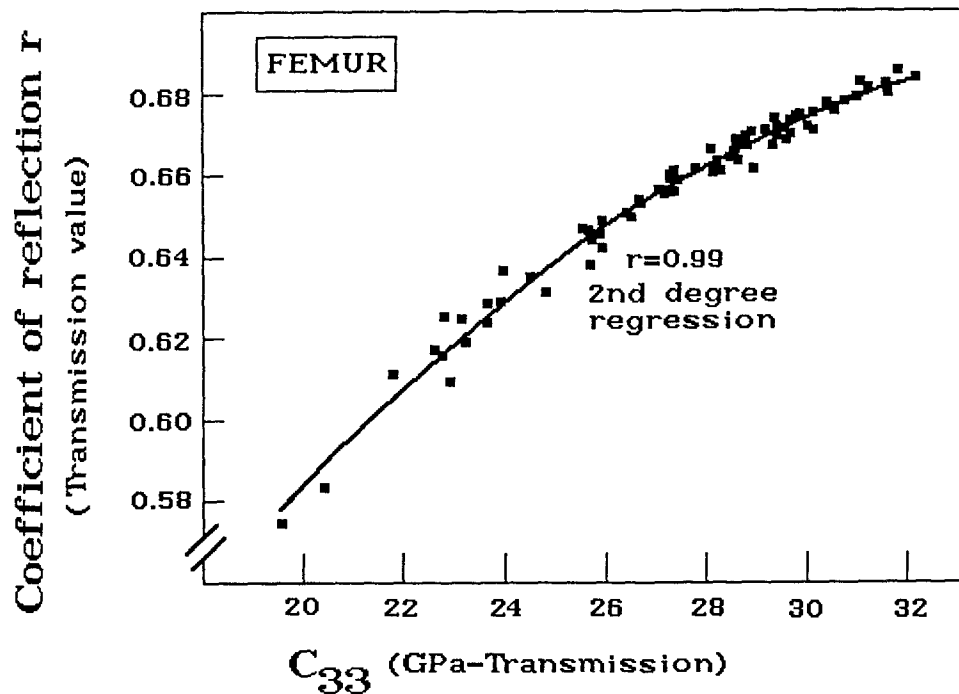


Fig. 1.12: Correlation between ultrasonic transmission and reflecting technique

The data obtained with these experiments show that there is a clear relationship between the acoustic impedance, density, and velocity [29]. Using this data it is possible to obtain the elastic stiffness properties, as Yoon and Katz [24] have already shown. From this work we know the velocity, v , from the transmission experiment. Knowing the material density, ρ , it is possible to obtain the

acoustic impedance: $Z = \rho \cdot v$ (6)

This acoustic impedance can also be obtained from the reflection factor r , and the acoustic impedance from the transmitting medium Z_w

using the relation
$$Z = Z_w \cdot \frac{1 + r}{1 - r} \quad (7).$$

Taking the same numbers we can also obtain the elastic stiffness (Young's modulus)

$$C_{ijkl} = \rho \cdot v^2 \quad (8)$$

and knowing the geometrical directions we can describe the mechanical properties in form of a matrix using:

$$\sigma_{ij} = c_{ijkl} \cdot \epsilon_{kl} \quad (9)$$

$$\begin{bmatrix} \sigma_1 \\ \sigma_2 \\ \sigma_3 \\ \sigma_4 \\ \sigma_5 \\ \sigma_6 \end{bmatrix} = \begin{bmatrix} C_{11} & C_{12} & C_{13} & 0 & 0 & 0 \\ C_{12} & C_{22} & C_{23} & 0 & 0 & 0 \\ C_{13} & C_{23} & C_{33} & 0 & 0 & 0 \\ 0 & 0 & 0 & C_{44} & 0 & 0 \\ 0 & 0 & 0 & 0 & C_{55} & 0 \\ 0 & 0 & 0 & 0 & 0 & C_{66} \end{bmatrix} \times \begin{bmatrix} \epsilon_1 \\ \epsilon_2 \\ \epsilon_3 \\ \epsilon_4 \\ \epsilon_5 \\ \epsilon_6 \end{bmatrix} \quad (10)$$

$$11 \rightarrow 1, \quad 22 \rightarrow 2, \quad 33 \rightarrow 3, \quad 23 \rightarrow 4, \quad 13 \rightarrow 5, \quad 12 \rightarrow 6,$$

In a number of preliminary experiments, scanning acoustic microscopy has been used in the study of bone remodelling about orthopaedic implants [10-13]. For hard tissue analysis, this technique offers the advantage of non-destructive testing of a sample which can then be processed and further analyzed with other techniques. Secondly, it provides an analysis of material properties on a scale not possible with conventional mechanical testing

techniques. Using this technique it is also possible to investigate and determine the different mechanical properties of pathological osteopetrotic and osteoporotic bone. Thus, this new reflection ultrasonic technique that determines the acoustic impedance of material can also be used to study bone remodelling. Subsequently, the acoustic maps produced with the reflection system can be compared to the elastic stiffness results measured with the transmission technique.

1.3 Rationale for Study

The remodelling of different functioning bony elements consisting of solid, nonhomogeneous structured materials becomes a very important issue in bone material remodelling research. The most significant aspect is the ability to present structures in the form of mathematical computer models (FEM) that can be simulated under different loading conditions. In orthopaedic research this technique can be used for remodelling analysis of entire bones. The geometrical shape of a bone is quite difficult to determine, as are the physical properties. A bone consists of a material that is nonhomogeneous; that is, the physical properties like the elasticity change greatly with respect to location within the structure. In order to find and determine these properties, which are required for an analysis of remodelling parameters, it has been necessary to develop a technique that could provide these parameters. The best method to realize this was by using different SAM techniques, connected with an ultrasonic microscope designed especially for this purpose and assembled in our lab. This device is a unique PC-based apparatus. The technical realization of this device and implementation for orthopaedic research is the main subject of this study.

A few experiments have been attempted to improve this scanning technique, data acquisition, processing and presentation of SAM images. A major portion of this thesis deals with improvement of the scanning methods. This involves the correct control of mechanical devices within dynamic limits, and data acquisition with optimized data sampling speed and timing. Using this equipment, an experiment was conducted to evaluate and analyze the acoustic properties of the cortical, diaphyseal bone of the human femur and some known objects such as coins. The acoustic data is compared to images taken with a normal optical microscope and an electron microscope used in the backscatter mode.

2. MATERIAL & METHODOLOGY

Using the ultrasonic microscope developed in the Orthopaedics Research Laboratory at the University of Medicine and Dentistry of New Jersey, SAM images were generated from human bone specimens and known objects such as coins. Due to some limits of the equipment used and the data acquisition technique, different scanning techniques have been used for improving the image resolution and data accuracy.

Briefly, the ultrasonic microscope which was assembled in our lab consists of two different parts: the hardware, based on a IBM Personal Computer and specially developed software for evaluation of ultrasonic images for use in orthopaedic research (see Fig. 2.1).

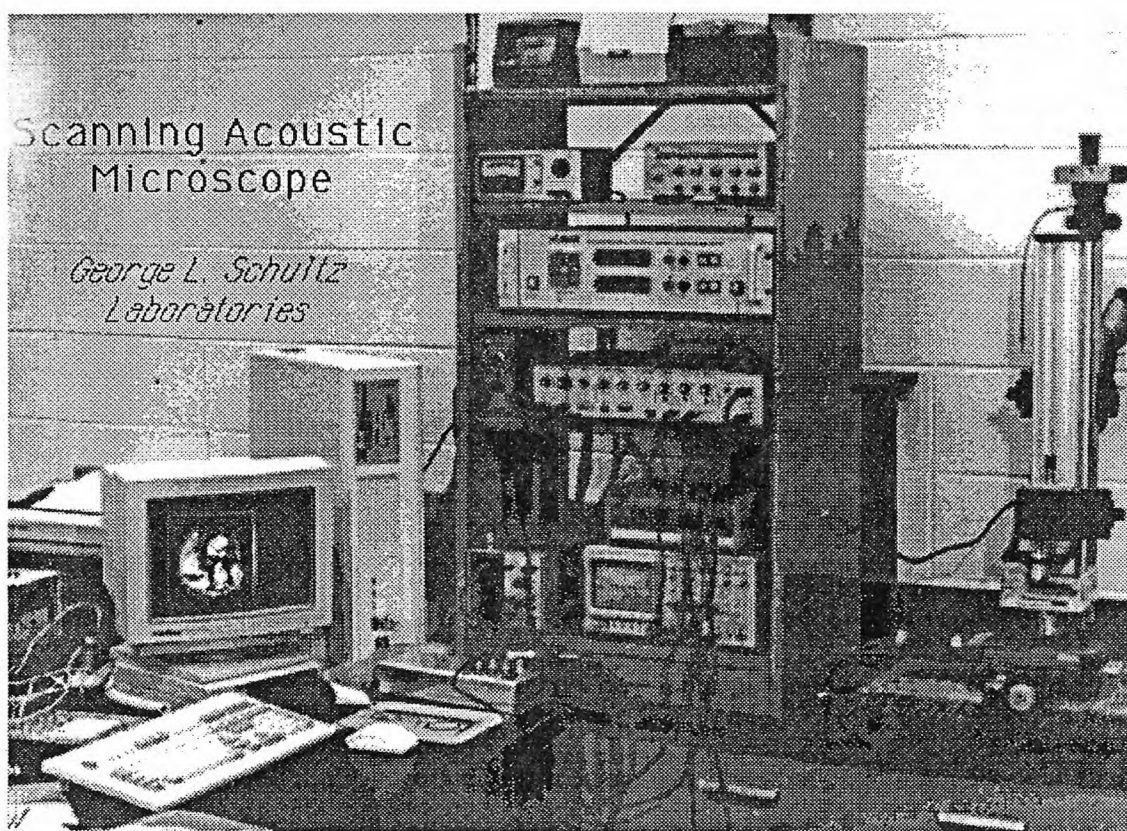


Fig. 2.1: PC based Ultrasonic Scanning Microscope (George L. Schultz Laboratories for Orthopaedic Research)

2.1 System Configuration & Improvements

The hardware can be divided into two major parts:

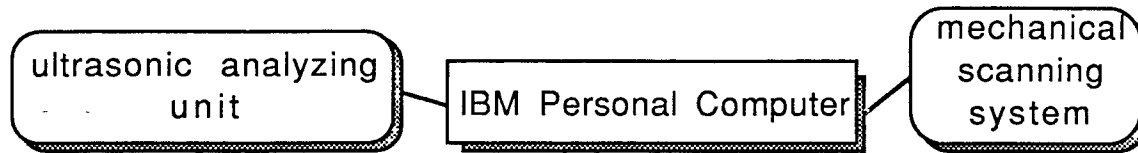
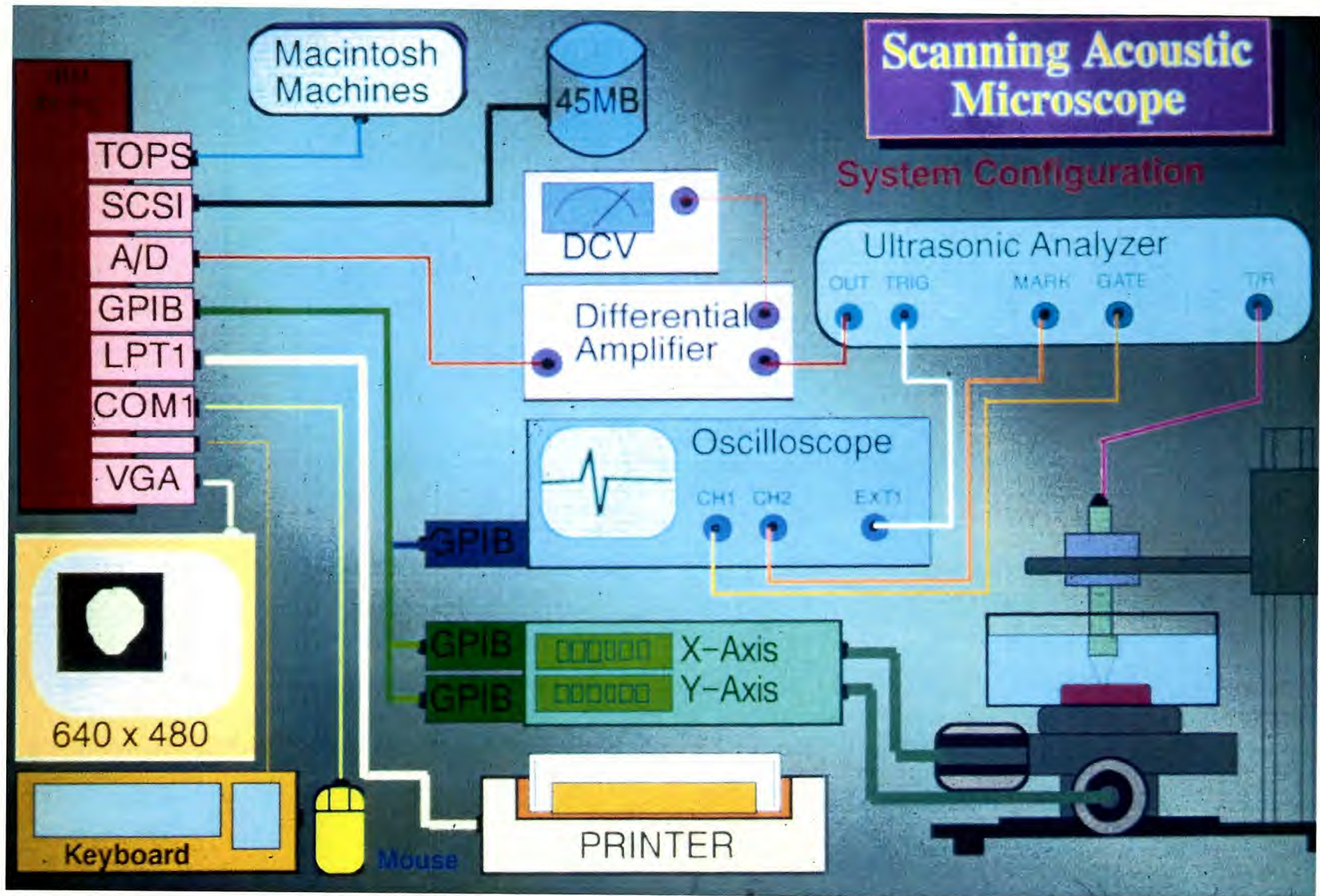


Fig. 2.2: System block diagram

- 1.) the mechanical scanning system with a stepping motor driving unit controlling the X-Y table.
- 2.) The data acquisition, processing and presentation block with the ultrasonic analyzing unit which includes a data acquisition board, screen for image presentation, and an external hard disc for image files storage (see Fig. 2.2).

The entire system consists of the following devices:

a 386 IBM-AT/PC as a system controller, with a VGA color screen (resolution 640x480 screen pixels) and several peripheral boards installed inside the computer, an X-Y table with a driving unit, an acoustic reflection and impedance analysis system connected to a differential amplifier, a digital oscilloscope, a DC voltage source, and a spherically focused transducer operating at 30 MHz (a schematic configuration of this system is shown on the following page in Fig. 2.3).



2.1.1 The Mechanical Scanning System

A number of brackets and mounts were custom designed for various applications. They included a bracket to secure the ultrasonic transducer attached to a vertical column with an optical microscope. The transducer than can be moved in the Z-axis (vertical) and adjusted in the focal plane. In order to obtain multiple measurements on the surface of the specimen, the sample had to be mounted in a special bracket that was fixed in a small tank of coupling fluid (H₂O). This tank was attached to a stage on a dual X-Y table system that consisted of two stages in the horizontal position, mounted perpendicular to each other and moved by stepper motors. Each rotational step of the motor was converted into 10 μm of translated motion on the X or Y stage. The entire raster area range that can be covered by these two stages is 72 x 72 mm. The stepper motors are driven and controlled by a Programmable Stepping Motor Controller CC 1,2 from Klinger® Corp. that can communicate with other devices through a GPIB-bus, RS-232 port or a non-standard parallel communication port. This non-standard communications port provides important signals and information about status of run, speed, actual position from the front display or even the control pulses to the stepper motor. The stages can be moved in single steps or in continuous movement with different speeds, accelerations, and decelerations. Depending on the weight of the tank, its load, the image size to be obtained and the required kinematics of the system, different movement characteristics have to be initialized and assigned to the controller.

2.1.2 Data Acquisition

The ultrasonic transducer is spherically focused with an f number of F 1.2, a frequency of 30 MHz, and a focal length of 25.4 mm with a maximum obtainable resolution of 100μm. The focal point is not truly a point, but an acoustic amplitude

distribution that follows a Bessel function. The width of the principal peak is approximately $100\ \mu\text{m}$ for a 30 MHz transducer. The geometrical characteristics of the transducer used in our system are suitable for C-SAM methods (see Fig.2.4).

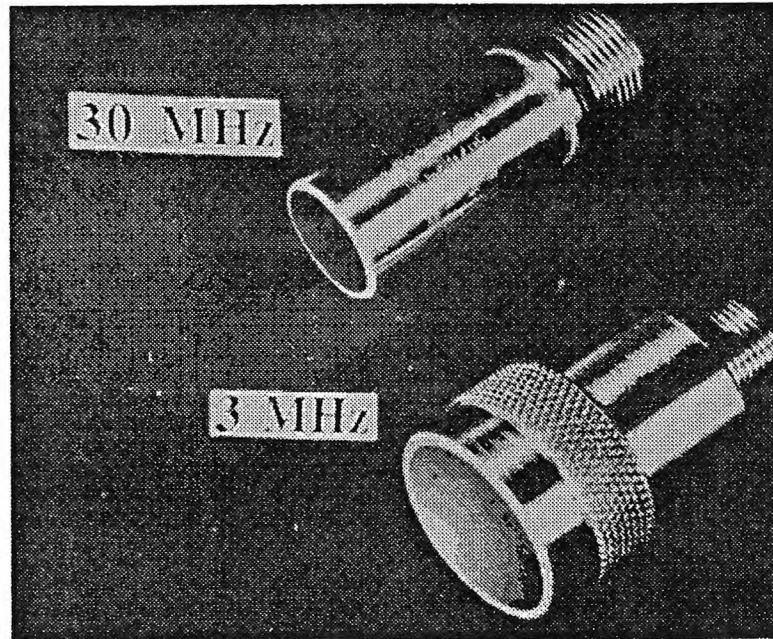


Fig. 2.4: *Ultrasonic transducers*

For our requirements, this transducer can also be used for SAM images. This piezoelectric transducer is excited by very short, high energy pulses from a broadband Ultrasonic Analyzer (model 5052-UA from Panametrics®), which includes a pulser, receiver, "steeples" gate adjustment, and a gated peak detector (see Fig. 2.5).

The pulser generates short, large-amplitude electric pulses of controlled high energy with a repetition rate of 100Hz to 5kHz that are sent to the ultrasonic transducer and converted into short ultrasonic waves. These ultrasonic waves are received either by the transmitting transducer after partial or total reflection, or by a separate receiving transducer. The received ultrasonic signal is converted by the transducers into a voltage value and amplified by the receiver section.

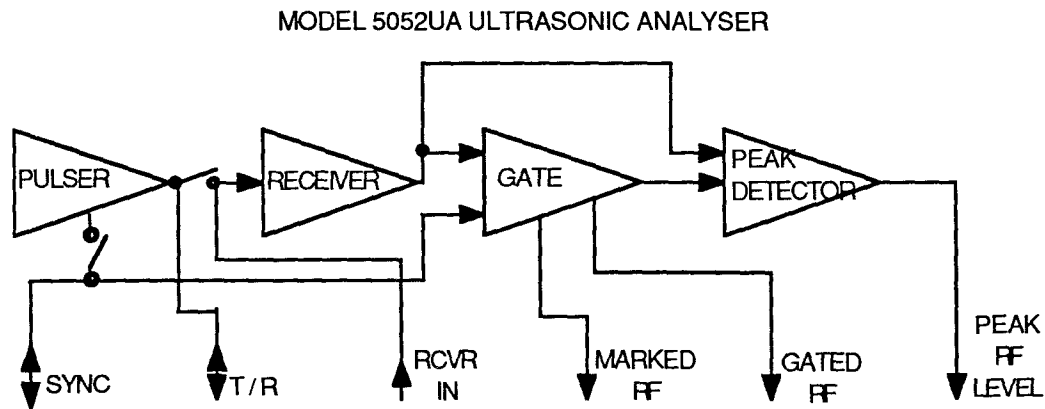
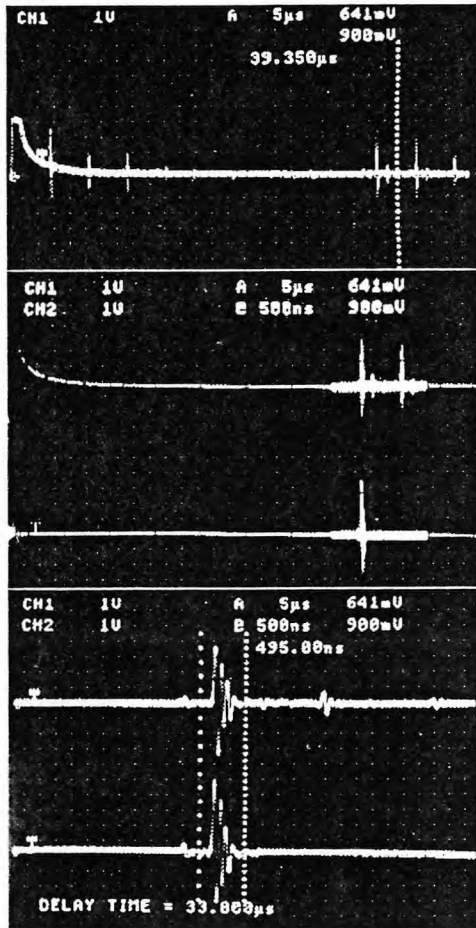


Fig. 2.5: Block diagram for the Ultrasonic Analyser

The amount of sound reflected is directly related to the acoustic impedance of the material. There exists a relationship between the acoustic impedance, the velocity and material density: $Z = v \cdot \rho$ (6), where Z = acoustic impedance, v = the velocity and ρ = material's density. Further, it also has been shown [24] that for bone material there is a strict correlation between these acoustic properties and the elastic stiffness, or elastic constant (C_{33} -the material axis is the same as the direction of sound propagation and reflection) as a function of the acoustic impedance. The correlation between data obtained using the reflection technique relative to the transmission technique has been also verified in previous experiments [10]. The "steeples" gate feature inside the ultrasonic analyzer provides the capability for selecting the part of the signal train to be analyzed. The gate pulse position and width are easily controlled to cover a wide range of values. A special digital oscilloscope (model 2430A from Tektronix) has the capability to present the A-scan or time-domain presentation that is taken from the marked signal (at the marked output connector), which is the RF output from the pulser-receiver signal with a superimposed voltage to mark the selected part of the signal train to be analyzed. This selected part of the signal can also be changed with respect to its duration and time delay after the sent pulse (main bang) or an interface reference pulse. The reflection pulse and the selected part of this signal is presented in Fig. 2.6.



The peak detector section generates a voltage level output which is proportional to the peak amplitude of the highest ultrasonic wave form within the superimposed gate window. The peak level output is held constant during the period the gate is inactive. Although the peak detector has an extremely fast response to a minimum number of narrow pulses, it still requires between 8 and 12 repetitions of a single pulse type to set the right output voltage level, which is then considered as the amplitude of the gated signal. This is illustrated schematically on next page in Fig. 2.7.

Fig. 2.6: Reflection signal (internal)

The peak detector section generates a voltage level output which is proportional to the peak amplitude of the highest ultrasonic wave form within the superimposed gate window. The peak level output is held constant during the period the gate is inactive. Although the peak detector has an extremely fast response to a minimum number of narrow pulses, it still requires between 8 and 12 repetitions of a single pulse type to set the right output voltage level, which is then considered as the amplitude of the gated signal. (see Fig. 2.7. on the next page)

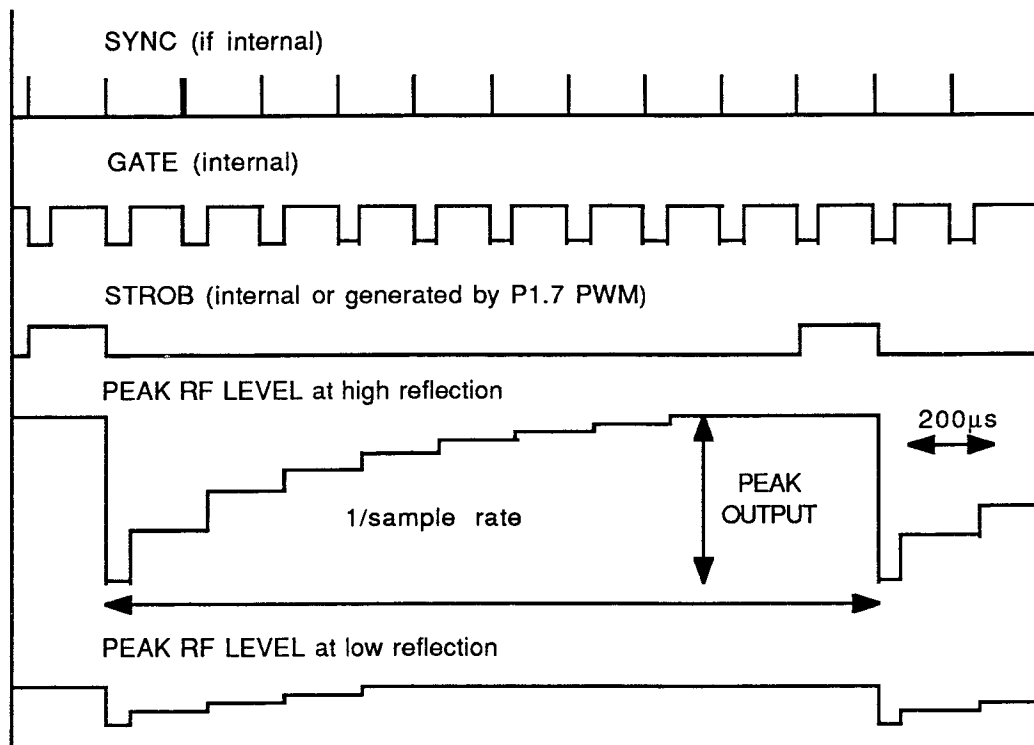


Fig. 2.7: *The Peak Level output from the ultrasonic analyzer*

This output signal is sent to a differential amplifier (model TM502A from Tektronix) which, using another DC-voltage reference, selects a window within the output voltage value that corresponds to a certain acoustic impedance and amplifies this windowed signal.

The signal provided by the output can reach values between 0 and 10V. This analog voltage value is connected to a 12-bit Analog to Digital (A/D) converter which is part of a data acquisition board (model 5525MF from ADAC Corp.) installed in the motherboard of the IBM-PC. This data acquisition board has 16 channels for A/D conversion, 2 digital 8-bit I/O channels with additional handshake connectors, an internal programmable timer, external trigger, interrupt connectors and two digital to analog converter outputs that can generate voltages in the range -10 to +10 volts. The maximal speed of the data acquisition of the A/D converter is 25kHz. This speed can only be reached by Direct Memory Access (DMA). Using assembler routines for single sampling it is necessary to define the

command registers and check the status registers of the acquisition board before each data register acquisition. This technique is slow and can only sample each A/D channel at a frequency of 14 kHz. This board gives the option of using four different techniques for A/D conversion: software triggering, external event triggering, clock triggering, and scan triggering. Our application has used mainly software triggering, and in a few experiments for improving the scanning quality, external event and scan triggering.

In the Software Triggering mode, a scanning program moves the X-Y table and scans the object in 256 lines, generating an image consisting of 256x256 points or pixels. Before beginning real data acquisition, the program scans just one line and generates a motion function to compute the displacements of each image point of the following raster lines. The computer sends a start signal to the stepping motor controller and while the X-Y table is in motion, an assembly subroutine polls the A/D channel with the Peak Detect output and an End of Scan signal provided by the X-Y table controller. The output voltage data is collected in 12 bit values into memory, and after finishing each line, another routine samples the maximum values and interpolates them according to the previously generated motion function, with respect to position. The 256 data values correspond to pixel positions on the screen after the interpolation. They can be presented in the form of a false color map or grayscale on the screen and stored on the external hard disk. An example of gray scale distribution modification is showed in Figure 2.8 (or in color in Fig. 2.21a ,b).

The external event triggering technique executes an A/D conversion only after an external trigger or interrupt impulse has been received by the data acquisition board. The external trigger impulse is generated by an internal strobe signal that comes from the ultrasonic analyzer and coincides with the highest peak detect value. The data is sampled in a similar way as described before.

Scan Triggering provides the possibility of scanning more data channels by doing just one initialization of control registers. This experimental approach has the advantage that it

is possible to acquire more data points, always at the highest peak output value from the ultrasonic analyzer. Using additional hardware, like a divide-by-N counter, it is possible to acquire position signals from the X-Y table controller and trigger the acquisition when a certain number of steps have occurred (see section 3. Results and discussion). The data obtained does not have to be interpolated (displaced) further and can be directly presented on the CRT screen and stored to the hard disk.

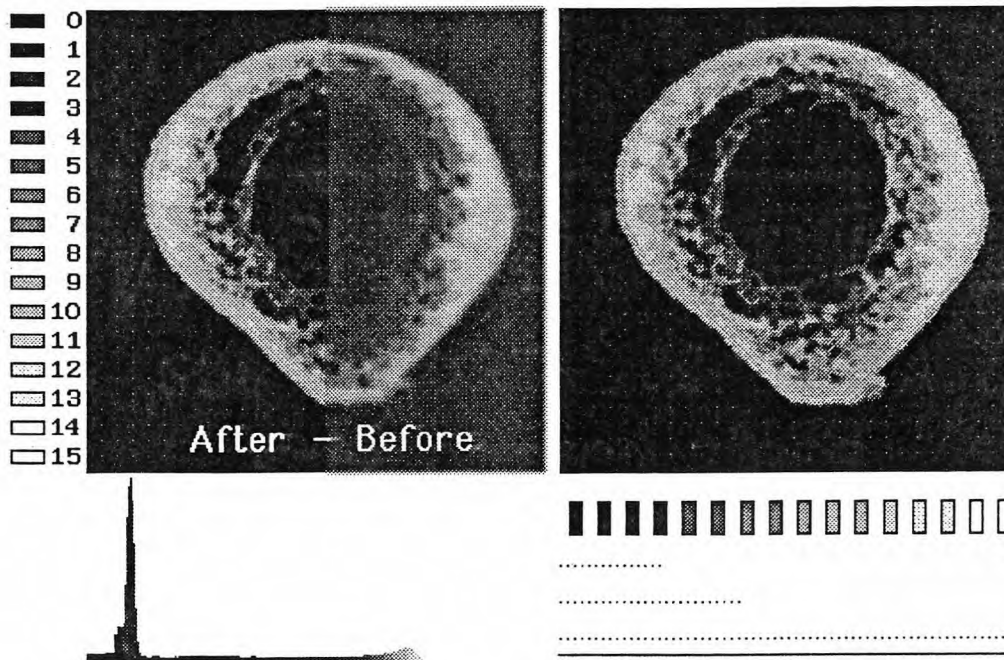


Fig. 2.8: *Grayscale distribution modification*

2.1.3 Data Processing and Presentation

Once the data is sampled and stored on a disk, it can be read, processed, and presented on the screen by using another program for image processing and evaluation. This software was developed by Meunier [29] and recently enhanced for our system. The image analysis software was written in TurboBasic, and has been modified for our

application. It also serves as a guideline for development of a new image processing program to be written in TurboC++. This program has different functions for image presentation, processing and evaluation. For instance, it reads the data from the disk and presents the image in 16 colors or gray level values. The color palette for each of the 16 colors can be individually assigned. Also the color distribution can be changed and stored as a specific histogram distribution [17]. This program can compute the area of the objects. Additionally this program can also present the ultrasound images from the investigated objects in three dimensional perspective. This is very important for designation of the real amplitude of the reflected image, that is sometimes not possible in 2-D presentation. Finally, another powerful property of this image program is computing of the properties with respect to the location on the object. First, it finds the center of gravity and breaks up this object into three different regions - the outer one-third, the middle one-third, and the inner one-third and it investigates these regions in 10° increments and proceeds with a circular weight averaging.

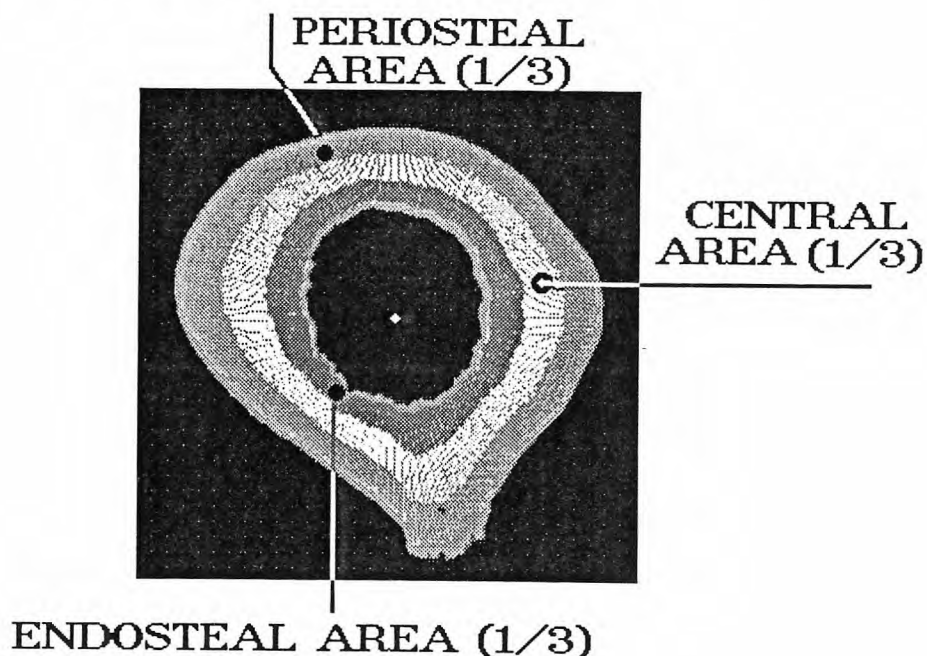


Fig. 2.9a: Center of gravity and three regions

This is particularly useful in analysis of endosteal, middle, and periosteal sections of a tubular bone section. Then the program calculates the average arbitrary ultrasonic impedance values for each of those three regions, as well as the average value for the entire section. This scheme is illustrated in Figure 2.9a. This is not a simple procedure and the following is a description of the algorithm.

The algorithm that provides this computation consists of few simple geometrical equations. But the implementation of the program and the connection with the image enhancement and processing is not intuitive.

Cross sections of long bones are approximately tubular, however differ widely depending on the bone and the cross section location. A typical midshaft region of a femur is shown below in Fig.2.9b

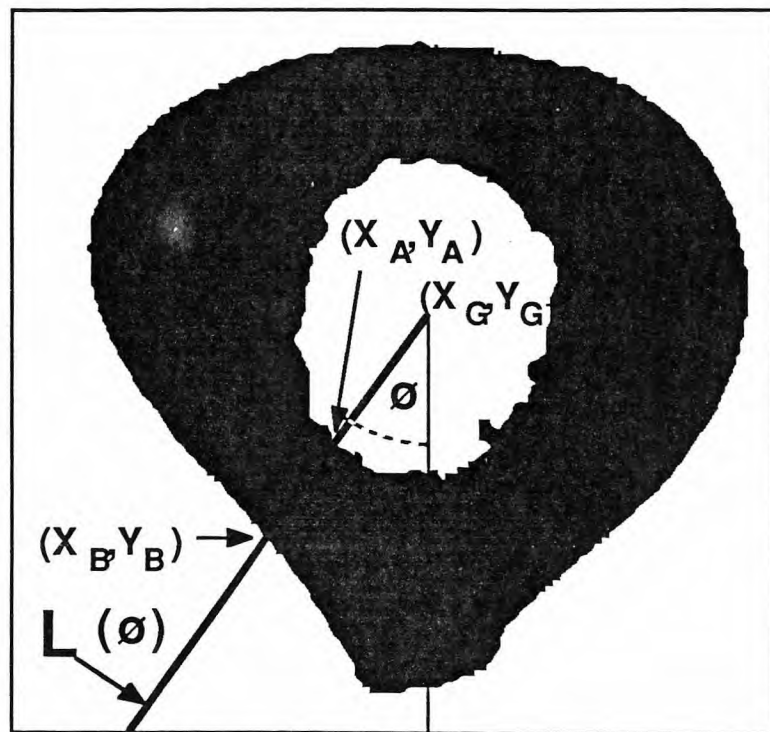
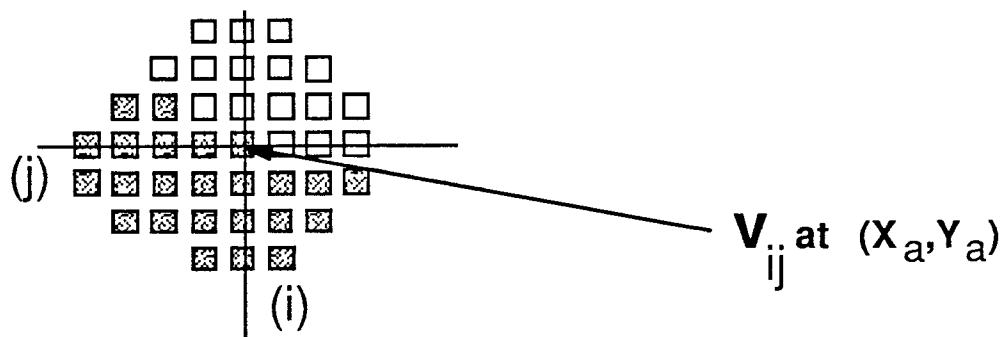


Fig. 2.9b: Creating the line $L(\theta)$.

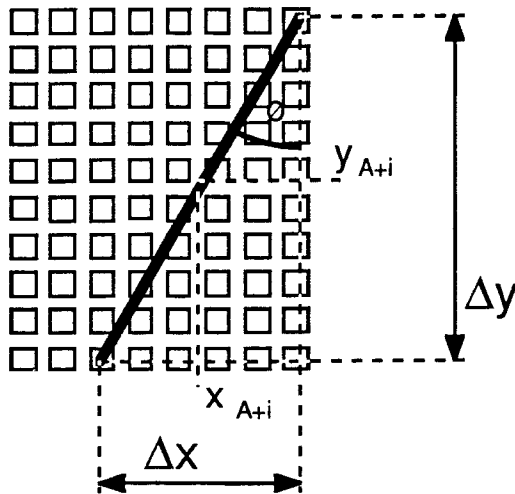
$L(\emptyset)$ is a line which defines pixels to be evaluated. In order to define and compare the geometric properties of different specimens, it is necessary to first find the geometric midpoint and center of gravity. Next a pseudo line is created, which determines the values (pixels on the screen) to be evaluated. This line begins at the center of gravity X_G, Y_G and ends on the image border. The coordinates of the center of gravity in screen pixels can be obtained using the following equation:

$$X_G = \frac{\sum(v_{ij} \cdot x_i)}{\sum(v_{ij})} \quad \text{and} \quad Y_G = \frac{\sum(v_{ij} \cdot y_i)}{\sum(v_{ij})} \quad (11)$$

where the index G represents the position in a 256×256 pixel image. The pseudo line is calculated as follows: Starting at the center of gravity, the algorithm evaluates each pixel close to the pseudo line. In the previous equation x_i is the distance in pixels along the line $L(\emptyset)$ to x_0 ; y_i is the distance to y_0 and $v_{ij} = \{1,0\}$ represents the pixel value in [grayscale values in 1 to 256, after threshold at value 51] at position ij within the investigated image array.



To define line $L(\emptyset)$ with the appropriate pixels the following equations are used.

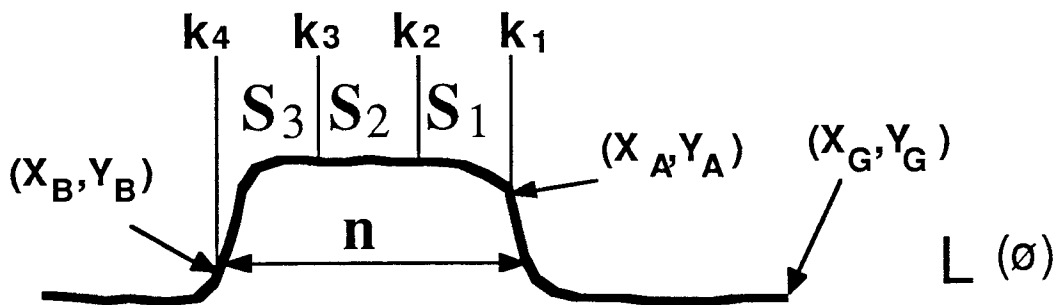


$$X_{A+i} = |\cos\theta \cdot n| \quad (12)$$

and

$$Y_{A+i} = |\sin\theta \cdot n| \quad (13)$$

Using this algorithm it is not possible to detect and evaluate all pixels, therefore it is necessary to assign only the values that are close to this pseudo line $L(\theta)$. Once the pixel values are obtained and assigned to the pseudo line, the next procedure is applied. First, the entire line is divided into points that belong and do not belong to the object [threshold]. All points belonging to the object create a region of n points. This region is divided into three equal sections $S_1(\theta)$, $S_2(\theta)$, and $S_3(\theta)$; corresponding to the endosteal, middle, and periosteal regions of the cross section. In each section the values are averaged as shown in the following diagram.



where

$$n = \sqrt{(X_B - X_A)^2 + (Y_B - Y_A)^2} \quad (14)$$

and the averaged values from each section can be expressed in :

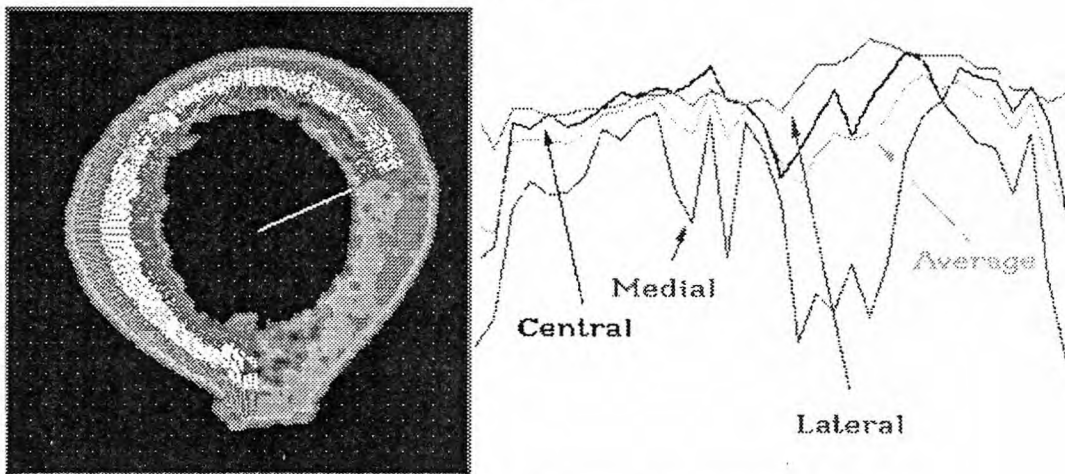
$$S_1(\varnothing) = \frac{1}{k_2-k_1} \sum_{i=k_1}^{k_2} V_{ij}(x_{A+i} y_{A+i}) \quad (15)$$

$$S_2(\varnothing) = \frac{1}{k_3-k_2} \sum_{i=k_2}^{k_3} V_{ij}(x_{A+i} y_{A+i}) \quad (16)$$

$$S_3(\varnothing) = \frac{1}{k_4-k_3} \sum_{i=k_3}^{k_4} V_{ij}(x_{A+i} y_{A+i}) \quad (17)$$

In addition to these three values, a fourth average value $S_G(\varnothing) = \frac{1}{3} \sum_{m=1}^3 S_m(\varnothing)$ (18)

is generated. This $S_G(\varnothing)$ value is an average of the three regions, and represents an overall average of the properties of the specimen along the designated line. Figure 2.10 shows in principle how the program executes this algorithm, how the data is primarily presented and what kind of results are provided.



**Averaging of acoustic properties
in 3 Regions of a transverse
Cross Section**

Fig. 2.10: Circular averaging - image computations

The image data is stored in the form of 12 bit values in large image data files. All image files and the results from computations are stored on a 45 Mbyte removeable hard drive that is connected to the computer through a Small Computer Standard Interface card (SCSI).

The IBM PC is also equipped with TOPS-network support, which connects the IBM PC with Macintosh IIx machines or mainframes. The Macintosh computers are equipped with several graphics packages for further image processing and presentation. Files with ultrasound images and computations results can be sent over the network to Macintosh machines, enhanced, and converted into slides for presentations.

2.1.4 System Improvements

A number of problems had to be solved in order to enhance the function of the system and improve the data accuracy. These problems involved coordination of data sample locations at the specimen with pixel locations on the CRT screen, data conversion, presentation, and storage. A problem existed of coordination between the sampling speed and the timing of the A/D board with specimen movement on the X-Y table. The conversion problem involved the A/D conversion speed and its timing with other devices. The presentation problem involved the optimization of imaging techniques and the speed of image presentation on a VGA screen. The data storage problem involved data format, the size of the data files for each image, and the choice of media for storage. Also, the peak level output of the Ultrasonic Analyzer is not constant over time, and provides the true voltage value corresponding to the reflected energy only in a region between the 8th and 12th trigger impulse. To obtain the correct data it is important to find and to sample only the largest values of this output signal. This is illustrated in Figure 2.11.

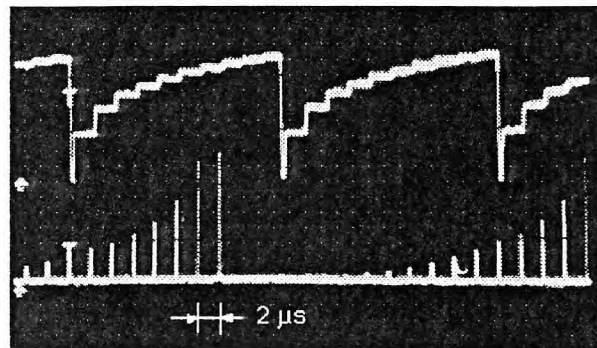


Fig. 2.11: Peak Level Output signal and external triggering

Another important problem is the kinematic characteristics of the X-Y table - the acceleration, deceleration, and different table speeds (as shown in Figures D1 to D14). If the data sampling occurs in equal time increments and not with respect to the actual table position, the generated image will be grossly distorted. The dislocation occurs because the left and right regions of the image are compressed, corresponding to where the specimen was accelerated and decelerated, prior to table reversal. This is illustrated in Figure 2.12.

This is an SAM image of a coin that has been scanned without respect to the data acquisition speed (sampling speed), the speed characteristics and location of the X-Y table over the specimen. This image shows quite sharp edges but it is too much distorted to be used for further processing and investigation.



Fig. 2.12: Image distortion due to acceleration or deceleration of table

Data sampling is random, and depending on the hardware, the programming language used, and the program structure, it can show quite different results in speed and accuracy (see Figure 2.13). In this diagram there are two examples of sampling data using two different data acquisitions board. The upper one was using QuickBasic and showed a very slow data acquisition. In order to obtain the resultant value of voltage this data had to be averaged. The lower part shows data sampled with a faster data acquisition board using assembler subroutines. The resultant voltage value was obtained in this case by directly reading the peak voltage amplitude from the sampling plot and later extracting the maximum values.

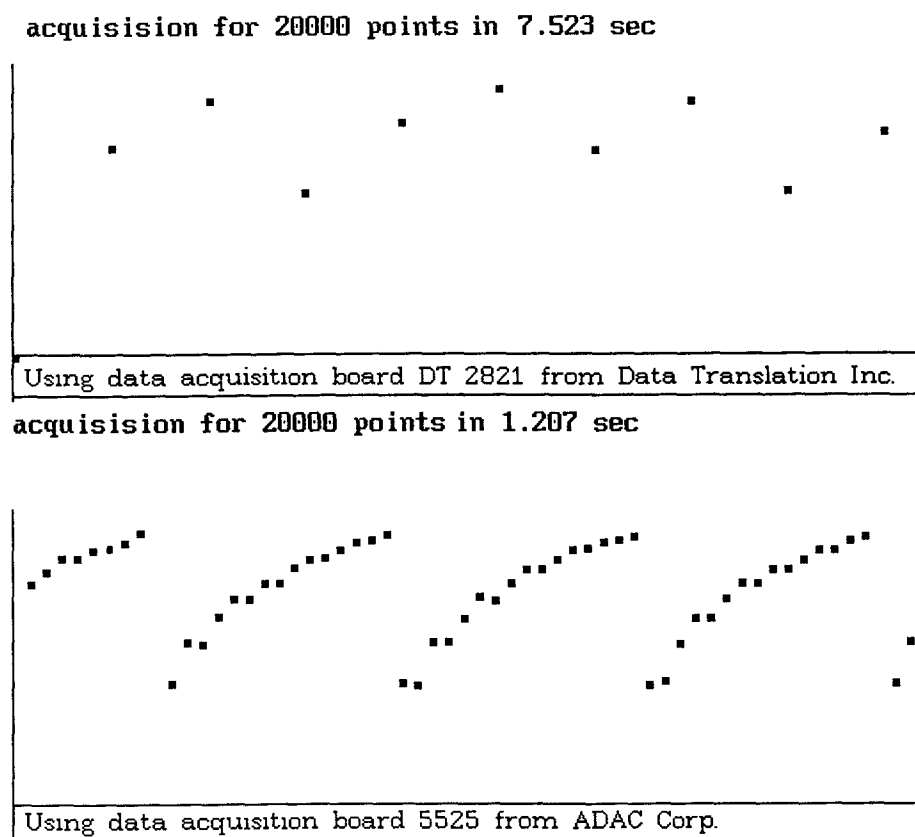


Fig. 2.13: *Computer sampling with two data acquisition boards*

In this thesis three different approaches are used to solve these problems: 1) the software solution through averaging, 2) the software solution through interpolation, and 3) the hardware triggering solution.

2.1.4.1 Software Solution Averaging:

This was the first method used to obtain ultrasonic images with the SAM system. The A/D signal conversion was provided by a data acquisition board from Data Translation® (Data Translation, Inc., Marlboro, MA) which operated in a Software Triggering mode and could only sample about 2000 samples per second. This data acquisition board had a complicated hardware structure and it was virtually impossible to run this board on the assembler level (see program SCAN1.BAS listed in Appendix C).

Using a trigger signal repetition rate from the ultrasonic device of 5 kHz, the output signal was modified by a low pass filter, and the values were sampled by the data acquisition board. They were averaged in order to avoid any large differences in the obtained output voltage values. The data did not show clear differences between the data points because a large portion of the signal was removed by the low pass filter. The resulting image was poor. (Figure 2.14 shows on the bottom the peak level output signal after applying a lowpass filter).

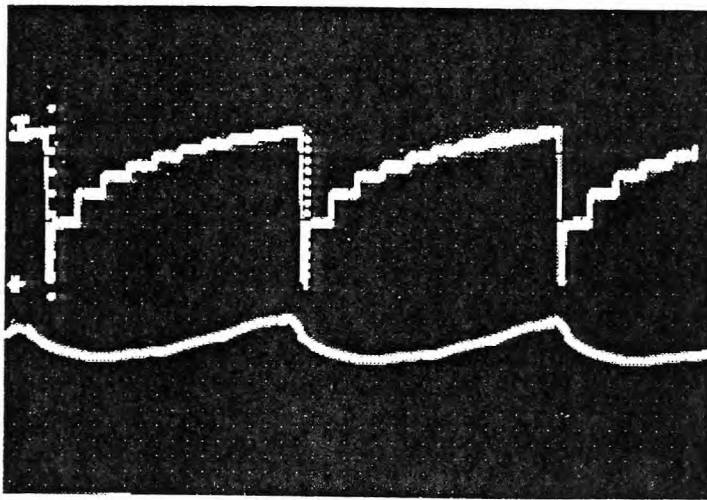


Fig. 2.14: Peak Level output signal before and after low pass filtration

2.1.4.2 Software Solution Interpolation

Another data acquisition board with much faster A/D conversion and a less complicated hardware structure was installed (ADAC Data Translation Board, ADAC Corp., Woburn, MA). Using assembler subroutines, this board is able to collect up to 14,000 samples per second and can therefore provide up to 2.8 A/D-conversions in each trigger signal sequence of 5000Hz (see Fig. 2.13 bottom). The scanning program moves the X-Y table as described before and samples all data points in a large array. After completing each scanning line, a special routine extracts the maximum data points from the array, interpolates the values for movement characteristics, stores them in a file, and presents them in color map or gray scale on the screen. Figure 2.15 (up) shows how the program detects the maximum sampled values when the signal is high.

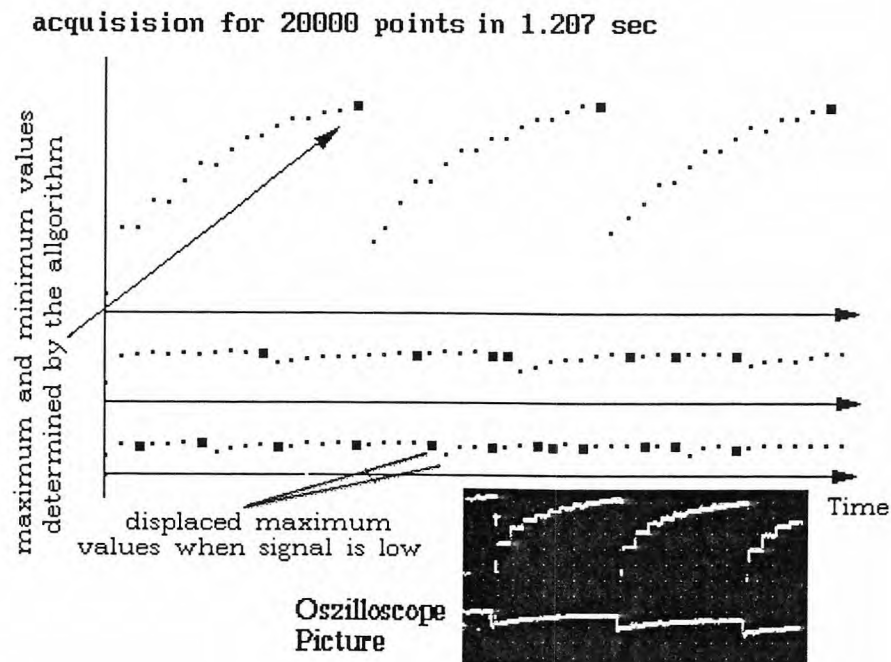


Fig. 2.15: *Sampling of the peak level output signal with maximal and minimal amplitude*

This Figure also shows that the detection of the maximal value when the peak level output signal is low appears more often, what leads to displacement of this maximum values. This reduces the image quality by shifting the image lines (see Fig. 2.16).

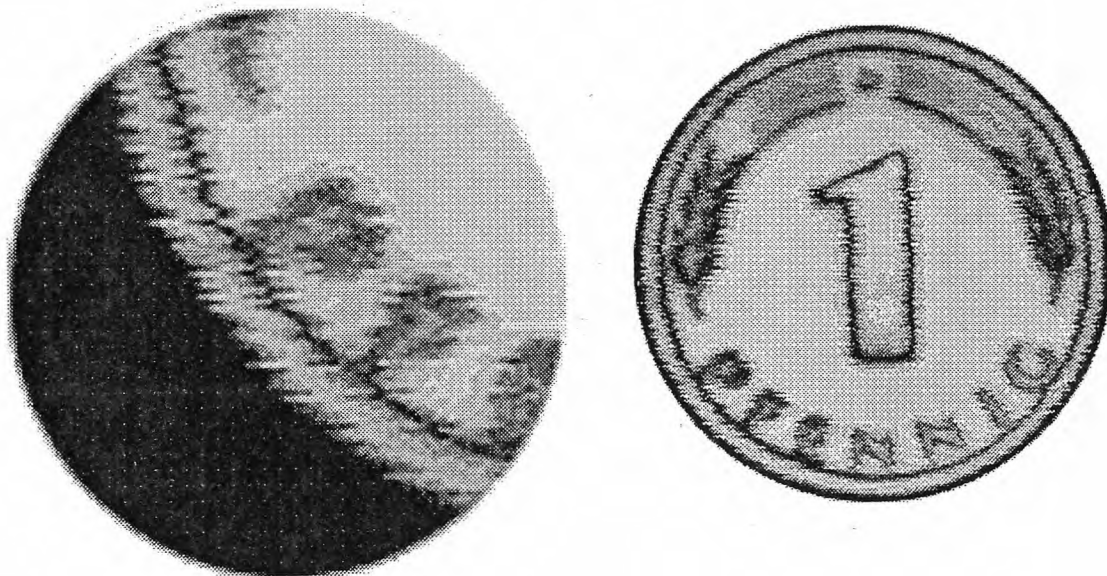


Fig. 2.16: Image line shifting

The image shows an additional problem that exists in determining each maximum value in the huge data array that corresponds to the exact pixel location within the screen line.

Using this approach it has been possible to more clearly differentiate the data points, and to obtain a more precise image. Because the points still have to be interpolated and averaged according to the movement function (especially on the left and right image edges) the image points that correspond to these regions are similarly distorted as in the previously described solution. These points are displaced according to the movement function obtained to the begin of each scanning procedure. In order to solve this problem it has been necessary to find a way to acquire only the data points from the ultrasonic analyzer with the maximum value and to determine the exact location within the image line on the screen.

2.1.4.3 Hardware Triggering Solution

The final solution implemented is the hardware triggering solution. This solution allows for the acquisition of the output signal exactly at its highest level. In order to find the time when the maximum output signal appears, it was necessary to analyze the electronic circuits of the ultrasonic analyzer device. The signal which resets the output signal, called STROBE (INTERNAL) was identified (see Figure 2.17 - bottom).

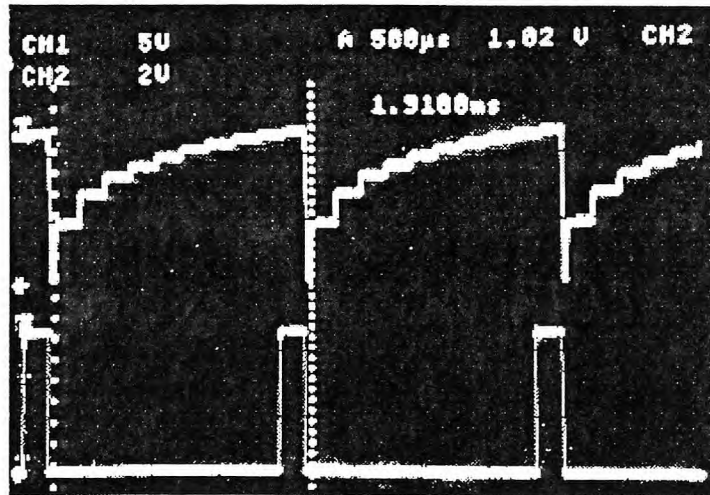


Fig. 2.17: Peak level output signal and internal strobe signal

It was necessary to amplify and interface this signal to the Trigger input of the data acquisition board. This was accomplished by using a TTL compatible bus driver (inside the ultrasonic analyzer device) and an open-collector NAND gate (see Figure 2.18).

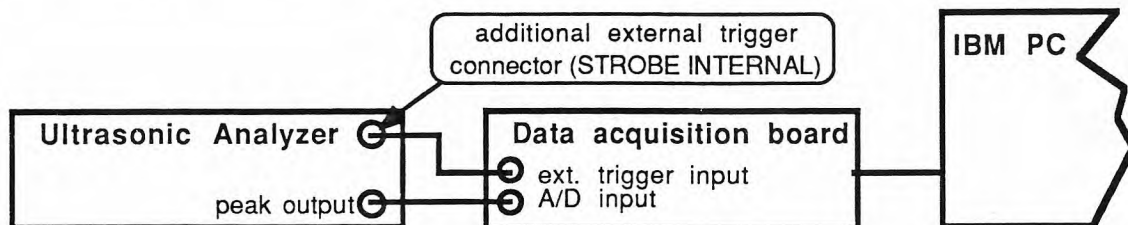


Fig. 2.18: Interfacing UA - device with data acquisition board.

The program ran as previously described, except there was no routine for extracting the maximum data points from an array of randomly sampled values. Using this hardware triggering solution, it has been possible to acquire the output signal data exactly at the maximum level of each A/D conversion and avoid the shifting of the image lines. Figure 2.19 shows a few SAM scans applying different speeds for the X-Y table and data acquisition.

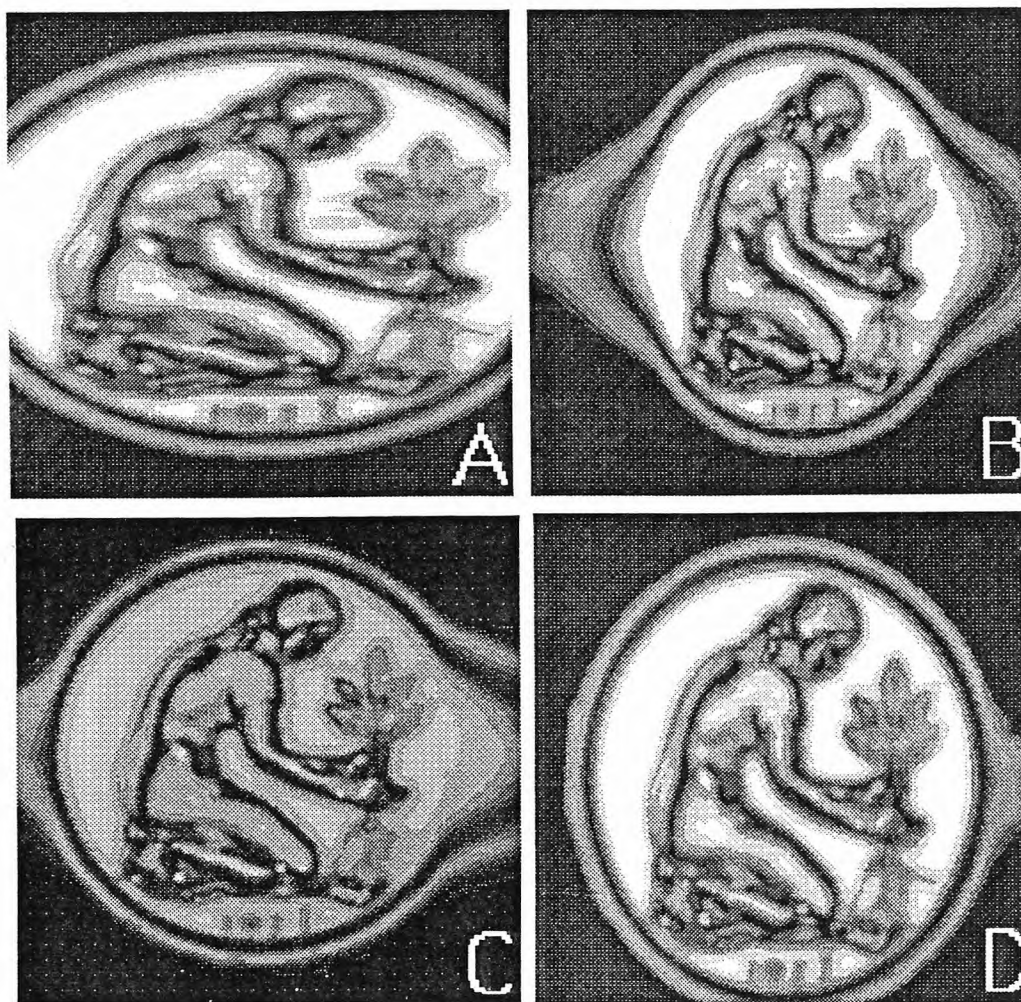


Fig. 2.19: Distorted images without application of displacement algorithms

But in order to obtain geometrically correct picture it was still necessary to apply the movement displacement function, which again averaged the pixel values and reduced the resolution quality of these images.

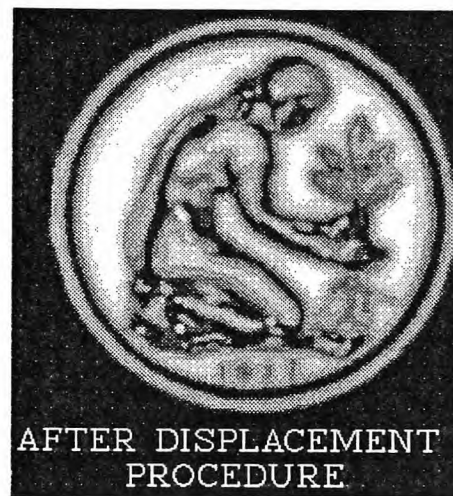


Fig. 2.20: The same SAM image as Fig. 2.19 after applying displacement algorithms

Comparison of Figs. 2.19 and 2.20 shows that without the movement interpolations and averaging, the image resolution has improved, but the non-linear displacement distortions change the shape of the scanned object. Of course, without any movement correction, the movement distortion makes this image useless for other investigations and further image enhancement. Trying to interpolate and average the edges of this image would again reduce this advancement. In order to eliminate the edge distortions without using any interpolation and averaging again, two techniques are currently under investigation. The first one is a software method and the second one is a hardware approach which still has not been tried because of the need of additional hardware devices. Details on this techniques are described in Chapter 3: Results and Discussion.

2.2 Data Acquisition and Triggering experiment

The described techniques for ultrasonic data acquisition provide improvement of data sampling and approach the technical limits of the employed devices. In addition to the software solution interpolation, which has been used for most of the experiments, the other techniques have been tested only experimentally. Therefore, the software solution interpolation will be described in more detail. The scanning program `SCAN2.BAS` in TurboBasic is presented in Appendix C. This program first defines the necessary data arrays and variable names and also initializes the GPIB interface using predefined functions. Since the data acquisition board from ADAC[®] Corp. has a very simple hardware structure, it is not necessary to initialize this board. Next, the GPIB interface must be reset and initialized. The X-Y table controller which is connected to the GPIB interface over an IEEE-bus connector must be loaded with acceleration, deceleration, speed and other interface and movement parameters. The digital oscilloscope is also connected to the IEEE bus and can be initialized with parameters for voltage and time range. The program asks for the image size to be scanned and the filename for data storage. With these parameters the program opens a file on the external hard disk drive and assigns the storage format for this data. Before the real scanning procedure begins, a subroutine moves the X-axis about the scanning range. While this axis is moving, the position of the X-stage is sampled in equal time intervals until the end-of-run position from the X-axis has been reached. This signal for the end of run is an external output signal from the stepping motor controller which has the value 5V while the table is running, and 0V if the end position has been reached. The obtained position values are used for creating a movement characteristics function, which is used for data point movement displacement in the entire scanning procedure. The tables with the motion and position parameters that are normally used by the program are presented in Appendix A and Appendix B. The scanning procedure is a loop that is repeated 256 times, one time for each line of the image. While

the X-axis starts to move, an internal loop is polling data from two A/D converter channels. One channel is connected to the peak output from the ultrasonic analyzer and the other is connected to the external output status signal from the stepping motor controller. The peak output value is stored in a large array and the status signal is checked for its value. Because of the shift displacements of the mechanical system it is only possible to scan in one direction. Therefore, while the stage is moving back, all necessary computations, data conversions and data storage can be performed. The first procedure is the evaluation of the randomly sampled peak output values for the highest values from peak output signal, which correspond to the real acoustic reflections. Because this signal varies strongly in its amplitude depending on the reflection, it is also very important to find the position at which this maximal signal can occur. For instance, for one line of an image 3 cm x 3 cm the board collects approximately 25,000 values and an algorithm determines approximately 1,500 maximum values. The maximum values have to be displaced according to the movement function and fit into 256 data points that represent one line of the image. Once these 256 data values have been computed and placed into an array, it is possible to store them on the disk and present them in the form of different colors on the screen. Figure 2.21a and 2.21b presents such an image.

The next program SCAN3.BAS presented in Appendix C is an experimental program designed to trigger the data acquisition from an external device. The program itself is only different from the previous one in the scanning procedure. Instead of randomly sampling a large number of data values and then extracting the maximum values like described before, this program only samples the peak output values when the ultrasonic analyzer triggers the data acquisition. The TTL - compatible trigger signal that is provided internally by the ultrasonic analyzer occurs only when the peak output has reached the maximum value. The high-level of this signal is connected to a NAND gate with open collector. The output of this gate, which is connected to the trigger input with a pull up resistor to +5V, pulls this trigger input to the logical ground and generates a trigger event.

The obtained data has to be displaced according to the movement characteristics and stored in the same way as described before. Because this program does not provide any significant improvements it is still necessary to find another technique which can ensure that the sampled data points are at the right position within the image without applying any displacement algorithms.

Currently, this approach is being tested to trigger the X-Y table displacement. As described in Chapter 4: conclusion, the stepper motor controller sends step pulses to an 8-bit counter. A comparator compares the two values and sends a trigger pulse when a certain number of pulses (steps) has been reached. This trigger signal combined with the peak detect signal gives the exact reference to calculate the exact time and location of the next data point to be acquired.

2.3 Experiment in scanning of four pairs of femural specimens

The purpose of this experiment was to evaluate bone remodeling and resorption in the human femur. Four pairs of human cadaveric femurs were harvested and frozen. At a later time, they were sectioned transversely with a low speed diamond saw such that a 1 cm section was removed from the central diaphyseal region. The superior side of the section was polished and scanned with the scanning acoustic microscope. Specimens from the proximal, distal, and midshaft section of the human femur (see Fig. 2.23 at the end of this chapter) were investigated with the SAM system. The midshaft region provided the best specimen for this analysis. A specimen was also prepared and imbedded in polymethylmethacrylate following standard histological protocol. Later, the superior side of the plastic block including the specimen was milled parallel to the bottom side, polished and prepared for ultrasonic scanning. The purpose of the embedding was to compare fresh

specimen properties to the properties measured when the bone is embedded in plastic. Figure 2.22 shows SAM scans of prepared specimens.

Besides scanning the bone specimens, it was also possible to obtain color SAM images of other objects (i.e. a NYC subway token, presented in Fig. 3.4 and 3.22). These results are presented in Chapter 3: Results and Discussion.

2.4 Mechanical Testing of Human Cadaveric Bone

The purpose of this experiment was to compare the mechanical properties of human bone to the material properties measured by the SAM system. One pair of HIV negative, fresh human cadaveric femurs (#2366) were harvested and stripped of all soft tissue. The diaphyseal shaft was then sectioned transversely using a slow speed diamond saw. The femoral sections were approximately 10cm in length (2 sections/femur for a total of 4 sections). All the segments (Right and Left) were transversely cut with a diamond saw into cross sections (bone rings) each approximately 1 cm in height. Six (6) "bone rings" were obtained from the proximal sections and five (5) from the distal. One pair of bone rings was non-destructively analyzed prior to mechanical testing with the SAM system (#2 rings, proximal Left and Right). For mechanical testing, each bone ring was turned on edge and tested in compression to failure with the application of force in the medial lateral direction. An MTS servohydraulic mechanical test system was used. The failure force was measured and a paired statistical analysis used to determine statistical differences.

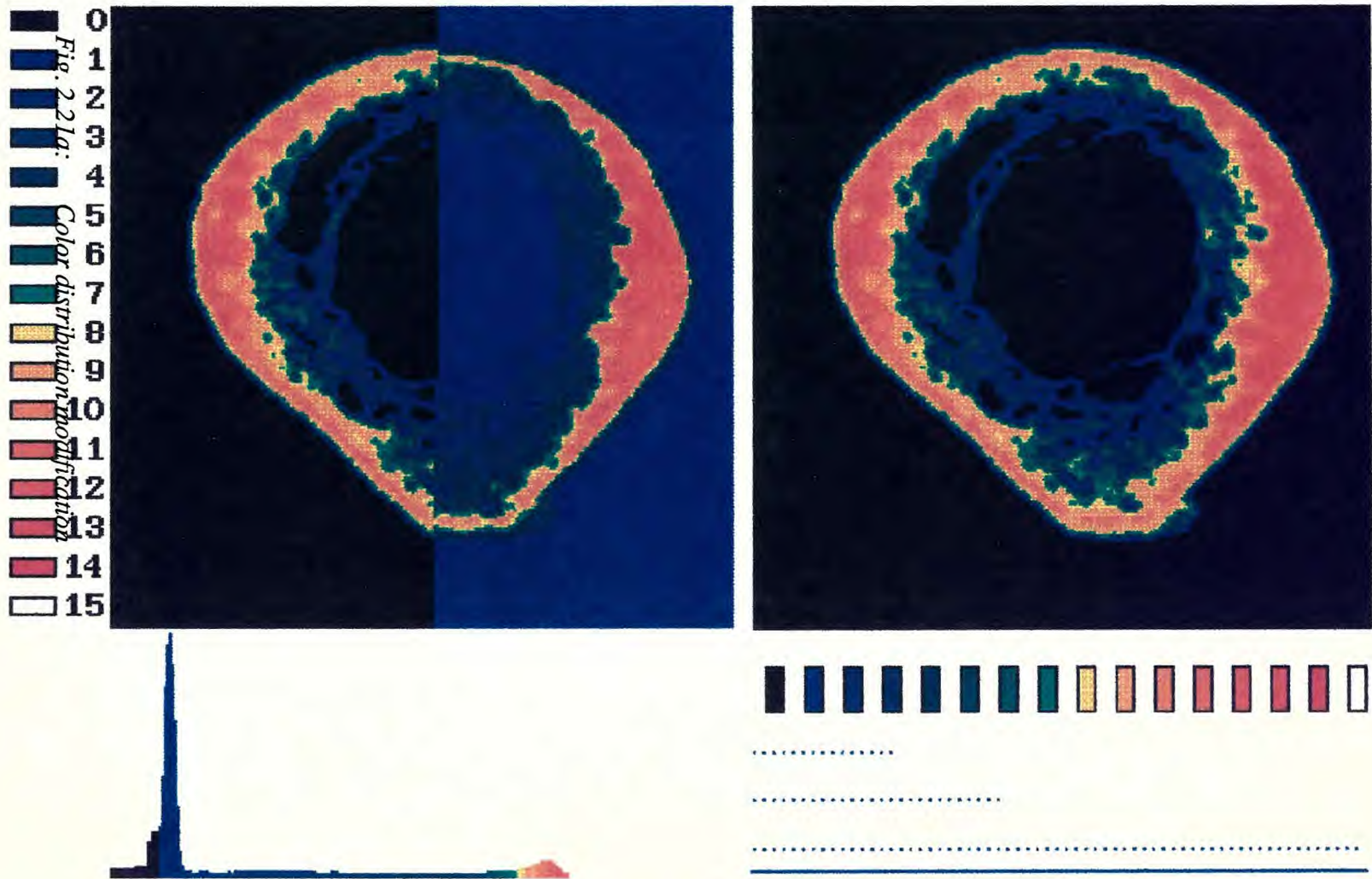
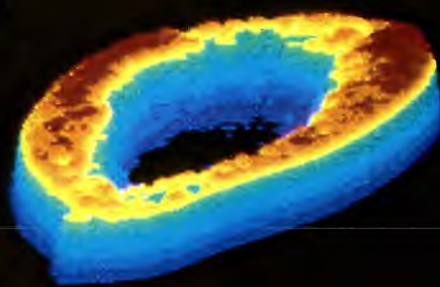


Fig. 2.21: Color distribution modification

Bone #2326R-M
3-D



GRAY SCALE
PRESENTATION

COLOR SCALE
PRESENTATION

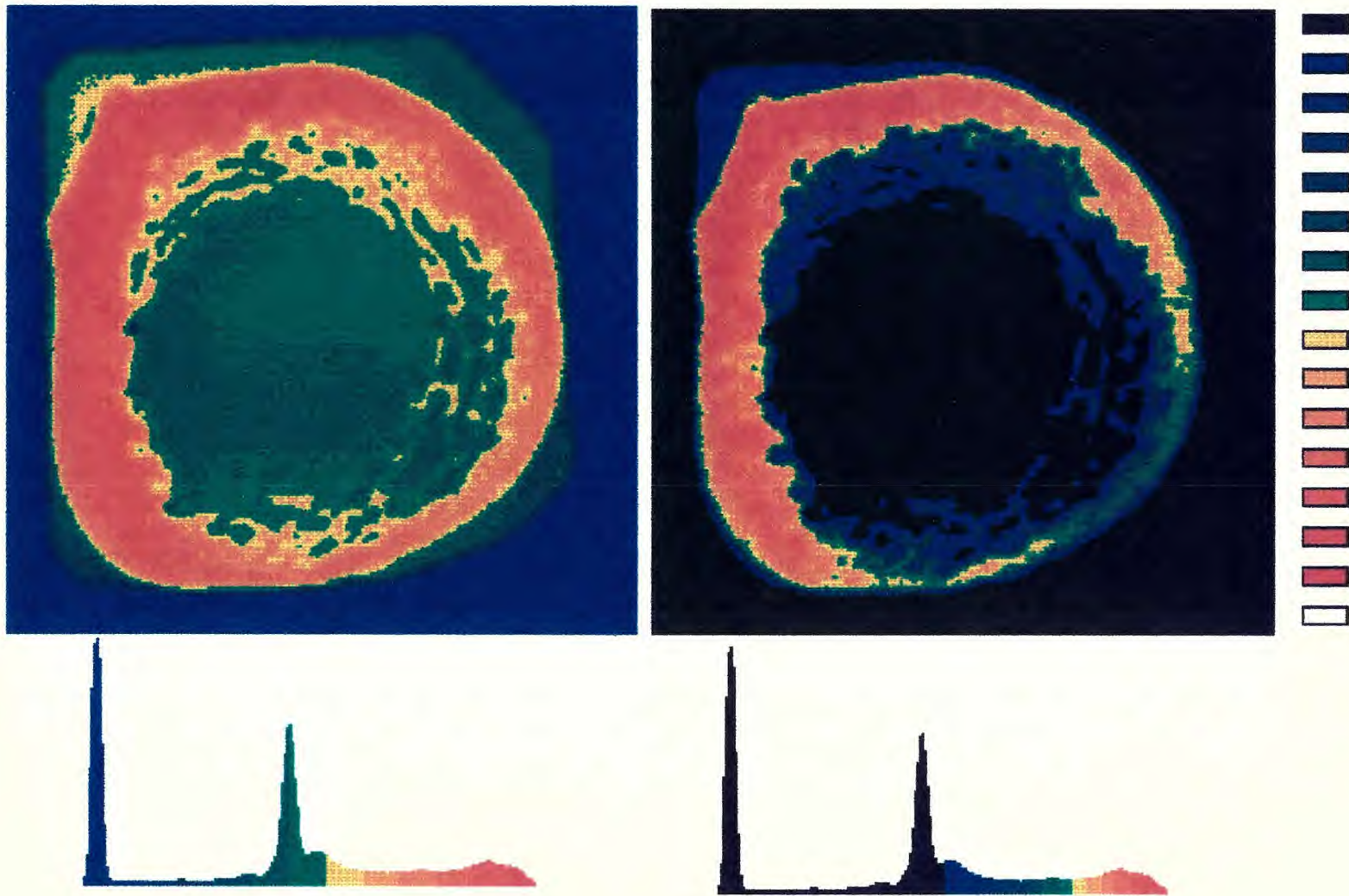
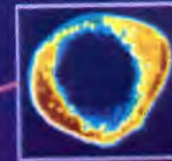
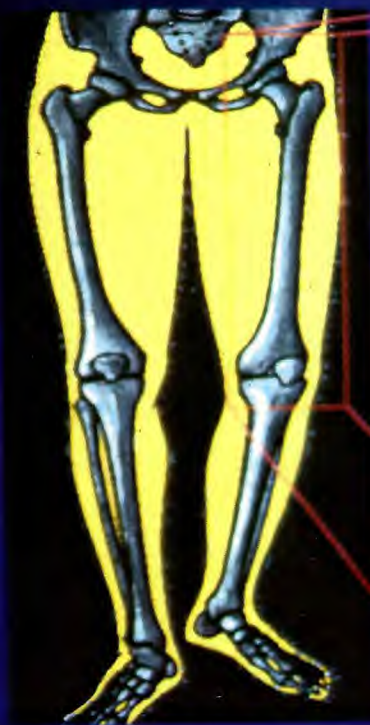
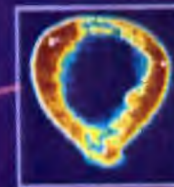


Fig. 2.22: Femoral Midshaft SAM Images of specimens imbedded in plastic

Femur specimen preparation



Proximal



Midshaft



Distal

3. RESULTS AND DISCUSSION

Brief, preliminary descriptions of SAM images have been presented in Chapter 2: Materials and Methodology. However, the present analysis deals primarily with the aspects of resolution and physical limits of the scanning acoustic microscope, and these are discussed in detail below.

3.1 Data Presentation and femoral section

The raw score data of SAM-scanned materials sampled using the experimental conditions described are presented in Tables 2 to 12, Appendix A. The title of this tables gives informations about the number of steps the table was moved [stp#], time difference between each position data acquisition[TimeDif=] and the R, S, and F parameters (see Appendix D.) The following numbers in these tables represent the actual XY-stage position as the distance from a given starting point as a function of time, sampled using uniform time intervals. Table 1 presents ranges of acoustic impedances for selected known materials, including human bone specimens.

Figures D.1 to D.14 represent the velocity as a function of time (v/t) and distance in steps as a function of time (s/t) extrapolated from data in Tables 2 to 8 (app. A). Here, a single motion experiment was carried out in separate trials (seven cases) where speed, acceleration, and deceleration parameters were changed. These parameter modifications were tested in order to assess how the speed of the XY-stage changed during the constant speed phase of the scan. These different device parameters gave information about the movement characteristics of the system, and allowed certain predictions about the accuracy and reliability of the scanning process.

Tables 9 to 12 (app. A) show the results from computing the acoustic properties of the sample with respect to the location within the femoral bone specimen sampled (circular averaging). In these cases, the endosteal, middle, and periosteal regions were investigated in 10° increments. Three data functions were obtained from these measurements; the fourth was the computed average. The most left column represents the location in 10° increments. The second left and the fourth from the right [av23??] represent the arbitrary averaged values from the left and right specimen, respectively. The abbreviations [endl-m] represent the endosteum of the left specimen, [medl-m] the middle left, [perl-m] the periosteum left, [endr-m] the endosteum right, [medr-m] the middle right and [perr-m] the periosteum right. The numbers in the columns represent arbitrary values for the reflection.

3.2 System configuration and Improvements

The experiments carried out were of two types. In one set of studies, the scanning apparatus was improved by applying different scanning techniques. In the second, ultrasonic images and data from human cadaver femurs and other known objects were obtained. The apparatus as already described in Material and Methodology is a unique combination of different devices driven and controlled by a Personal Computer. In order to make this system function and to obtain images such as those shown in some of the presented figures, unexpected problems had to be solved. In this work, only a number of problems connected with improvement of the resolution and the scanning procedure have been addressed and are described below.

3.3 Triggering Experiment (improving accuracy of device)

The problems connected with correct data acquisition and image presentation have been already described in the previous chapter. To obtain the highest image quality it is important to know the physical limits of this technique and the mechanical restrictions of the scanning device. The resolution of the system, the most important aspect in the data and image presentation, is limited by the transducer characteristics and the mechanical apparatus. The 30MHz transducer used for the imaging experiments had a resolution of 100 μm . A single step of a stepper motor is translated into 20 μm displacement.

In other words, the smallest increments that could be applied are

$$5 \text{ steps} = 100\mu\text{m} \quad (5 \text{ step} \cdot 20\mu\text{m}/\text{step} = 100\mu\text{m}) \quad (19)$$

In these experiments, scanning different coins with minor topographic features have shown that a displacement above 100 μm was still below the required resolution. Of course, scanning coins is not the best method for determining the resolution. The maximum scanning speed has been measured with the computer by acquiring the x-y axis locations over the GPIB bus and computing the time differences (see Table 2 - 8). The greatest speed measured was 1500 steps $\cdot \text{sec}^{-1}$. Utilizing this speed, and knowing that the resolution was beyond 100 μm and that the smallest displacement is at least 5 steps for each data acquisition, we obtain a maximum sampling rate of 300 sec^{-1} with the maximum speed. These speed position increments have to be interfaced with the data acquisition speed from the ultrasonic analyzer. This device operates at a repetition rate of 5KHz and can provide a valid peak level output signal every 10 to 12 trigger repetitions (like shown in Fig. 2.7), obtaining about 500 peak output values per sec. Therefore, the sampling frequency from the ultrasonic analyzer can vary only slightly between 500 and 420 sec^{-1} . The XY stage speed and the sampling rate can be changed to any value, depending on the

adjusted speed, acceleration and decelerations parameters, and the image size to be scanned. According to the operating manual for the stepper motor controller, there are four parameters that can be set to describe the movement characteristics of the XY-table: the R, S, F parameters and the number of steps N. These descriptions are provided in Appendix D. According to the operating manual, the speed at any time can be calculated using the given formula:

$$\text{Steps per second} = \frac{10^6}{(256-r) \cdot (80) + z \cdot (10) + 75 \pm 7.5} \quad (20)$$

and some other formulas included in the operation manual (see Appendix D). The kinematic characteristics are also different for the positive or negative direction. The results obtained in an experiment designed to evaluate movement characteristics are presented in the form of data in Tables 2 to 8 and Figures D.1 to D.14 relative to Velocity-Time (V/T) and Position-Time (S/T) diagrams. In the constant speed phase, it appears on the V/T diagram that the speed is severely fluctuating. In reality, the changes are zero or negligibly small. The fluctuations that appear in the diagram are because the data was collected as integer values and not fractions. These diagrams show unequal movement characteristics especially in the acceleration and deceleration phases. The choppy shape of the acceleration curve demonstrates that the load of the mechanical stage is too large to accelerate smoothly as per the defined preset parameters. Another reason for the choppy acceleration characteristic is that the motors are driven at two different speeds, the slow rate speed and the maximum speed. If the distance is less or equal to the number of steps that are necessary for acceleration and deceleration, the motor operates only at the slow rate and will never switch to the maximum speed. If the distance is larger, then as the motors are accelerating up to the slow rate speed, the system checks if the number of remaining steps is still large enough to reach the maximum speed. If the number of remaining steps is large

enough, it continues with the acceleration up to the maximum speed. For some of the V/T diagrams, this switch to the maximum speed is clearly indicated by a sharp velocity increase. In order to eliminate this velocity change distortion, which has a significant influence on the image quality, it is necessary to develop a technique which can exactly interface the position of the X-Y table with the appropriate pixel position on the screen. There are two techniques that are now being experimentally tested. One is the software method and the other one is the hardware solution.

In the software method, the data sampling is delayed, depending on the speed at a certain position during the acceleration or deceleration period. The scanner accelerates and the microscope starts taking data at some predefined locations. An acoustic measurement is triggered as the transducer is eventually moved equal increments as a function of the constant velocity of the X-Y table. Each position corresponds to one pixel of the image that is displayed. These positions are determined by counting pulses from the stepper motor with a divide-by-N counter, realized in the form of an array with different delay values. At the beginning of the scan line a delay counter is loaded with the first value from the delay array, which is the largest number. After each acquisition the next smaller number from this array is taken and placed into the delay counter. This decreases the delay times between the acquisitions according to the movement characteristic of the table. In the deceleration phase the delay counter starts with small numbers at the beginning and increases until the final position of the scanned line has been reached. The disadvantage of this approach is that it is very difficult to define the accelerations and deceleration parameters for the delay loops for each step. For each different scanning size, speed, and kinematic characteristics there must exist a different array of parameters assigned especially for this movement. To avoid this problem and configure this system for more flexibility, it was necessary to search for another solution, based on hardware modifications.

The hardware approach requires additional electronic devices in order to recognize the mechanical displacement and position of the X-Y table, and to interface it to the data acquisition board inside the PC. The data acquisition and A/D conversion are only enabled if a certain number of steps from the stepper motor has been completed and the peak level output has reached its maximum level. The stepping motor controller sends a pulse for each step completed. This pulses are counted by an 8-bit counter and the result is compared with a value that is preset through a digital I/O channel from the PC (refer to Fig. 3.6 and Fig. 3.7).

The software solution averaging approach mentioned above has been used previously with a slower data acquisition board. The results (images) have been taken from the scans already done in the past. The other software solution approach of doing interpolation between obtained values has been applied to this application using a faster data acquisition board. In order to improve this method it was necessary to apply different algorithms and change some of the parameters within them. That was necessary to avoid the line shifting (Fig. 2.16), minimize the image distortions on the edges (Fig. 2.12) and obtain geometrically correct image (Fig. 2.19 and 2.20).

In general the SAM images of coins show poorly-defined edges and almost no small surface features. There are several reasons for this. Firstly, coins are not adequate for determination of resolution and secondly, the transducer that has been used has a small angle and is therefore more suitable for subsurface scans rather than investigations on the surface. Poorly defined edges occur because when the acoustic beam hits the edge or a surface which is not perpendicular to the transducer axis, the beam is scattered and not reflected straight back to the receiver (it then detects a lower reflection factor). These effects can be seen in Figure 3.1, where the very black area around Lincoln's head (U.S. penny) is due to scatter or in the three dimensional presentation, the low attenuation is not representative of lower acoustic impedance but rather due to different reflection angles.

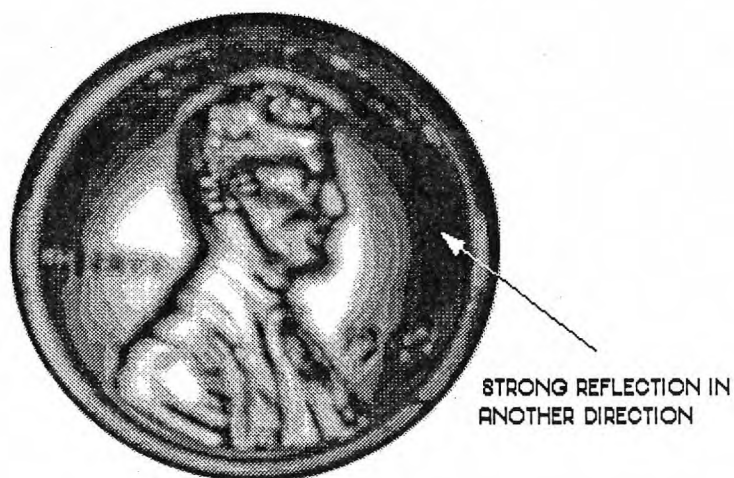


Fig. 3.1: *One US penny in grayscale*



Fig. 3.2: *One US quarter in grayscale*

The same features can also be observed in Figure 3.2, for the scan of a US quarter. Areas on this coin, that are not perpendicular to the transducer axis, especially on the edges are presented in quite dark gray colors.

Another SAM image of a coin but with equal surface is presented in Figure 3.3. Flat surfaces in some areas of this coin shows very high reflection factors and the sharp edges appear very dark, corresponding to lower amplitude in the 3D presentations. Especially the 3-D image shows higher reflection properties at surfaces perpendicular to the transducer axis and lower properties at the edges.



Fig. 3.3: Other coins with a flat surface in grayscale

Examples where a SAM image presents more closely the real acoustic material properties and less the topographic changes are presented in Figures 3.4 and 3.22. These are scans of a NYC subway token which consists of two different metals. The metal in the middle is harder and has a higher reflection coefficient than the surrounding metal. Panel B, the 3-D representation, shows these differences clearly. In Fig. 3.22, a New York City subway token was scanned and the 2D and 3D image is provided. The token consists of two metals, a copper outer ring with a stainless steel center. There are topographical characteristics of the copper ring that alter the reflected signal. However, the inner stainless steel center has consistently higher properties than the copper ring. The lack of topography also provides a more consistent signal.

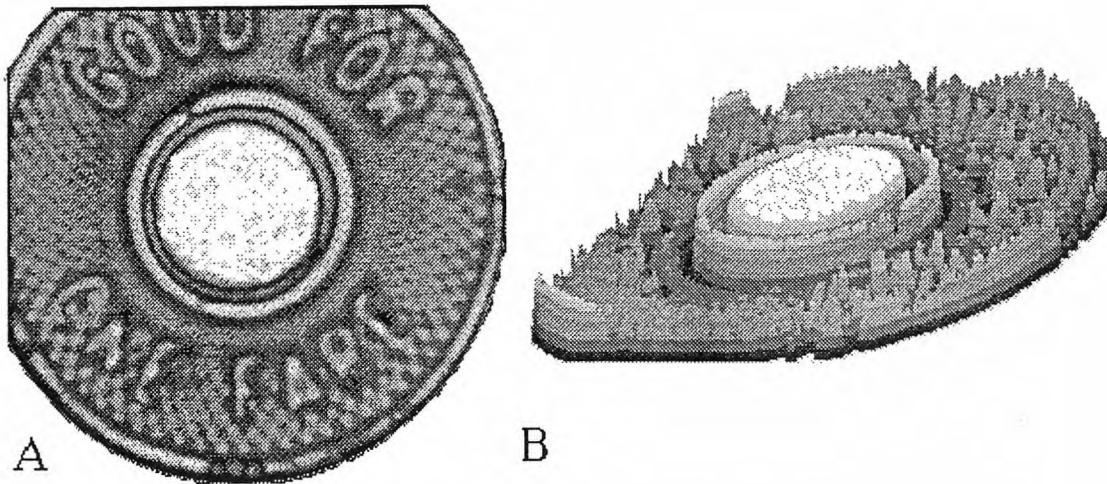


Fig. 3.4: SAM image of a NYC subway token

In another experiment a coin was scanned with different X-table increments, in order to reach higher magnification and be able to recognize the limits of the resolution. Figure 3.5 shows briefly the results of this experiment. One step increment is translated into $20\ \mu\text{m}$ displacement.

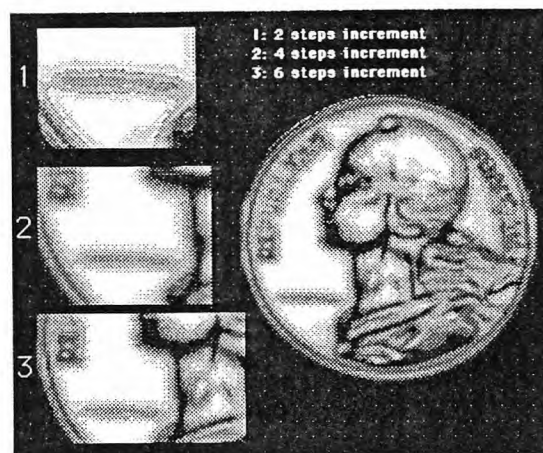


Fig. 3.5: SAM image with different sampling increments

The last experiment is a continuation of the triggering experiment - the hardware approach and involves implementation of additional hardware. This approach can improve the scanning device, determining the location of the X-Y table, by counting the steps from the stepper motor and sending a trigger signal to the computer. A block diagram of this approach is shown in Fig. 3.6

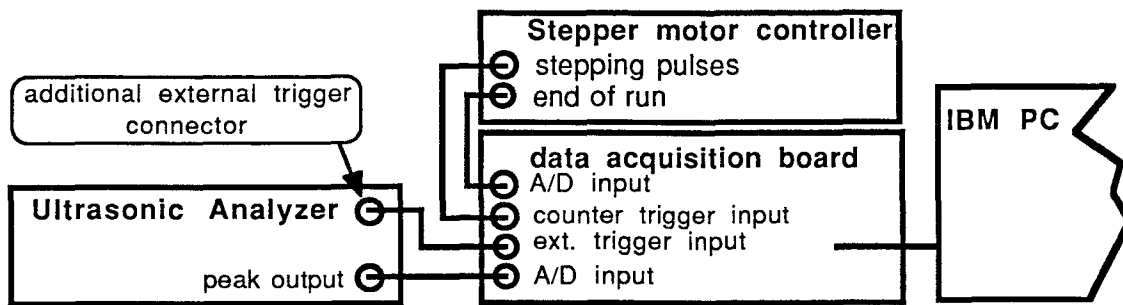


Fig. 3.6: Block diagram demonstrating interfacing of the external trigger and counter

The stepper motor controller is connected with a counter. The counter counts the motor steps and compares the number with a value preset from the computer. Each time a certain number corresponding to the scanning steps increments has been reached, this counter triggers the PC which executes a single data acquisition.

The electronic blockdiagram of this counter and its interfacing to other devices is shown in Fig. 3.7 on the next page. This circuit works according to the following description. Each time the counter has reached the preset value, a comparator sends a trigger signal which sets a RS-Flip-Flop and resets the counter. A trigger signal from the peak level detector, ANDed with the Flip-Flop output, triggers the data acquisition and resets the Flip-Flop again. This hardware solution acquires data only if the displacement between points has a minimum distance of N points. Using this technique it is important

that the speed of the stage be relatively slow with respect to the image size and displacement distance N , so that the position triggering is not faster than the maximal peak level triggering.

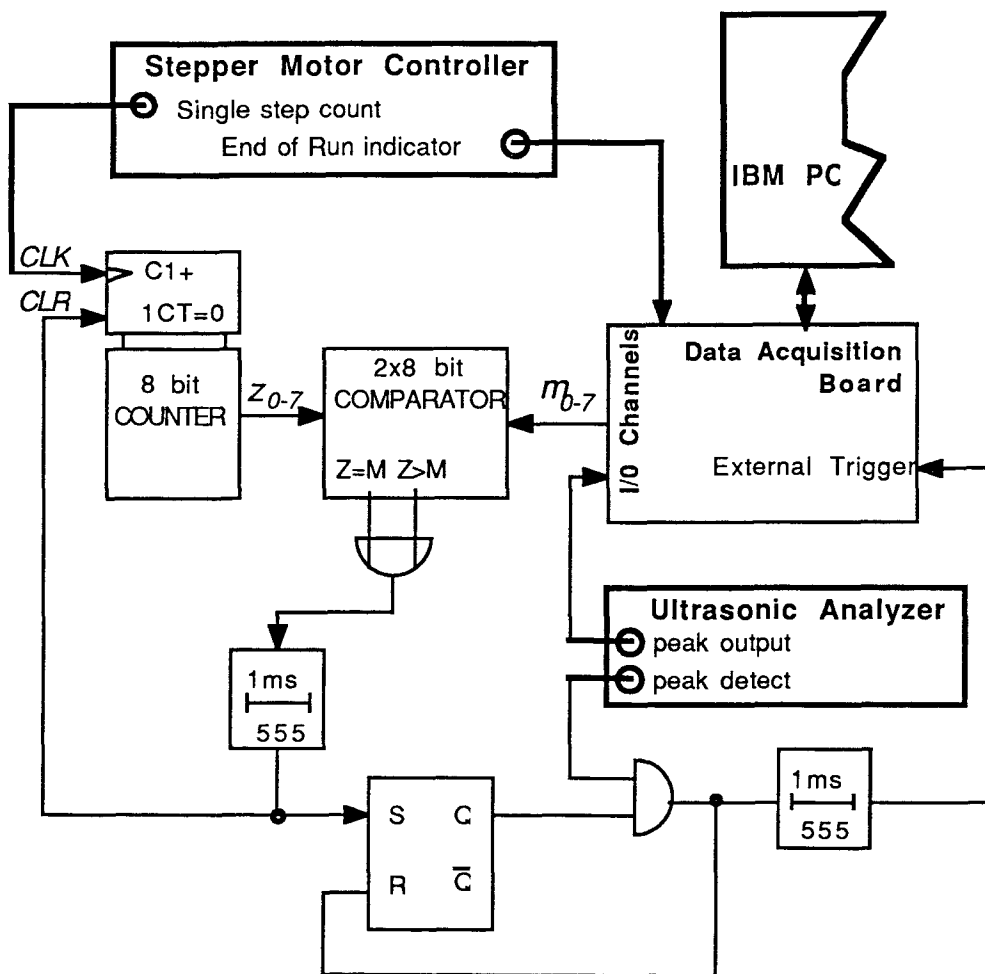


Fig. 3.7: Electronic circuit of counter trigger

3.4 Results from scanning of four pairs of femurs

The data presented in this section has been obtained from four different pairs of femurs. The SAM scans present the midshaft region investigated from the superior side. The circular averaging procedure was done according to the description in Fig. 3.8

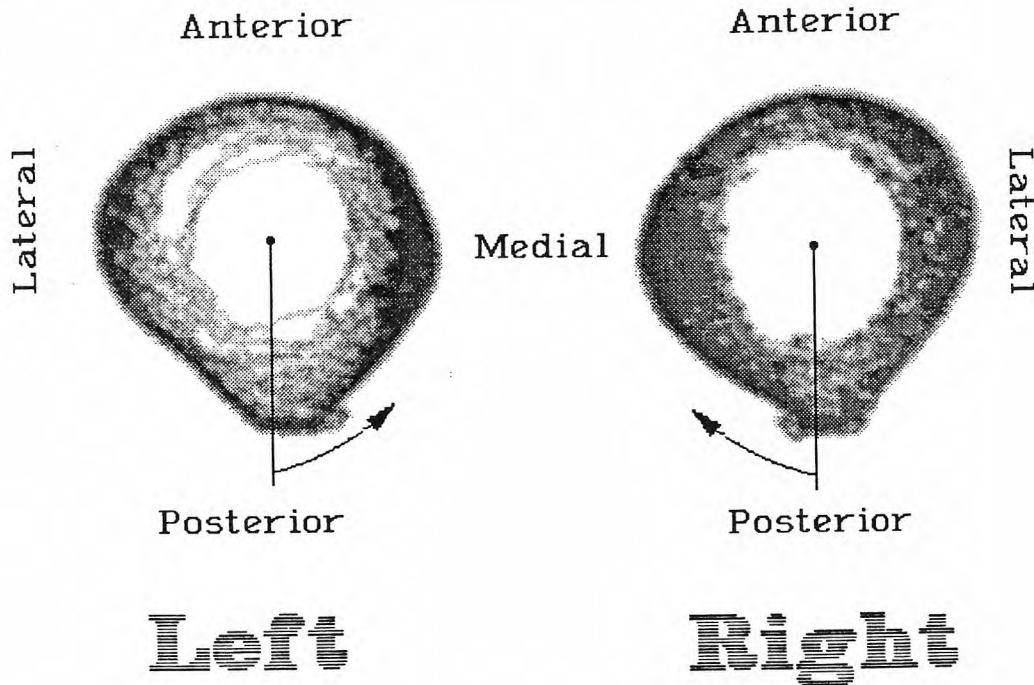


Fig. 3.8: Femoral section position and anatomic orientation

The following figures and scans were generated from this data. The same color scale was used for all sections. Figure 3.9 is an image of a femoral cross section taken from a 75 year old female (#2363). This scan is a prime example of left and right consistency regarding both form and properties. The geometry is nearly identical and the quantity of bone of different properties is also nearly identical. For example, the amount of bone represented by the orange part of the scale is equivalent for both sections.

A number of other observations can be made with this analysis that are not possible with conventional microscope techniques. The lower property endosteal and periosteal regions (blue and green) are quite evident. These are areas of active bone growth or remodeling and the presence of immature freshly remodeled bone is verified with this technique.

Figures 3.10 and 3.11 are graphic presentations of the averaged data of the 3 regions and the overall average of the section properties. Left to right consistency of the properties is evident. Lower endosteal properties are also evident for both sections, with the posterior endosteal zone of the left femur being very low. As illustrated in Fig. 3.9 significant resorption is evident in this region given the color distribution chosen. This is a consistent finding regarding femoral bone remodeling. Posterior resorption usually occurs first, followed by anterior resorption, and finally lateral and medial resorption.

Figure 3.12 is a scan of left and right femoral sections taken from a 84 year old male (#2329). This scan demonstrates how left and right geometry can be consistent, while the properties can vary significantly. The SAM image shows the right femur with a much larger percentage of low impedance bone than the left femur. Figures 3.13 and 3.14 present the data in graphic form, and one can quickly appreciate right to left differences. Firstly, this analysis is very sensitive as evident by the decreased properties of the posterior medial and anterior lateral endosteal zones. The two lowest values in Fig 3.13 are evidenced and verified in the scan. Consistent periosteal and middle properties are demonstrated, with an overall R value average of about 170. Figure 3.14 demonstrates a much more erratic, inconsistent, set of properties over all zones. This result contrasts to the previous pairs of sections analyzed. Again a qualitative light microscopic technique would not have provided the materials information obtained with the acoustic system.

Left and right sections of #2326 (Fig. 3.15) show another remodeling phenomenon. The scans are very similar with severe endosteal remodeling evident around the entire sections with significant resorption occurring in all three zones of the anterior and

posterior regions. Figures 3.16 and 3.17 demonstrate the inconsistent properties through all regions and zones when compared with Figs. 3.9 - 3.11 . Finally, if one assesses the average properties (delta symbols) of both Figs 3.16 and 3.17 the peak values attained approach 160, where the average values in Figs. 3.10 and 3.11 average about 165 with the lowest values attained were approximately 160.

Finally, Figure 3.18 presents femoral cross-sections taken from a 68 years old female (#2366), and Figures 3.19 and 3.20 present the averaged data in graphic form. These sections provide good examples of how left and right femurs can have very different form and material properties. The left femoral section has significantly lower acoustic properties with a widely scattered distribution when compared to the right. This significant resorption and reduction in endosteal properties was responsible for the left section shape change relative to the right section. The remodeling of the left is so severe that it demonstrates how, although most of the section has very low properties, a thin section of periosteal bone with very high properties is evident. Figure 3.19 shows how periosteal values were as high as 180 in the left medial specimen, and the right had lower albeit more consistent values.

Figure 3.21 demonstrates the 3D capabilities of the software. Besides producing a small 2D image for orientation, the 3D image provides an image of the real amplitude of the peak signal measured.

The SAM system is very useful for very quickly ascertaining the properties of the bone with unprocessed specimens. The system can determine interpair differences as demonstrated by the four pairs of scans presented. Bone remodeling such as severe endosteal resorption is also quite evident, as is the transition of the properties from periosteal to endosteal bone.

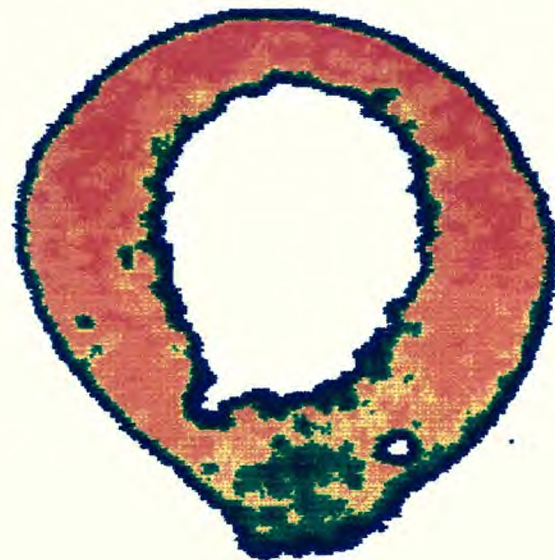
All of these variations can be observed with conventional techniques such as light or backscatter electron microscopy. However, there are two important differences between this technique and conventional techniques. The quantitative acoustic data shows averaged

values over 360° and three regions of every section. Second, and most importantly, Meunier et. al. [29] have demonstrated that the acoustic impedance is directly related to elastic modulus of bone. This is not true for all materials, but because of the composite nature of bone, and the material properties of the constituent materials, a unique correlation between the acoustic impedance and the elastic constant exists. Therefore, the acoustic scans represent a mapping of the elastic properties of the bone on a microscopic scale.

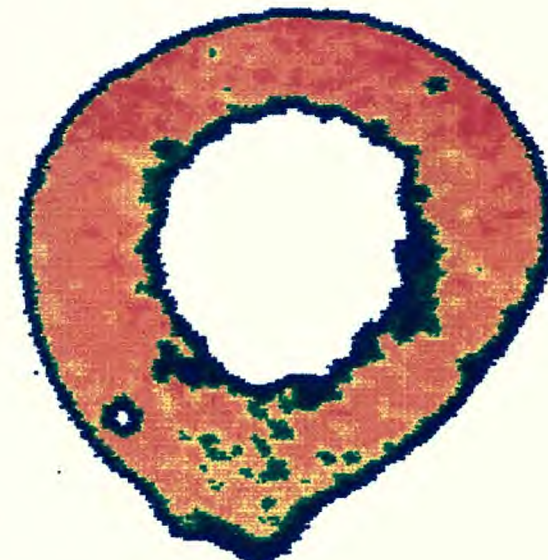
3.5 Mechanical Testing of Human Cadaveric Bone

The mechanical test results for the human bone are provided in Table 13. The mean force to failure for the left femur ring sections was 568.0 N and 594.0 N for the right. There was no statistically significant difference at $p < 0.05$ for the two groups of mechanical test data. Structurally the bones were very similar as evidenced by these results. This particular specimen #2366, was also the specimen with the severe resorption and low impedance properties as measured by the SAM. Although the material properties were very low, the left femur remodelling that included, geometric as well as a reorganization of bone with very high acoustic properties, resulted in a bone with structural properties similar to the right femur. Thus, the patient had a structurally functional bone in spite of severe resorption and remodelling.

Femoral Midshaft SAM Scans



2363 left



2363 right



Age: 75 sex: F

Fig. 3.9

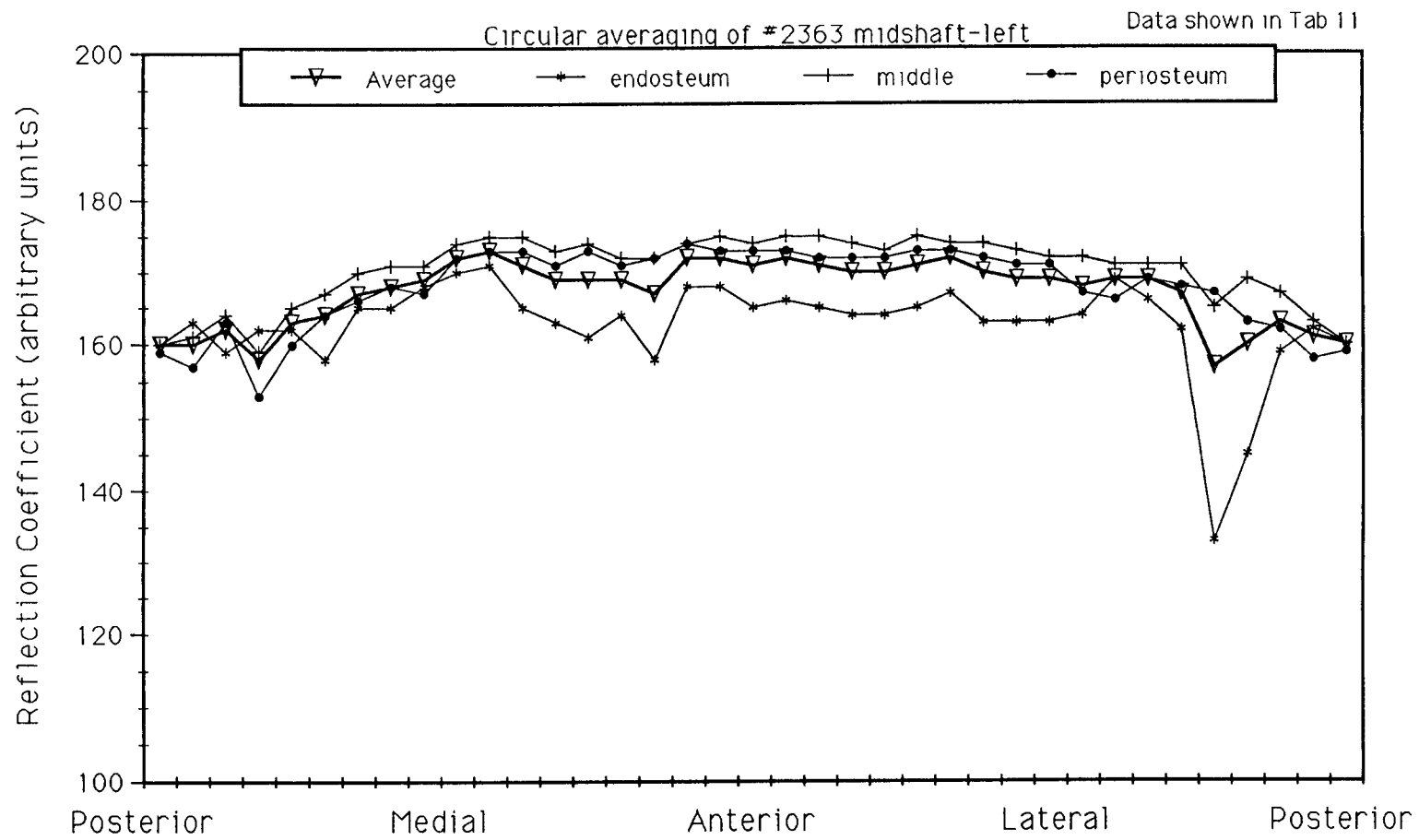


Fig. 3.10: Diagram with results of circular averaging of femur #2363 left

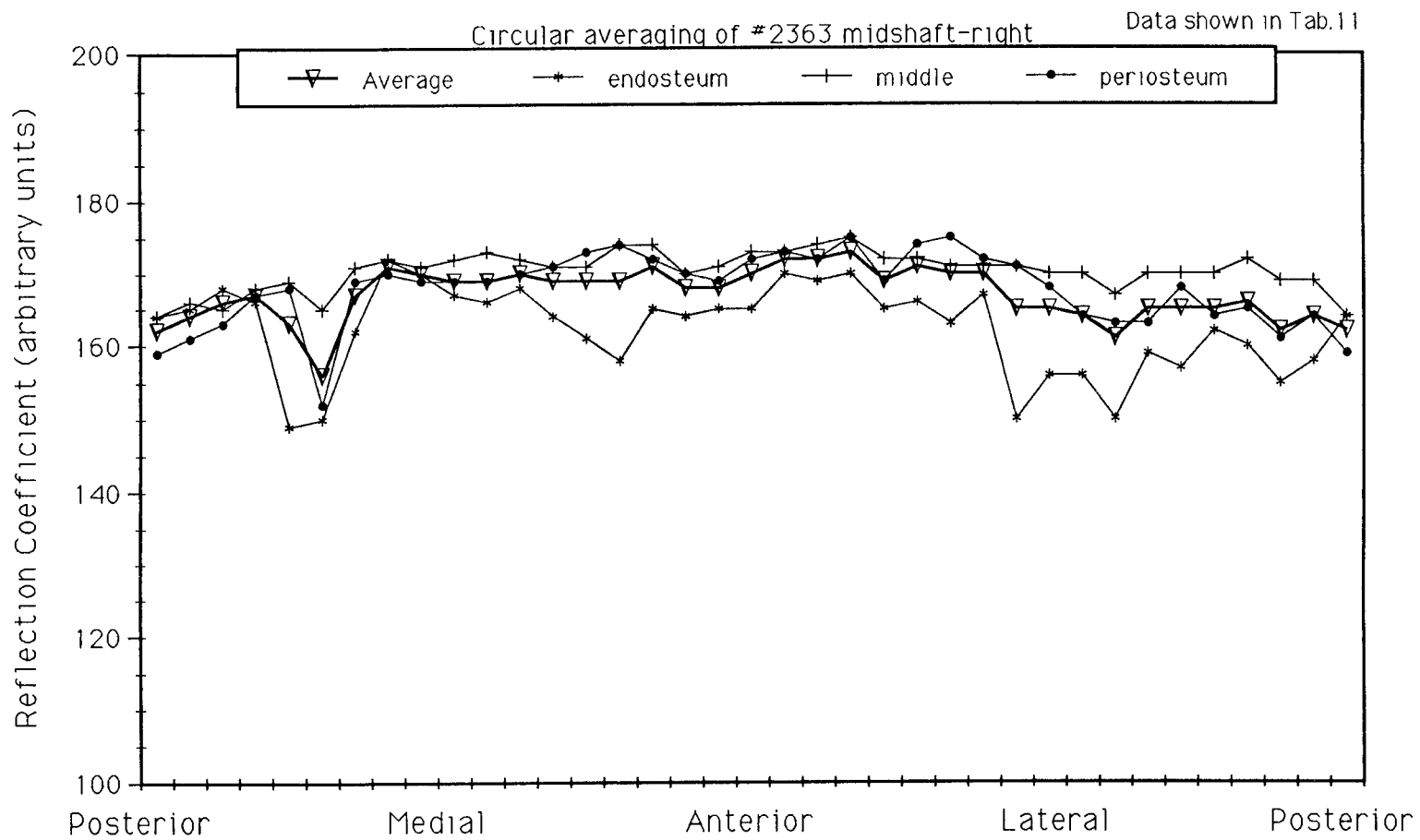
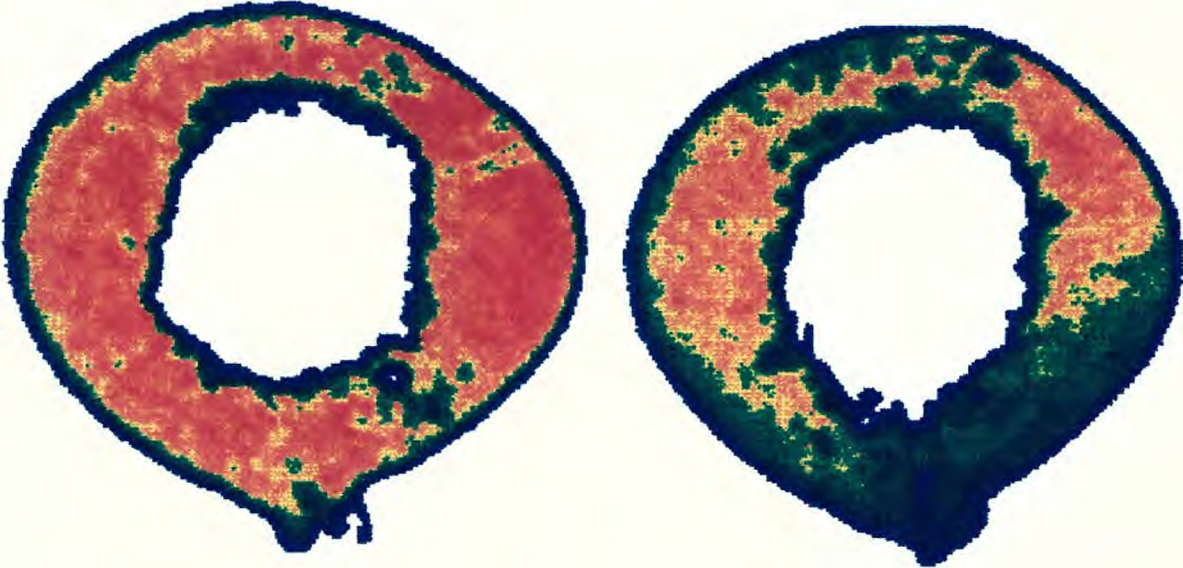


Fig. 3.11: Diagram with results of circular averaging of femur #2363 right

Femoral Midshaft SAM Scans



2329 left

2329 right



Age: 84 sex: M

Fig. 3.12

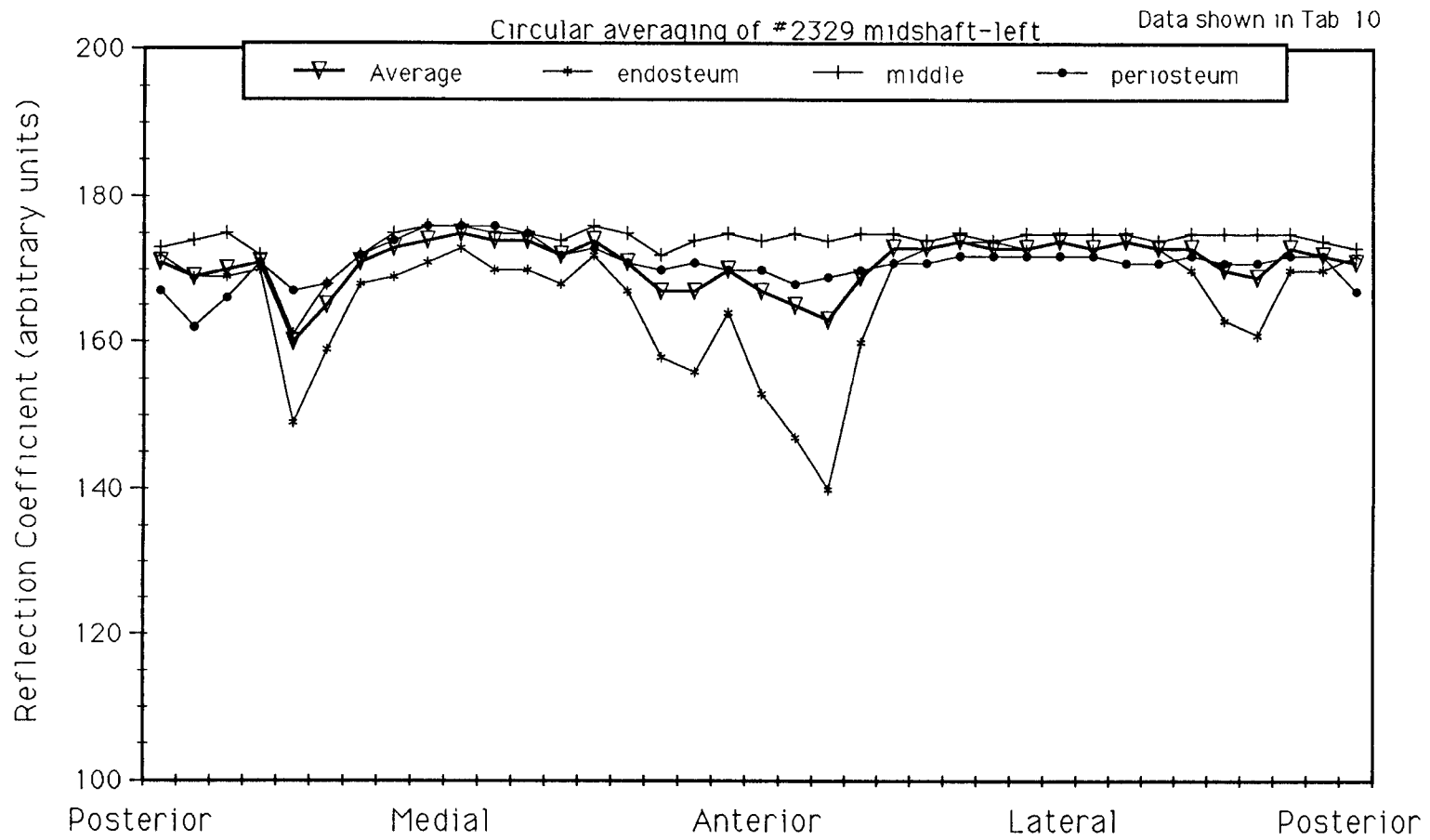


Fig. 3.13: Diagram with results of circular averaging of femur #2329 left

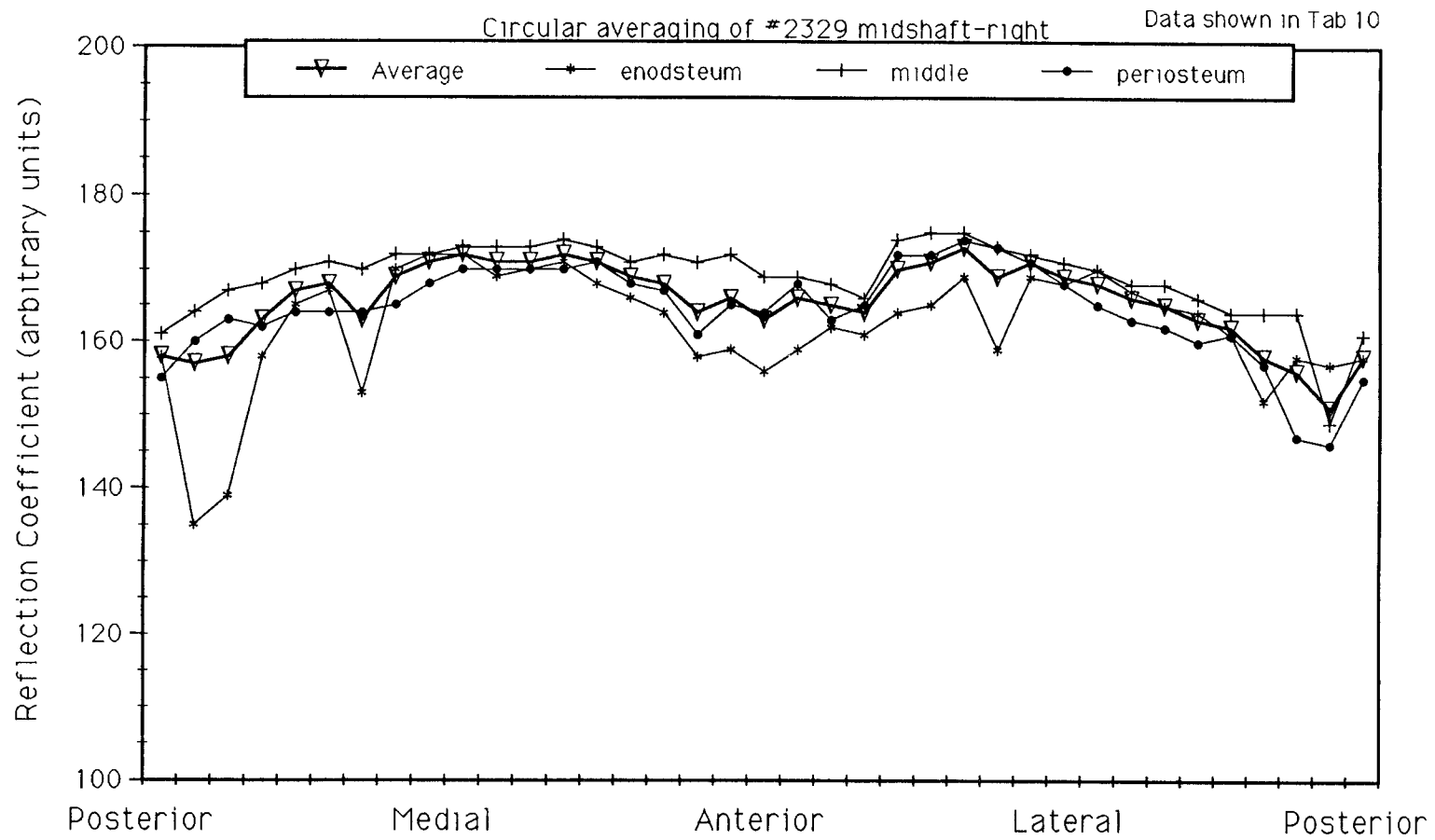
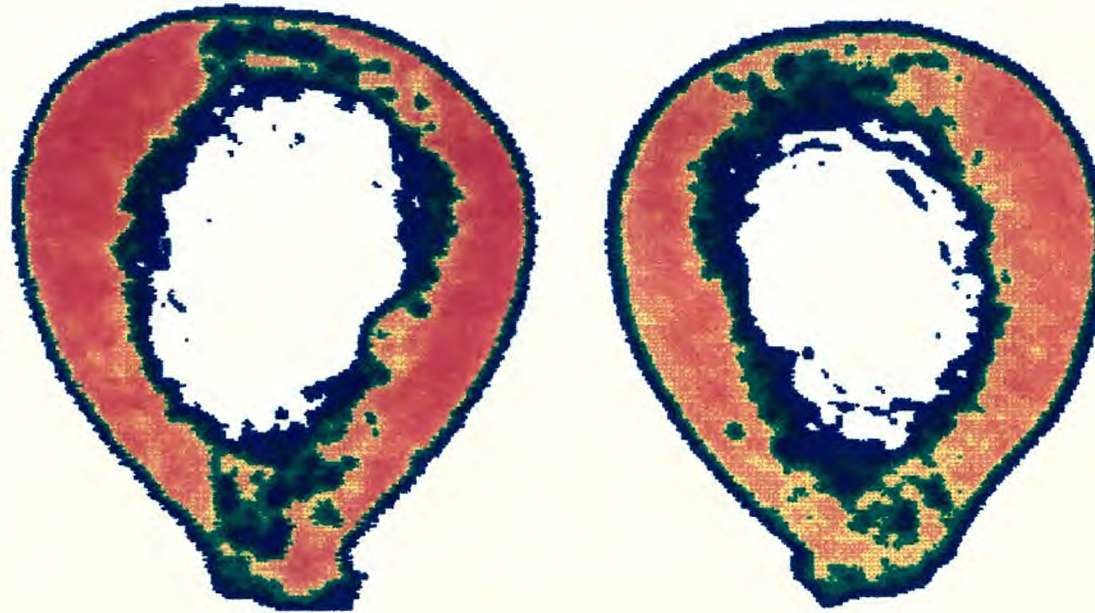


Fig. 3.14: Diagram with results of circular averaging of femur #2329 right

Femoral Midshaft SAM Scans



2326 left

2326 right



Age: 93 sex: F

Fig 3.15

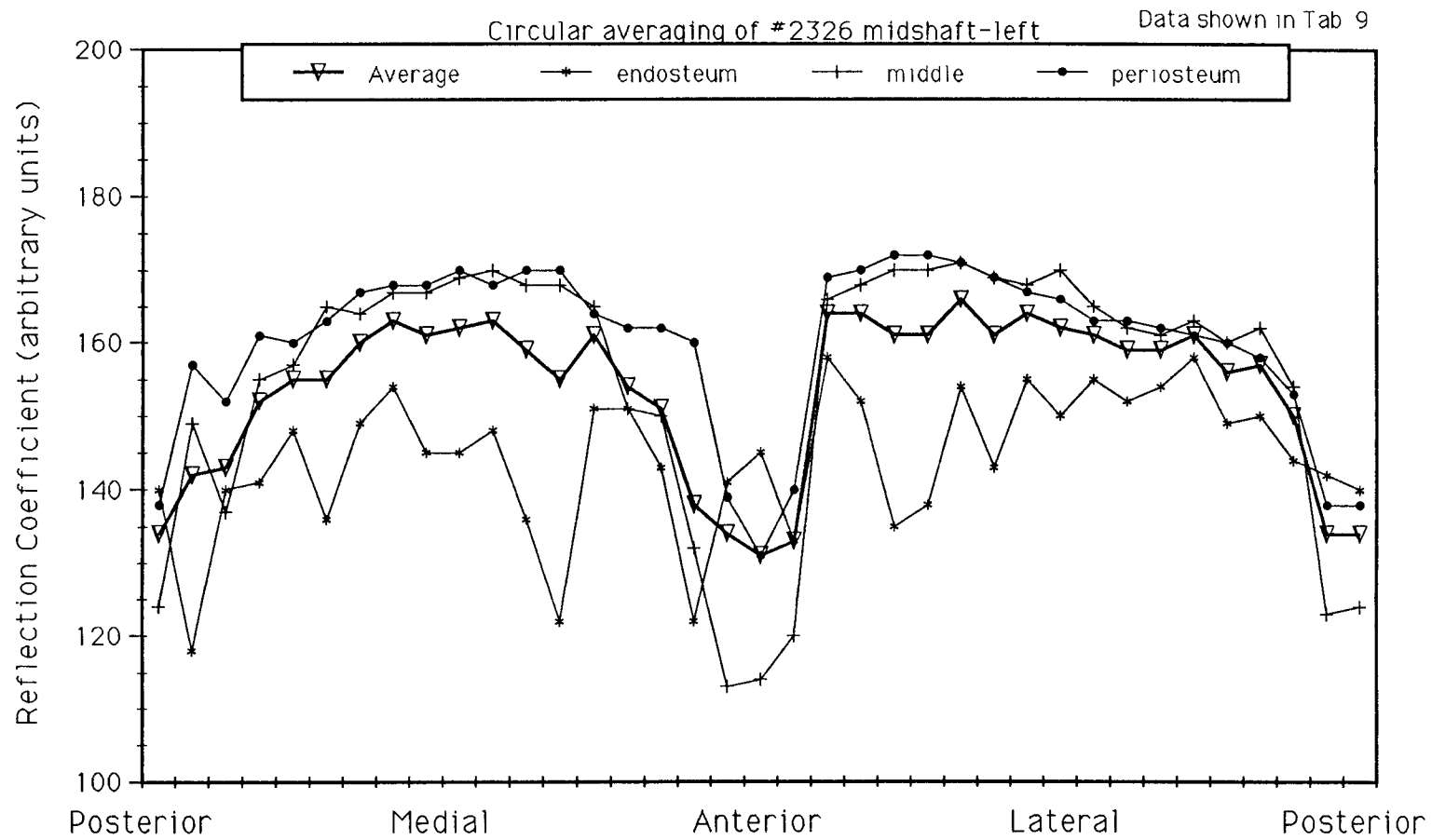


Fig. 3.16: Diagram with results of circular averaging of femur #2326 left

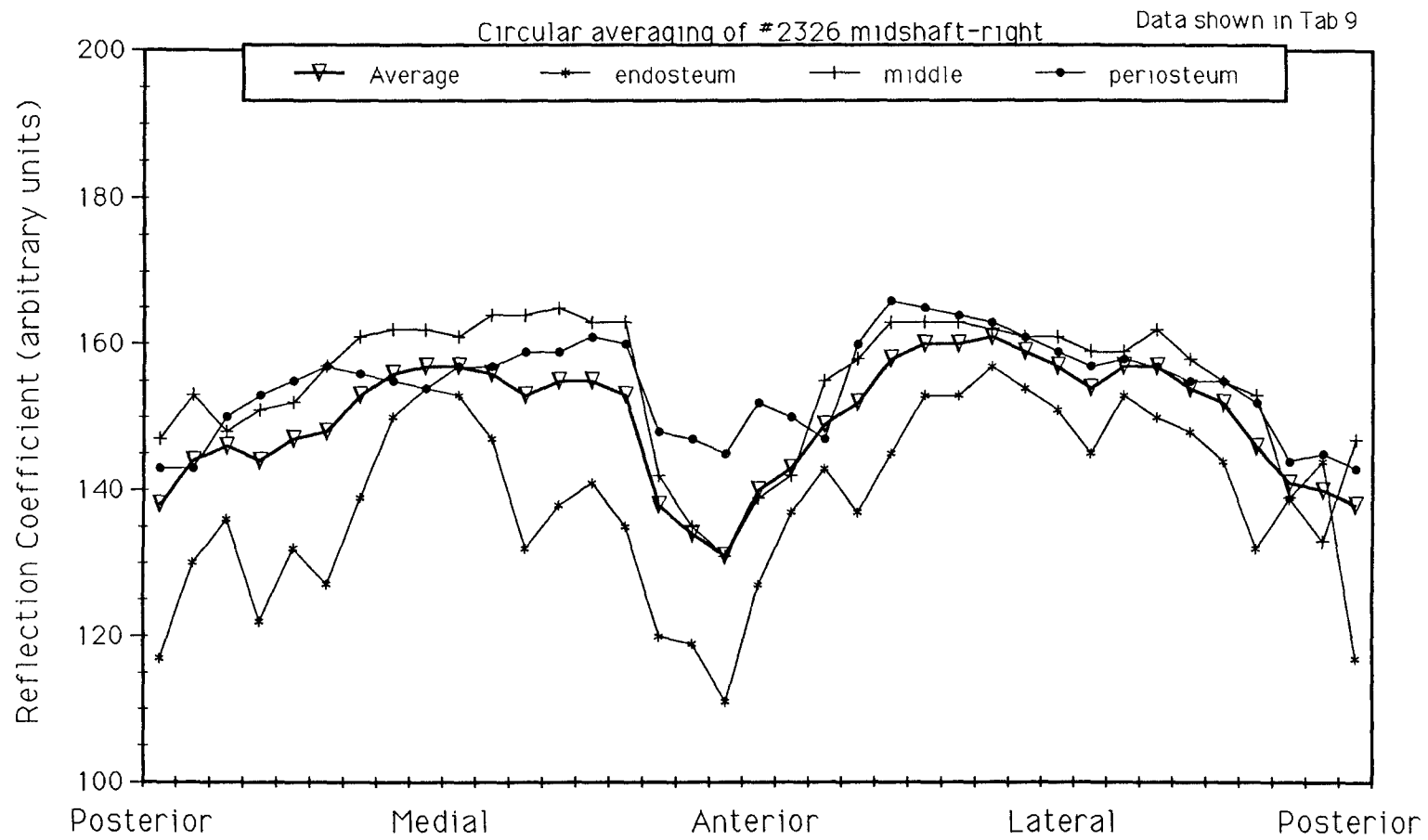
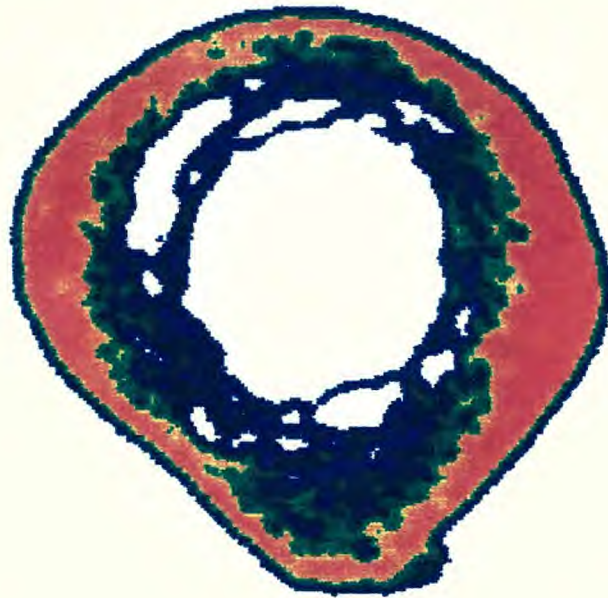
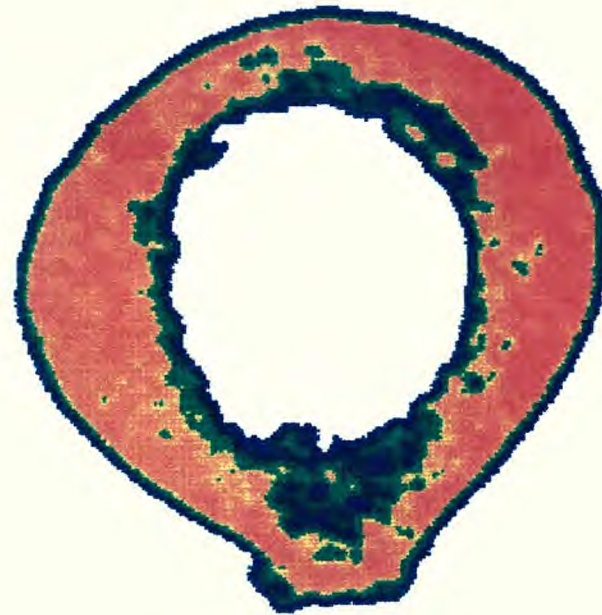


Fig. 3.17: Diagram with results of circular averaging of femur #2326 right

Femoral Midshaft SAM Scans



2366 left



2366 right



Age: 68 sex: F

Fig 3.18

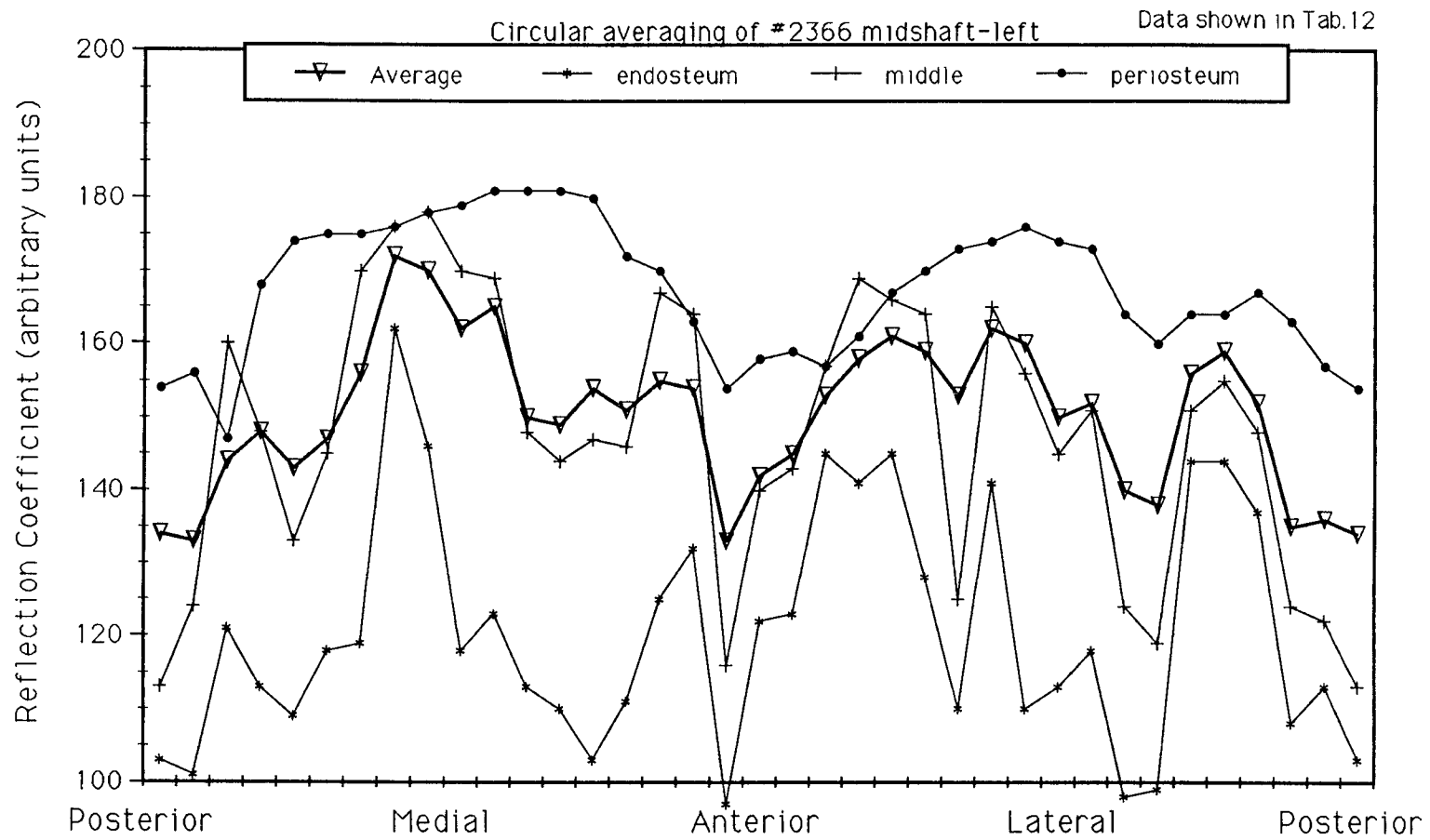


Fig. 3.19: Diagram with results of circular averaging of femur #2366 left

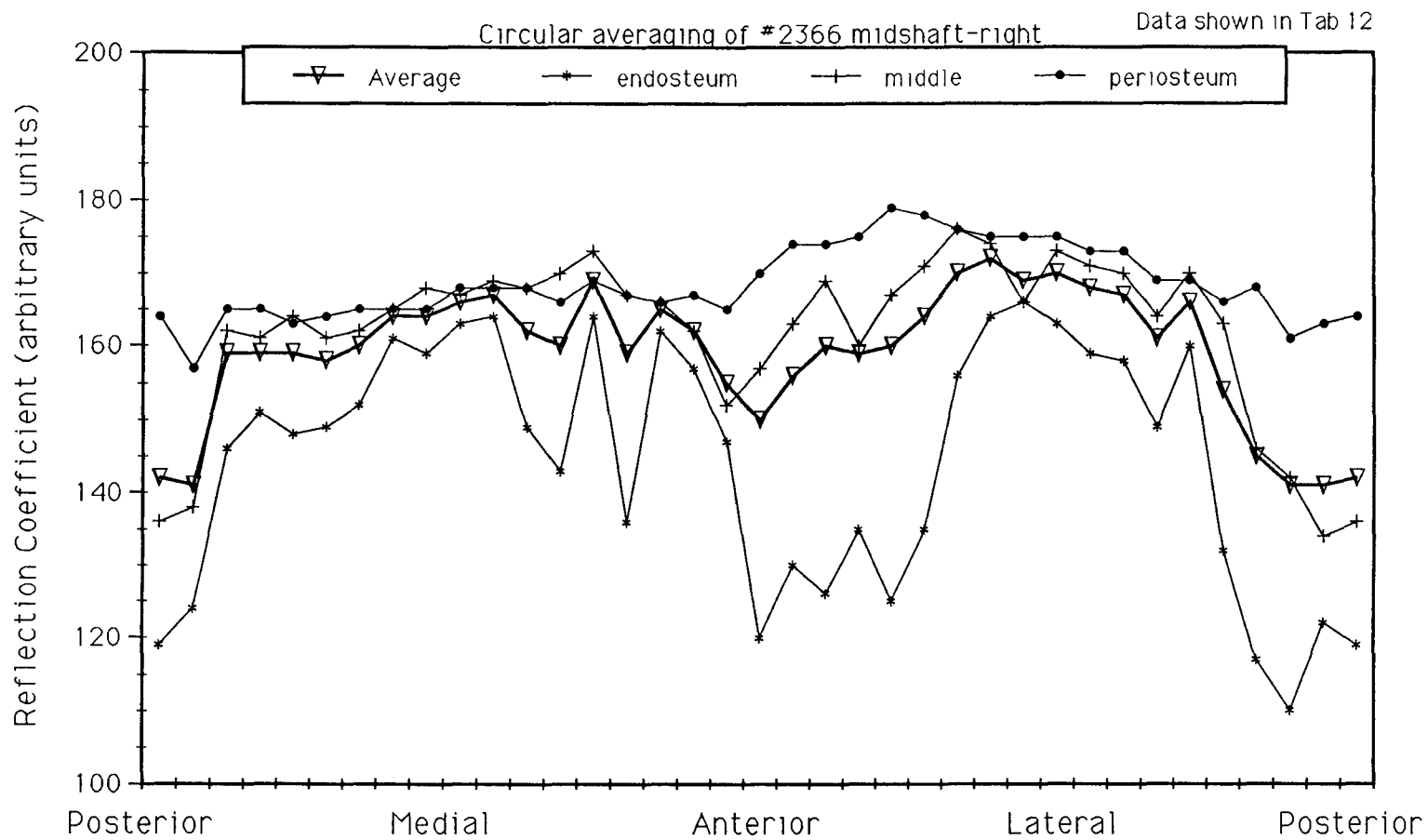
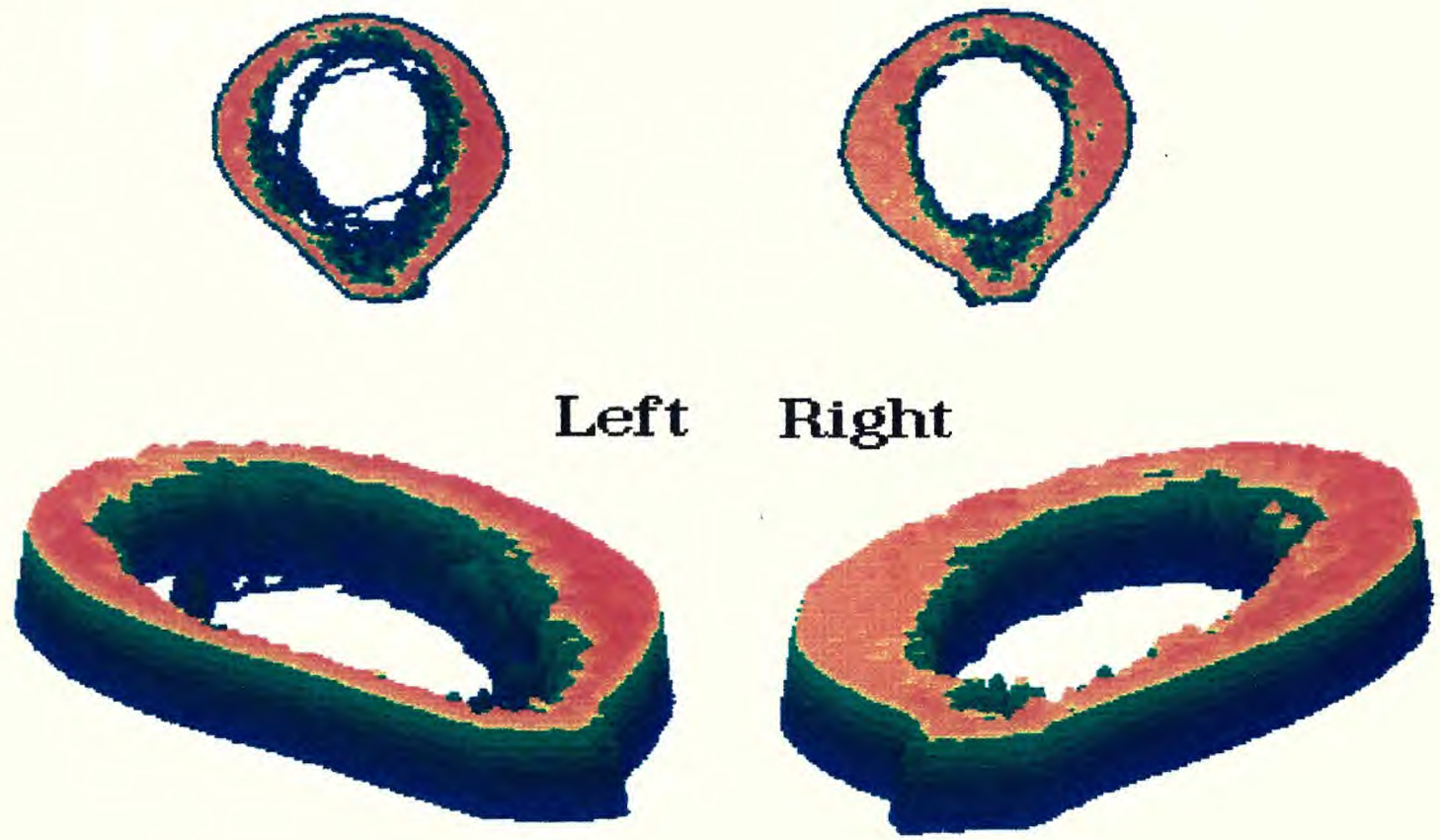


Fig. 3.20: Diagram with results of circular averaging of femur #2366 right



Left

Right

Fig. 3.21: 3-D presentation of Femoral Midshaft SAM image #2366

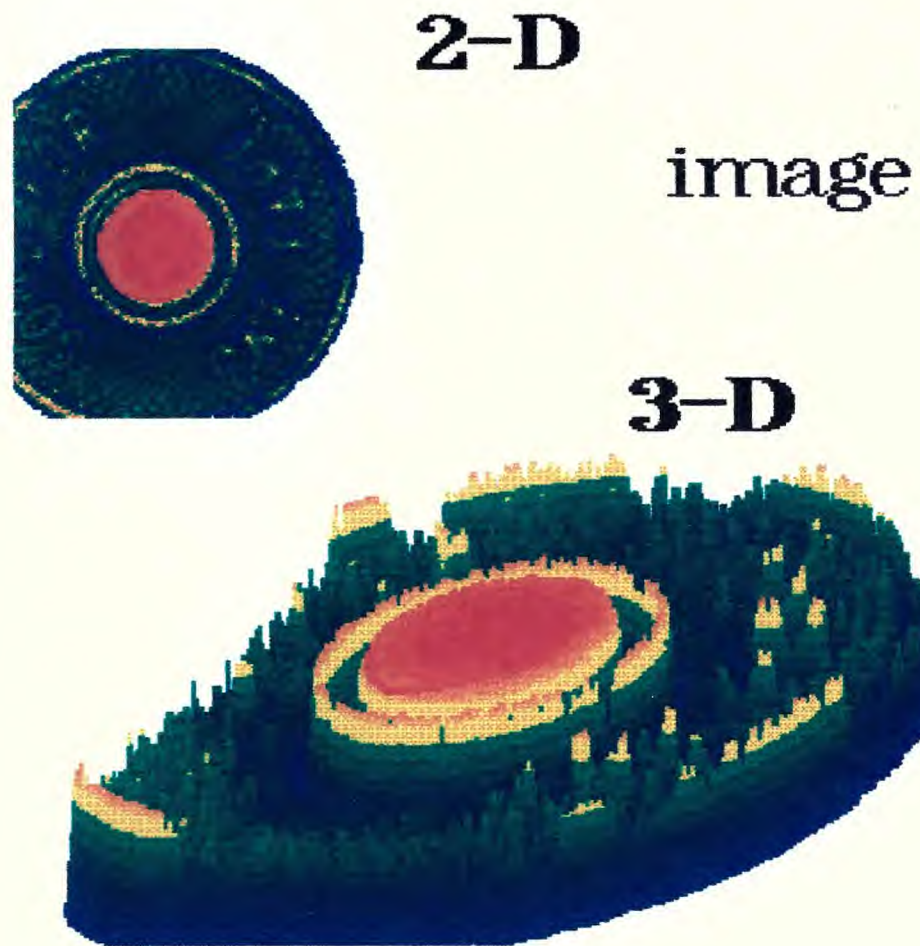


Fig 3.22: Color SAM image of a NYC subway token

4. CONCLUSIONS

The software solution averaging approach was used in the primary testing of the system with a relatively slow data acquisition board. The other software solution approach which includes interpolation of the obtained values has been applied using a faster data acquisition board. In order to improve this method it was necessary to apply different algorithms and change some of the parameters within them. Some of the problems included line shifting (Fig. 2.16), image distortion on the edges (Fig. 2.12), and geometrically incorrect images (Fig. 2.19 and 2.20).

In general, the SAM images of coins show relatively unsharp edges and almost no details regarding small surface features. There are a number of reasons for this. First, coins are not ideal for the determination of resolution. Secondly, the transducer used in the experiments had a small angle and was more suitable for subsurface analysis rather than surface analysis. The edges are not sharp because when the acoustic beam hits the edge or a surface which is not perpendicular to the transducer axis, the beam is reflected in other directions and not straight back to the receiver.

Regarding the femoral section scanning, an experiment is presented demonstrating the efficacy of scanning acoustic microscopy for the study of bone remodelling. Differences between individual pairs as well as the transition of properties between the periosteal and endosteal bone were observed. Circular averaging over the sections as well as the generation of quantitative graphical data was presented. This technique provides a very quick quantitative analysis of the material properties of an unprocessed section of bone.

REFERENCES

1. LEMONS, RA and QUATE, CF: "Acoustic Microscope Scanning Version," *Appl. Phys. Lett.*, **24**, 163, 1974.
2. JIPSON, V and QUATE, CF: "Acoustic Microscopy at Optical Wavelengths," *Appl. Phys. Lett.*, **32**, 789, 1978.
3. GILMORE, RS, JOYNSON, RE, TRZASKOS, CR and YOUNG, JD: "Acoustic Microscopy: Materials Art and Material Science," GE Research and Development Center, Schenectady, NY.
4. KESSLER, LW: "Acoustic Microscopy", In *Metals Handbook*, Volume 17, 9th Edition: Nondestructive Evaluation and Quality Control, ASM International, Materials Park, Ohio, 465-482, 1989.
5. KASAHARA, S, YOSHIDA, K, KUSHIBIKI, J and CHUBACHI, N: "Application of Acoustic Microscopy in Dental Research," In *Acoustical Imaging*, H, Schimizu, N, Chubachi and J-I, Kushibiki (eds.), New York: Plenum Press, 1989, pp. 153-158.
6. BRIGGS, GAD, DAFT, CMW, FAGAN, AF, FIELD, TA, LAWRENCE, CW, MONTOTO, M, PECK, SD, RODRIGUEZ, A and SCRUBY, CB: "Acoustic Microscopy of Old and New Materials," In *Acoustical Imaging*, H, Schimizu, N, Chubachi and J-I, Kushibiki (eds.), New York: Plenum Press, 1989, pp. 1-16.
7. NONAILLARD, B, ROUVAEN, JM and IMOULOUDENE, NE: "Non Destructive Evaluation of Composite Materials Using Acoustic Microscopy," In *Acoustical Imaging*, H, Schimizu, N, Chubachi and J-I, Kushibiki (eds.), New York: Plenum Press, 1989, pp. 111-119.
8. GILMORE, RS, HEWES, RA, THOMAS III, LJ and YOUNG, JD: "Broadband Acoustic Microscopy: Scanned Images with Amplitude and Velocity Information," In *Acoustical Imaging*, H, Schimizu, N, Chubachi and J-I, Kushibiki (eds.), New York: Plenum Press, 1989, pp. 97-110.
9. BREITER-HAHN, J, LITNIEWSKI, J, HILLMANN, K, KRAPOHL, A and ZYLBERBERG, L: "What Can Scanning Acoustic Microscopy Tell About Animal Cells and Tissues?" In *Acoustical Imaging*, H, Schimizu, N, Chubachi and J-I, Kushibiki (eds.), New York: Plenum Press, 1989, pp. 27-38.
10. MEUNIER, A, KATZ, JL, CHRISTEL, P and SEDEL, L: "A Reflection Scanning Acoustic Microscope," *J. Orthop. Res.*, **6**, 770-775, 1988.
11. MARTIN, RB and BURR, DB: "Structure, Function, and Adaptation of Compact Bone," New York: Raven Press, 1989, pp. 57-84.
12. ZIMMERMAN, MC, MEUNIER, A, KATZ, JL and CHRISTEL, P: "The Evaluation of Cortical Bone Remodeling with a New Ultrasonic Technique," *IEEE Transactions on Biomedical Engineering*. Vol. **37**, No. 5, May, 1990, pp. 433-441.

13. ZIMMERMAN, MC, MEUNIER, A, CHRISTEL, PS, KATZ, JD and SEDEL, L: "The Evaluation of Bone Remodeling about Orthopaedic Implants with Ultrasound," *J. Orthop. Res.*, 7:4, 607-611, 1989.
14. REINTHOLSEN, PA: "Image Processing for an Amplitude and Phase Acoustic Microscope," Ph.D. Dissertation, Dept. of Applied Physics, Stanford University, Palo Alto, CA, 1989.
15. GENERAZIO, ER, ROTH, DJ and BAAKLINI, GY: "Imaging Subtle Microstructural Variations in Ceramics With Precision Ultrasonic Velocity and Attenuation Measurements," In *NASA Technical Memorandum 100129*, Cleveland, Ohio, 1987, pp. 1-6.
16. KWONG, LL: "Techniques of Acoustic Microscopy," Ph.D. Dissertation, Dept. of Electrical Engineering, Stanford University, Palo Alto, CA, 1984.
17. ROSENFELD, A and KAK, AC: "Digital Picture Processing," Vol. 1, Chapters 3,4, & 6, Vol. 2, Chapters, 3 & 6, San Diego: Academic Press, Inc., 1982.
18. LI, HU and NEGISHI, K: "Visualization of Ultrasonic Waves Propagating in Scanning Acoustic Microscope," In *Acoustical Imaging*, H, Shimizu, N, Chubachi and J-I, Kushibiki (eds.), New York: Plenum Press, 1989, pp. 79-86.
19. KULIK, A, GREMAUD, G and SATHISH, S: "Continuous Wave Reflection Scanning Acoustic Microscope (SAMCRUM)," In *Acoustical Imaging*, H, Shimizu, N, Chubachi and J-I, Kushibiki (eds.), New York: Plenum Press, 1989, pp. 71-78.
20. FRAZER, JD: "The Design of Efficient Broadband Ultrasonic Transducers," In *G.L. Report No. 2973*, Stanford University, Palo Alto, CA, 1979.
21. TATENTO, H, IWASHITA, Y, KAWANO, K and NOIKURA, T: "Image of Ion Beam Excited Acoustic Microscope of the Teeth," In *Acoustical Imaging*, H, Shimizu, N, Chubachi and J-I, Kushibiki (eds.), New York: Plenum Press, 1989, pp. 167-171.
22. ABENDSCHEIN, W and HYATT, GW: "Ultrasonic and Selected Physical Properties of Bone," *Clin. Orthop.*, 69, 294-301, 1970.
23. COWIN, SC: *Bone Mechanics*, Florida: CRC Press, 1989, pp. 97-127, 253-277.
24. YOON, HS and KATZ, JL: "Ultrasonic Wave Propagation in Human Cortical Bone-I Theoretical Considerations for Hexagonal Symmetry," *J. Biomech.*, 9, 407-412, 1976.
25. SIDNEY, LB: "Ultrasonic Method for Measuring Elastic Coefficients of Bone and Results on Fresh and Dried Bovine Bones," *IEEE Trans. Biomed. Engy*, vol. BME-17, Feb. 1970.
26. VAN BUSKIRK, WC and ASHMAN, RB: "The Elastic Moduli of Bone," In *1981 Biomechanics Symposium*, WC, Burskirk and SL-Y, Wood (eds.), New York: ASME, 1981, pp.131-143.

27. KHURI-YAKUB, BT, REINHOLDTSEN, P, CHOU, C-H, PARENT, P and CINBIS, C: "Amplitude and Phase Acoustic Microscopy and its Application to QNDE," In *Acoustical Imaging*, H, Shimizu, N, Chubachi and J-I, Kushibiki (eds.), New York: Plenum Press, 1989, pp. 173-182.
28. TIETZE, U and SCHENK, CH: "Halbleiter Schaltungstechnik," 9th edition, Berlin: Springer-Verlag, 1989, pp. 232-270.
29. MEUNIER, A: Personal communication.
30. GILMORE, RS: Personal communication.

Appendix A:

Tables of acoustic impedance data from human femoral sections and regarding X-Y table position

Material	Acoustic impedance, 10^6 rayl
Air, vacuum	0
Water	1.5
Plastic	2.0-3.5
Bone (human)	9-12
Glass	15
Aluminum.....	17
Silicon.....	20
Beryllia.....	32
Copper	42
Alumina	21-45
Tungsten	104

Table 1. Ranges of acoustic impedance.

Tab.2: stp# 1000 TimeDif=6.64 ms R=250 S=2 F=20																			
2	5	7	9	11	14	16	19	21	24	26	29	31	34	37	40	43	46	49	52
55	59	62	66	70	74	78	82	87	92	98	104	111	119	128	137	146	154	163	172
180	189	198	206	215	224	232	241	250	258	267	276	284	293	302	310	319	328	336	345
354	362	371	380	389	397	406	414	423	432	441	449	458	466	475	484	493	501	510	519
527	536	545	554	562	571	580	588	597	606	614	623	632	640	649	658	666	675	684	692
701	710	718	727	736	744	753	762	770	779	788	797	805	814	822	831	840	849	857	866
874	883	891	898	904	909	914	919	923	927	931	935	939	942	946	949	952	955	958	961
964	966	969	972	974	977	979	982	984	987	989	991	994	996	998	999				

Tab. 2: X-Y table positions with: R = 250; S = 2; F = 20; N = 1000

Tab. 3: stp# 1000 TimeDif=6.66 ms R=252 S=2 F=20																			
2	5	8	10	12	15	18	20	23	26	28	31	34	37	40	43	46	50	53	57
61	65	69	73	78	83	88	94	101	109	119	130	142	153	164	175	186	197	208	219
230	242	252	263	274	286	297	308	319	330	341	352	363	374	385	396	407	418	430	441
451	462	474	485	496	507	518	529	540	551	562	573	584	596	606	618	629	640	651	662
673	684	695	706	717	728	739	750	762	773	784	795	806	817	828	839	850	861	872	883
893	901	907	913	918	923	928	932	936	940	944	947	951	954	958	961	964	967	970	972
975	978	981	983	986	988	990	993	995	998	999									

Tab. 3: X-Y table positions with: R = 252; S = 2; F = 20; N = 1000

Tab.4: stp# 1000 TimeDif=6.62 ms R=254 S=2 F=20																			
3	6	8	10	13	16	18	21	24	27	30	33	36	39	43	46	50	54	58	62
66	70	76	81	87	94	102	111	125	141	157	172	187	202	218	233	248	263	278	294
309	324	340	355	370	386	401	416	431	446	462	477	492	507	523	538	553	569	584	599
614	630	645	660	675	690	706	721	736	752	767	782	798	813	828	843	858	874	889	898
906	913	919	925	930	934	939	943	947	950	954	958	961	964	967	970	974	977	979	982
985	987	990	993	995	998	999	999												

Tab. 4: X-Y table positions with: R = 254; S = 2; F = 20; N = 1000

Tab. 5: stp# 1000 TimeDif=6.59 ms R=254 S=1 F=20																			
2	5	8	10	13	15	18	20	23	25	28	30	33	36	38	41	44	47	50	53
56	58	62	65	68	71	74	77	81	84	87	91	94	98	102	105	109	113	117	121
126	130	134	139	144	149	154	159	165	171	177	184	191	198	207	217	228	242	258	273
288	304	319	334	350	365	380	395	410	426	441	456	472	487	502	517	533	548	563	578
594	609	624	639	655	670	685	701	716	731	746	762	776	786	796	804	812	819	825	831
837	843	848	853	858	863	867	872	876	880	884	889	892	896	900	904	907	911	914	918
921	924	927	930	934	937	940	943	946	949	952	954	957	960	963	966	968	971	974	976
979	981	984	986	989	991	994	996	999	999										

Tab. 5: X-Y table positions with: R = 254; S = 1; F = 20; N = 1000

Tab. 6: stp# 500 TimeDif=6.39 ms R=252 S=1 F=30																			
2	5	7	10	12	14	17	19	22	24	26	29	31	34	37	39	42	44	47	50
53	55	58	61	64	67	70	73	76	79	82	85	88	91	95	98	102	105	109	112
116	120	123	127	131	136	140	144	149	154	158	163	168	174	179	186	192	198	206	214
222	232	241	251	260	270	279	288	295	302	309	315	321	327	332	337	342	347	352	356
361	365	369	373	377	381	384	388	392	395	398	402	405	409	412	415	418	421	424	427
430	433	436	439	442	445	447	450	453	455	458	461	463	466	468	471	473	476	478	481
483	486	488	490	493	495	497	499	499											

Tab. 6: X-Y table positions with: R = 252; S = 1; F = 30; N = 500

Tab. 7: stp# 500 TimeDif=6.33 R=252 S=2 F=20																			
2	5	8	10	12	15	18	20	23	26	28	31	34	37	40	43	46	50	53	57
61	65	69	73	78	83	88	94	101	109	119	131	142	153	164	175	186	197	208	219
230	241	252	263	274	286	297	308	319	330	341	352	363	374	385	394	402	408	414	419
424	429	433	437	441	445	448	451	455	458	461	464	467	470	473	475	478	481	483	486
488	491	493	495	498	500	499													

Tab. 7: X-Y table positions with: R = 252; S = 2; F = 20; N = 500

Tab. 7: stp# 500 TimeDif=6.52 ms R=254 S=1 F=30																				
2	5	8	10	13	15	18	20	23	25	28	30	33	36	39	41	44	47	50	53	
56	59	62	65	68	71	74	77	81	84	87	91	94	98	102	106	109	113	117	122	
126	130	134	139	144	149	154	159	165	171	177	184	191	199	207	217	228	241	253	266	
278	289	298	306	313	320	327	333	338	344	349	354	359	364	369	373	377	381	386	390	
393	397	401	405	408	412	415	418	422	425	428	431	434	438	441	444	446	449	452	455	
458	461	463	466	469	471	474	477	479	482	484	487	489	492	494	497	499	499			

Tab. 8: X-Y table positions with: R = 254; S = 1; F = 30; N = 500

Degrees	av2326	endl-m	medl-m	perl-m	av2326	endr-m	medr-m	perr-m
10	134	140	124	138	138	117	147	143
20	134	142	123	138	144	130	153	143
30	150	144	154	153	146	136	148	150
40	157	150	162	158	144	122	151	153
50	156	149	160	160	147	132	152	155
60	161	158	163	161	148	127	157	157
70	159	154	161	162	153	139	161	156
80	159	152	162	163	156	150	162	155
90	161	155	165	163	157	154	162	154
100	162	150	170	166	157	153	161	157
110	164	155	168	167	156	147	164	157
120	161	143	169	169	153	132	164	159
130	166	154	171	171	155	138	165	159
140	161	138	170	172	155	141	163	161
150	161	135	170	172	153	135	163	160
160	164	152	168	170	138	120	142	148
170	164	158	166	169	134	119	135	147
180	133	133	120	140	131	111	131	145
190	131	145	114	131	140	127	139	152
200	134	141	113	139	143	137	142	150
210	138	122	132	160	149	143	155	147
220	151	143	150	162	152	137	158	160
230	154	151	151	162	158	145	163	166
240	161	151	165	164	160	153	163	165
250	155	122	168	170	160	153	163	164
260	159	136	168	170	161	157	162	163
270	163	148	170	168	159	154	161	161
280	162	145	169	170	157	151	161	159
290	161	145	167	168	154	145	159	157
300	163	154	167	168	157	153	159	158
310	160	149	164	167	157	150	162	157
320	155	136	165	163	154	148	158	155
330	155	148	157	160	152	144	155	155
340	152	141	155	161	146	132	153	152
350	143	140	137	152	141	139	139	144
360	142	118	149	157	140	144	133	145

Tab. 9: Results of circular averaging of femur #2326 - left and right

Degree	av2329	endl-m	medl-m	perl-m	av2329	endr-m	medr-m	perr-m
10	171	172	173	167	158	158	161	155
20	172	170	174	172	157	135	164	160
30	173	170	175	172	158	139	167	163
40	169	161	175	171	163	158	168	162
50	170	163	175	171	167	165	170	164
60	173	170	175	172	168	167	171	164
70	173	173	174	171	163	153	170	164
80	174	174	175	171	169	170	172	165
90	173	173	175	172	171	172	172	168
100	174	174	175	172	172	172	173	170
110	173	173	175	172	171	169	173	170
120	173	174	174	172	171	170	173	170
130	174	174	175	172	172	171	174	170
140	173	173	174	171	171	168	173	171
150	173	171	175	171	169	166	171	168
160	169	160	175	170	168	164	172	167
170	163	140	174	169	164	158	171	161
180	165	147	175	168	166	159	172	165
190	167	153	174	170	163	156	169	164
200	170	164	175	170	166	159	169	168
210	167	156	174	171	165	162	168	163
220	167	158	172	170	164	161	166	165
230	171	167	175	171	170	164	174	172
240	174	172	176	173	171	165	175	172
250	172	168	174	172	173	169	175	174
260	174	170	175	175	169	159	173	173
270	174	170	175	176	171	169	172	171
280	175	173	176	176	169	168	171	168
290	174	171	176	176	168	170	170	165
300	173	169	175	174	166	167	168	163
310	171	168	172	172	165	165	168	162
320	165	159	168	168	163	164	166	160
330	160	149	161	167	162	161	164	161
340	171	170	172	171	158	152	164	157
350	170	169	175	166	156	158	164	147
360	169	169	174	162	151	157	149	146

Tab. 10: Results of circular averaging of femur #2329 - left and right

Degree	av2363	endl-m	medl-m	perl-m	av2363	endr-m	medr-m	perr-m
10	160	160	160	159	162	164	164	159
20	161	162	163	158	164	165	166	161
30	163	159	167	162	166	168	165	163
40	160	145	169	163	167	166	168	167
50	157	133	165	167	163	149	169	168
60	167	162	171	168	156	150	165	152
70	169	166	171	169	167	162	171	169
80	169	169	171	166	171	172	172	170
90	168	164	172	167	170	170	171	169
100	169	163	172	171	169	167	172	169
110	169	163	173	171	169	166	173	169
120	170	163	174	172	170	168	172	170
130	172	167	174	173	169	164	171	171
140	171	165	175	173	169	161	171	173
150	170	164	173	172	169	158	174	174
160	170	164	174	172	171	165	174	172
170	171	165	175	172	168	164	170	170
180	172	166	175	173	168	165	171	169
190	171	165	174	173	170	165	173	172
200	172	168	175	173	172	170	173	173
210	172	168	174	174	172	169	174	172
220	167	158	172	172	173	170	175	175
230	169	164	172	171	169	165	172	169
240	169	161	174	173	171	166	172	174
250	169	163	173	171	170	163	171	175
260	171	165	175	173	170	167	171	172
270	173	171	175	173	165	150	171	171
280	172	170	174	172	165	156	170	168
290	169	168	171	167	164	156	170	164
300	168	165	171	168	161	150	167	163
310	167	165	170	166	165	159	170	163
320	164	158	167	164	165	157	170	168
330	163	162	165	160	165	162	170	164
340	158	162	159	153	166	160	172	165
350	162	159	164	163	162	155	169	161
360	160	163	161	157	164	158	169	164

Tab. 11: Results of circular averaging of femur #2363 - left and right

Degree	av2366	endl-m	medl-m	perl-m	av2366	endr-m	medr-m	perr-m
10	134	103	113	154	142	119	136	164
20	136	113	122	157	141	124	138	157
30	135	108	124	163	159	146	162	165
40	152	137	148	167	159	151	161	165
50	159	144	155	164	159	148	164	163
60	156	144	151	164	158	149	161	164
70	138	99	119	160	160	152	162	165
80	140	98	124	164	164	161	165	165
90	152	118	151	173	164	159	168	165
100	150	113	145	174	166	163	167	168
110	160	110	156	176	167	164	169	168
120	162	141	165	174	162	149	168	168
130	153	110	125	173	160	143	170	166
140	159	128	164	170	169	164	173	169
150	161	145	166	167	159	136	167	167
160	158	141	169	161	165	162	166	166
170	153	145	157	157	162	157	162	167
180	145	123	143	159	155	147	152	165
190	142	122	140	158	150	120	157	170
200	133	97	116	154	156	130	163	174
210	154	132	164	163	160	126	169	174
220	155	125	167	170	159	135	160	175
230	151	111	146	172	160	125	167	179
240	154	103	147	180	164	135	171	178
250	149	110	144	181	170	156	176	176
260	150	113	148	181	172	164	174	175
270	165	123	169	181	169	166	166	175
280	162	118	170	179	170	163	173	175
290	170	146	178	178	168	159	171	173
300	172	162	176	176	167	158	170	173
310	156	119	170	175	161	149	164	169
320	147	118	145	175	166	160	170	169
330	143	109	133	174	154	132	163	166
340	148	113	148	168	145	117	146	168
350	144	121	160	147	141	110	142	161
360	133	101	124	156	141	122	134	163

Tab. 12: Results of circular averaging of femur #2366 - left and right

#2366 FEMORAL CROSS SECTIONS

SAMPLE		MAXIMUM LOAD (N)	STROKE AT MAX. LOAD (mm)
PROXIMAL	RIGHT #2	550.00	0.75
	RIGHT #3	525.00	0.80
	RIGHT #4	850.00	0.88
	RIGHT #5	750.00	0.59
	RIGHT #6	875.00	0.60
	MEAN SD	710.00 164.51	0.72 0.13
PROXIMAL	LEFT #2	600.00	0.98
	LEFT #3	600.00	0.98
	LEFT #4	600.00	1.19
	LEFT #5	725.00	0.95
	LEFT #6	813.00	1.28
	MEAN SD	667.60 97.65	1.08 0.15
DISTAL	RIGHT #1	613.00	0.75
	RIGHT #2	440.00	0.83
	RIGHT #4	380.00	0.88
	RIGHT #5	363.00	1.10
	MEAN SD	449.00 114.21	0.89 0.15
DISTAL	LEFT #1	505.00	0.70
	LEFT #2	470.00	0.83
	LEFT #4	435.00	0.83
	LEFT #5	365.00	1.23
	MEAN SD	443.75 59.77	0.90 0.23
RIGHT MEAN		594.00	0.80
RIGHT SD		193.25	0.16
LEFT MEAN		568.11	1.00
LEFT SD		141.52	0.20

Tab. 13. Maximum load (N) and stroke load (mm) prior to fracture for #2366 femoral cross section

Appendix B:

Graphic presentation of data regarding X-Y table
position

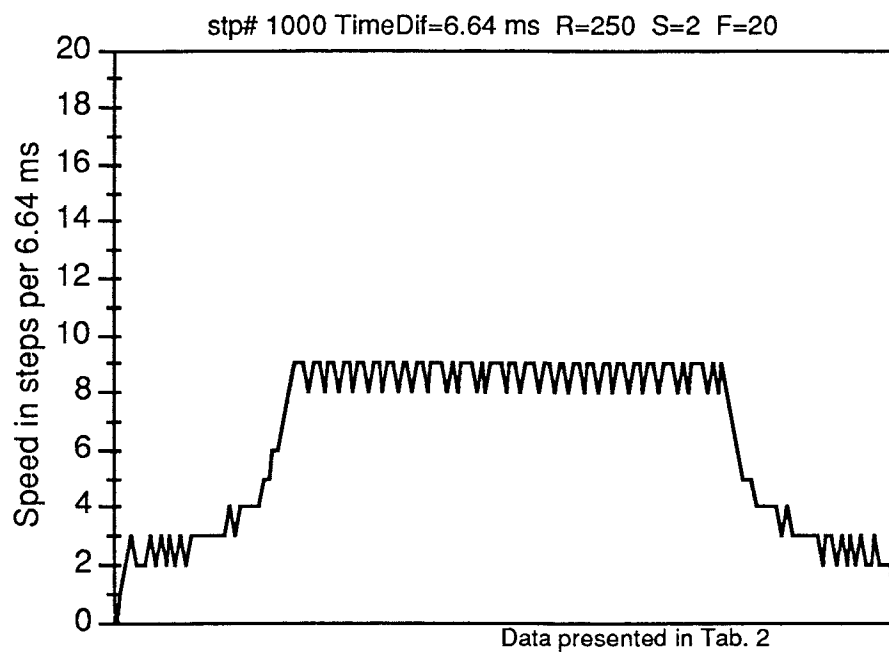


Fig. D1: Velocity-Time (V-T) diagram with parameters: R250;S2;F20;N1000

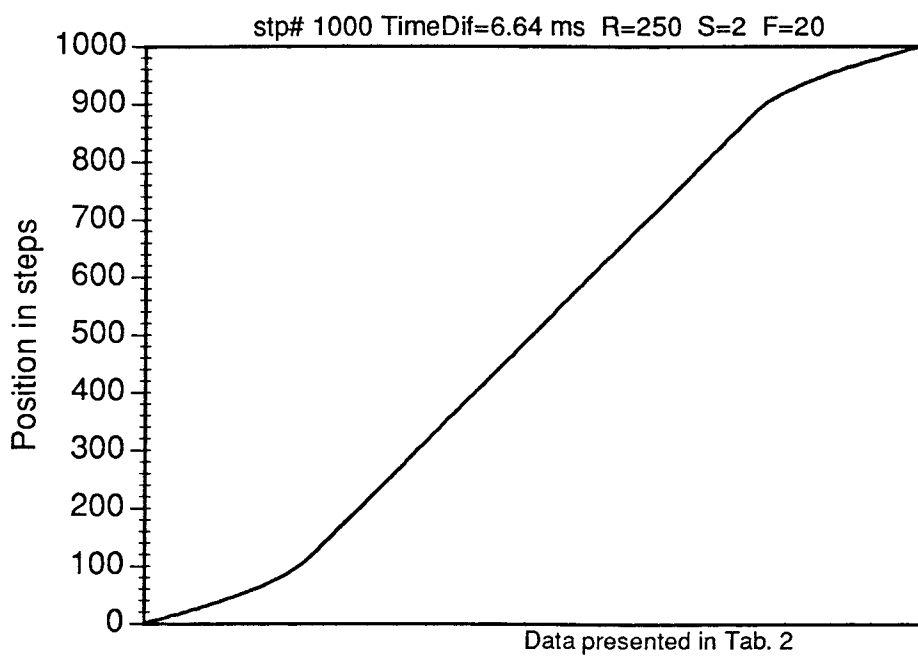


Fig. D2: Position-Time (S-T) diagram with parameters: R250;S2;F20;N1000

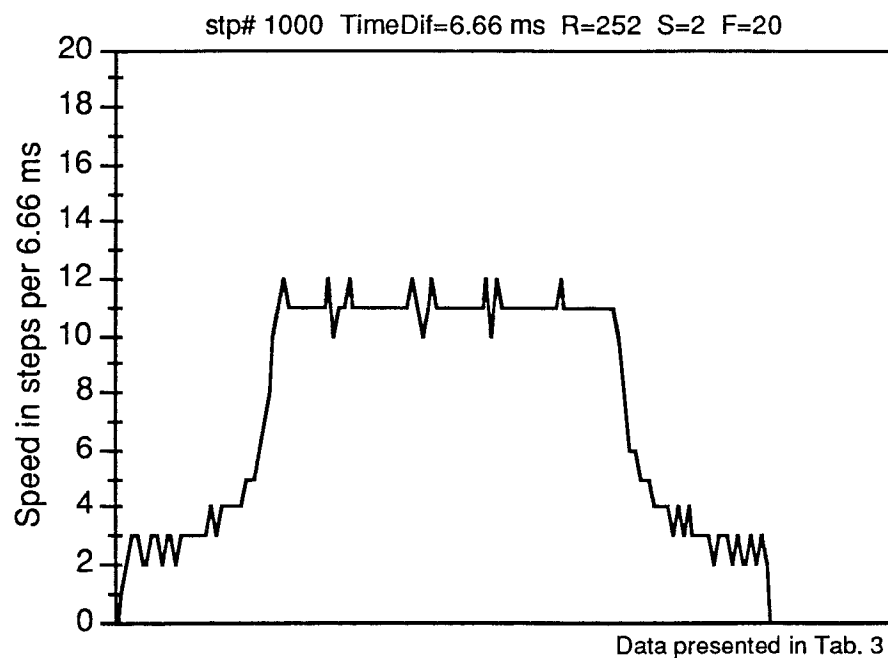


Fig. D3: Velocity-Time (V-T) diagram with parameters: R252;S2;F20;N1000

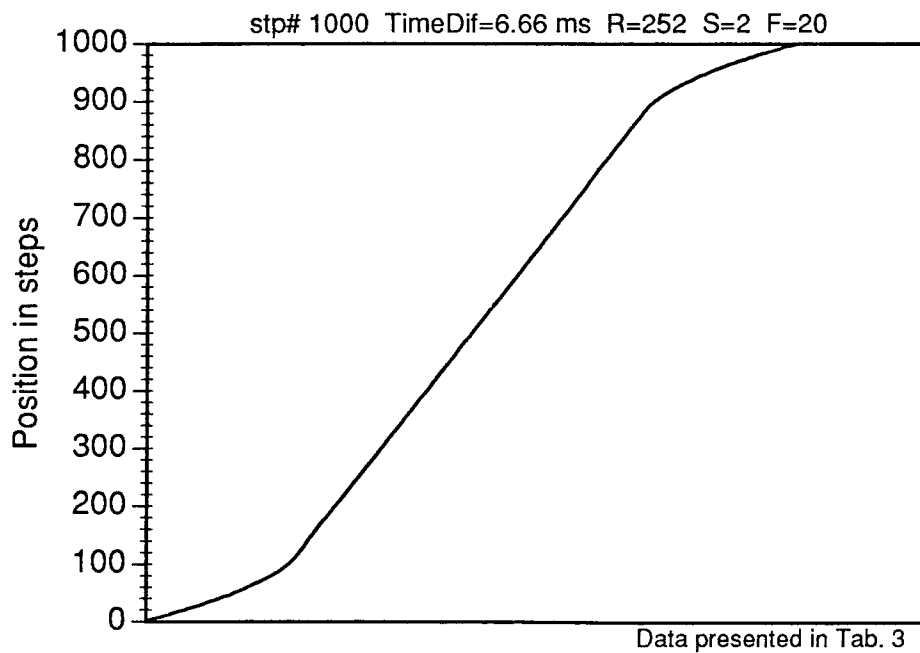


Fig. D4: Position-Time (S-T) diagram with parameters: R252;S2;F20;N1000

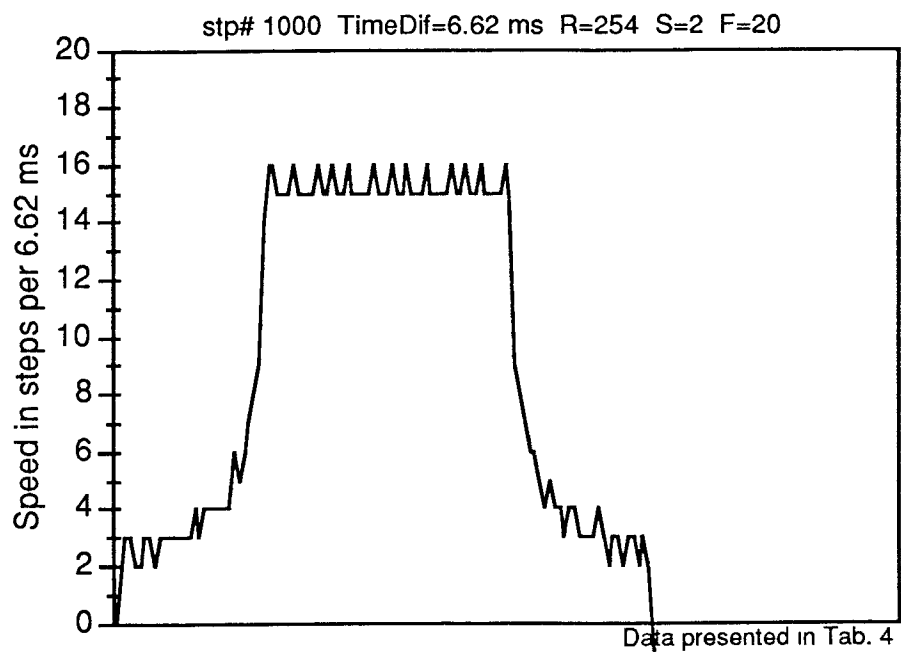


Fig. D5: Velocity-Time (V-T) diagram with parameters: R254;S2;F20;N1000

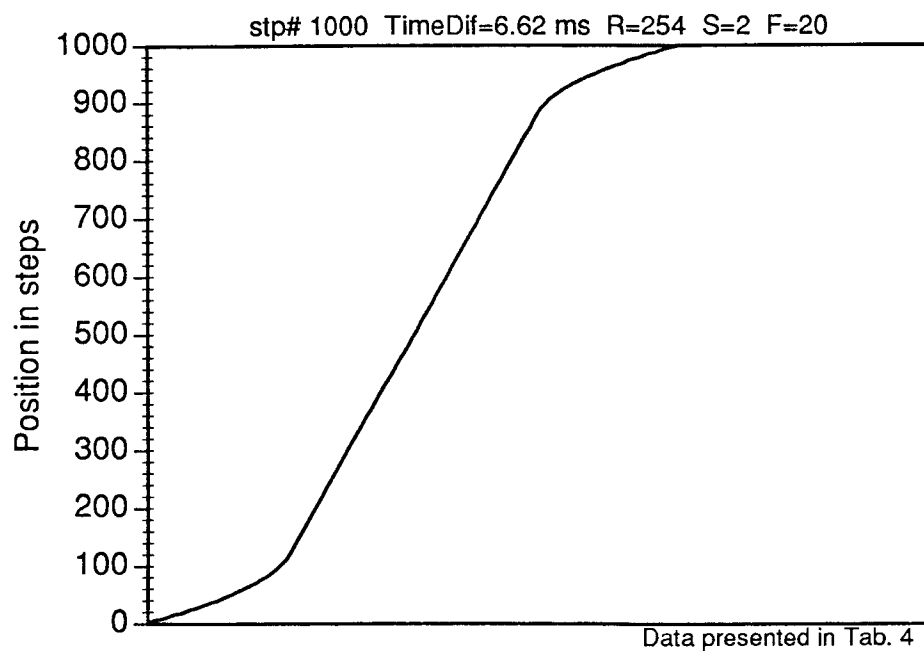


Fig. D6: Position-Time (S-T) diagram with parameters: R254;S2;F20;N1000

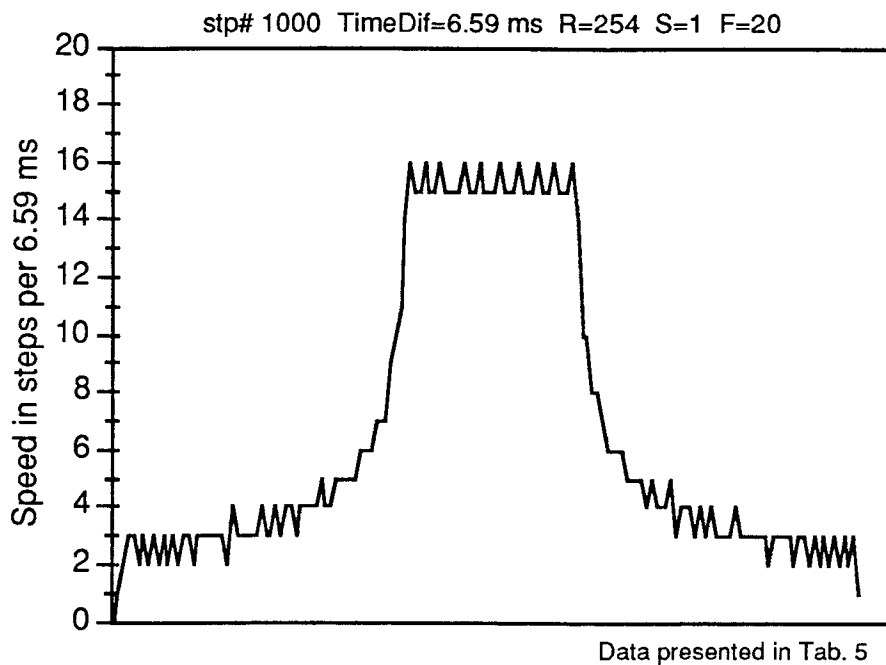


Fig. D7: Velocity-Time (V-T) diagram with parameters: R254;S1;F20;N1000

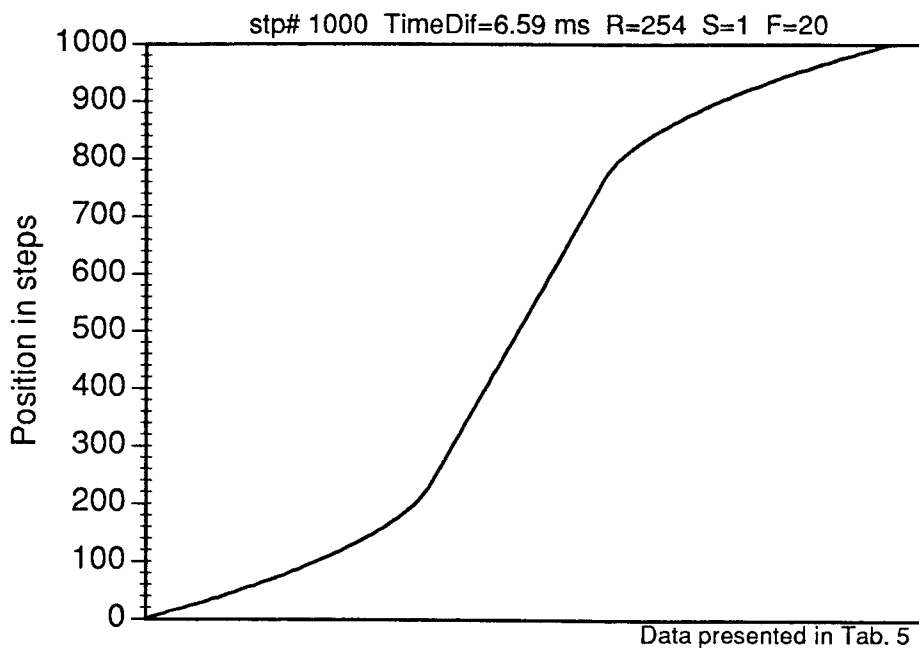


Fig. D8: Position-Time (S-T) diagram with parameters: R254;S1;F20;N1000

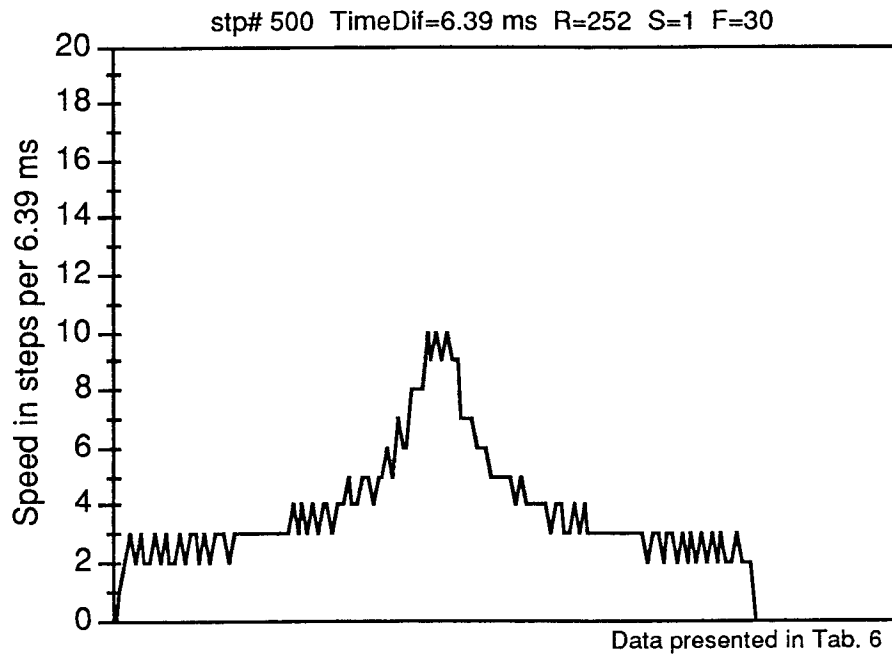


Fig. D9: Velocity-Time (V-T) diagram with parameters: R252;S1;F30;N500

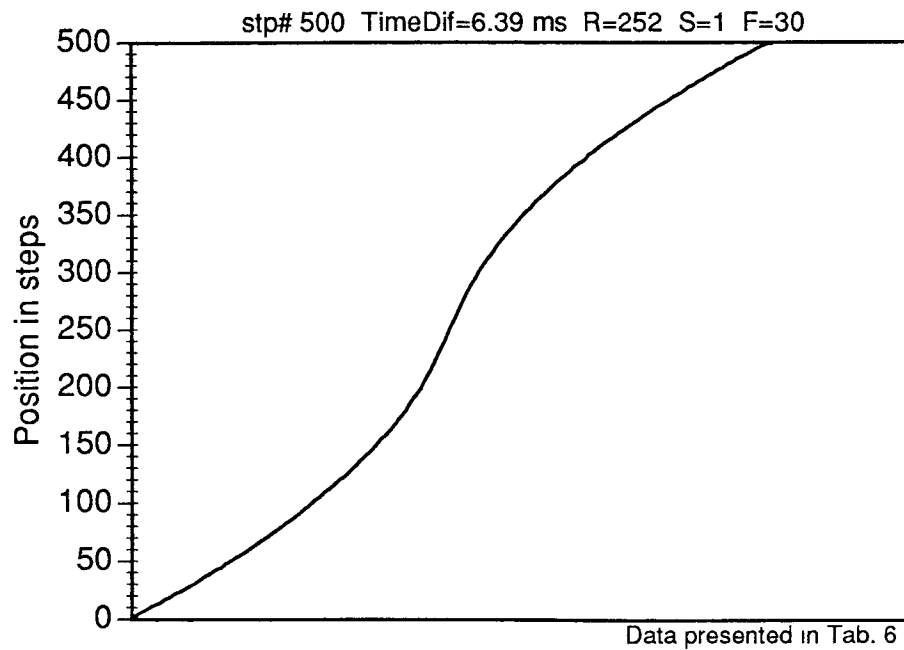


Fig. D10: Position-Time (S-T) diagram with parameters: R252;S1;F30;N500

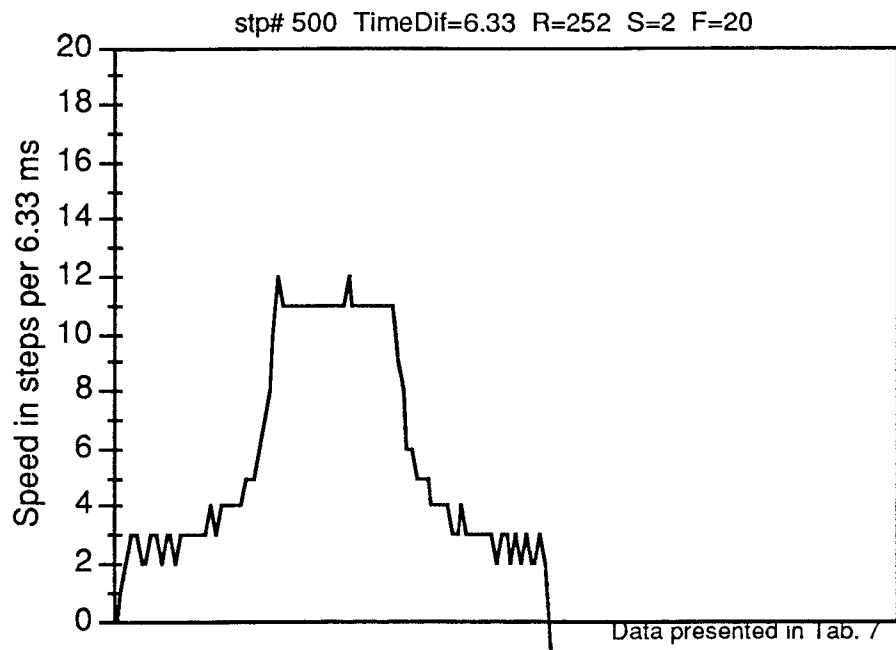


Fig. D11: Velocity-Time (V-T) diagram with parameters: R252;S2;F20;N500

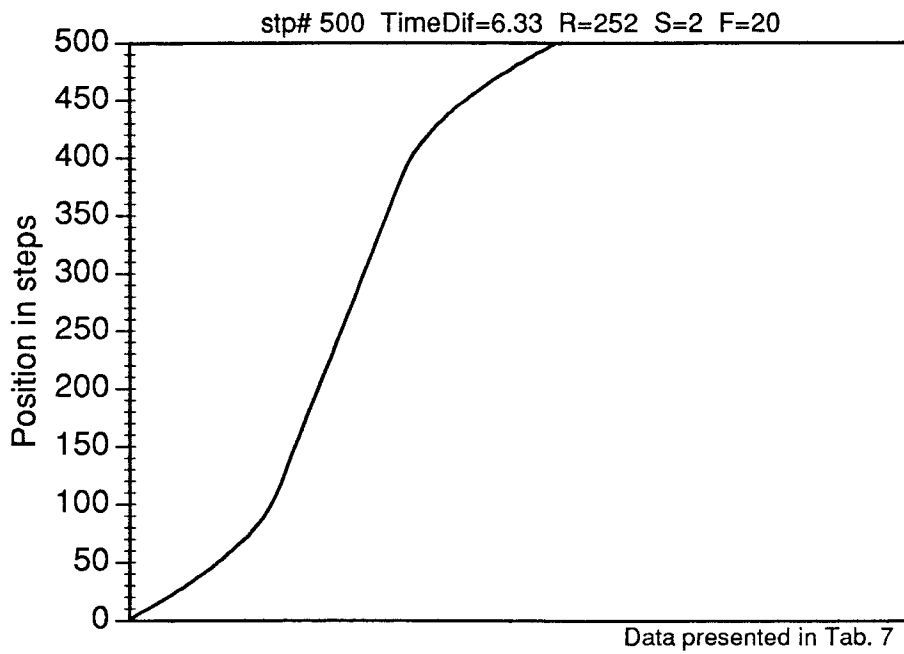


Fig. D12: Position-Time (S-T) diagram with parameters: R252;S2;F20;N500

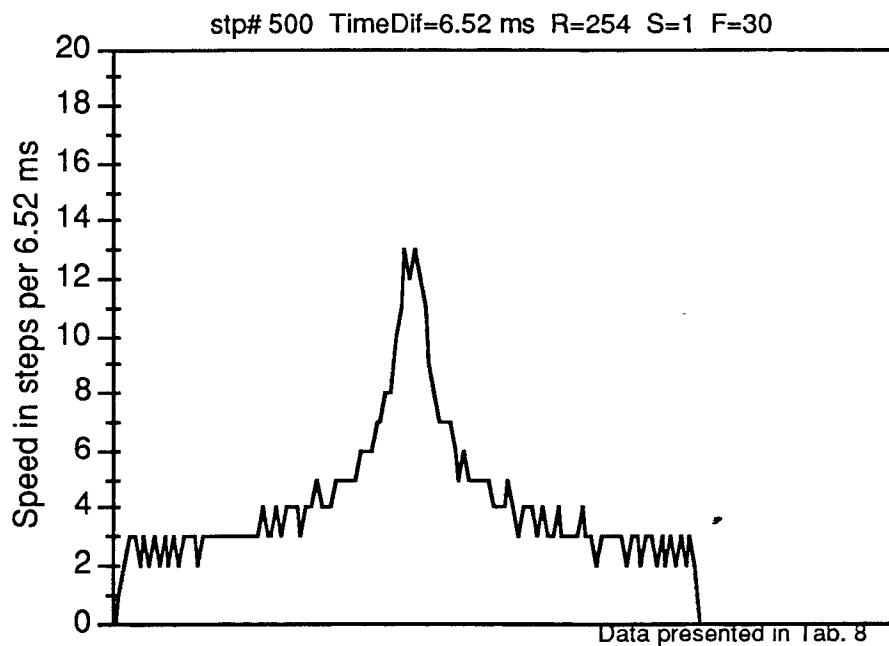


Fig. D13: Velocity-Time (V-T) diagram with parameters: R254;S1;F30;N500

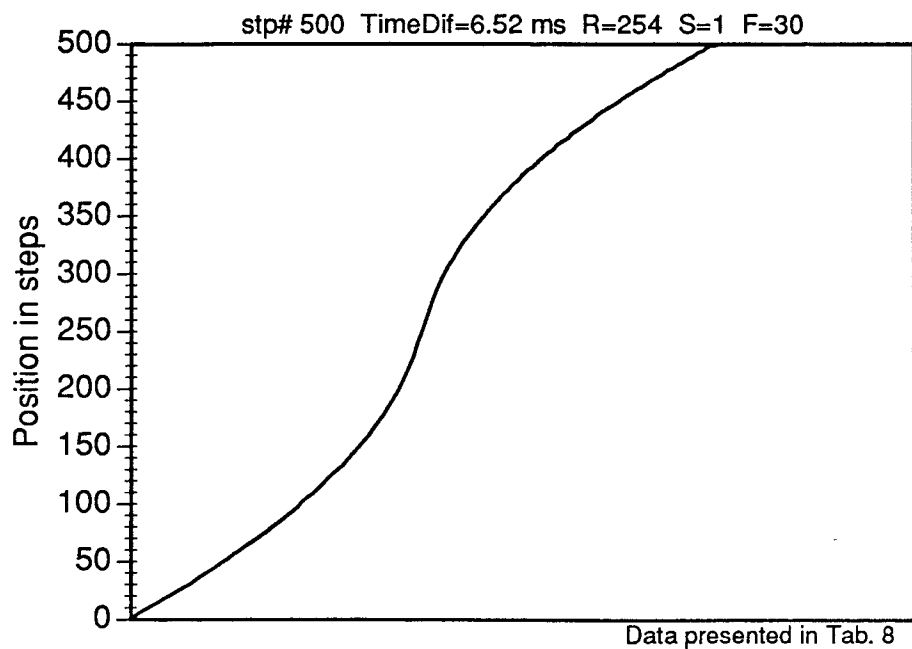


Fig. D14: Position-Time (S-T) diagram with parameters: R254;S1;F30;N500

Appendix C:

Computer programs

Program 1:

PROGRAM LISTING OF SCAN1.BAS

```
' $INCLUDE: 'atdefs.bi'           ' ATLAB function definition file.
' $INCLUDE: 'atlerrs.bi'         ' ATLAB error definition file.
' $INCLUDE: 'atlexsub.bi'       ' ATLEXSUB definitions

DEFINT A-X
DEFDBL Z
CONST TRUE = 1
CONST FALSE = 0
CONST BUFFERSIZE = 2000
COMMON /space0/ Configuration AS AIConfiguration

    DIM value(3000), V(256), xpos(1000), dist(3000)
    DIM S(16), R(16), F(16)
    DIM IM$(256)
CLOSE
BEGPROG:

CLS

COLOR 14
PRINT "CHOOSE THE LATERAL SIZE OF THE IMAGE"
    PRINT "-----"
PRINT

COLOR 12
FOR i = 1 TO 16
PRINT USING "          ## & ##.## &; i; " - "; i * 256 / 100; "mm"
NEXT i

COLOR 9
PRINT : PRINT "YOUR CHOICE 1-16", : INPUT imagesize
CLS
COLOR 12
LOCATE 7, 25: PRINT " ADJUST THE X-Y TABLE !"
COLOR 3
SLEEP 2
LOCATE 12, 13: PRINT " The Data Files will be stored on drive E: "
COLOR 15
SLEEP 3
LOCATE 20, 10: PRINT " ENTER THE NAME OF THE IMAGE FILE >"; : INPUT IMAGE$
OPEN "R", #3, "E:" + IMAGE$ + ".DAT", 32
FIELD #3, 2 AS IM$(1), 2 AS IM$(2), 2 AS IM$(3), 2 AS IM$(4), 2 AS IM$(5), 2 AS IM$(6),
2 AS IM$(7), 2 AS IM$(8), 2 AS IM$(9), 2 AS IM$(10), 2 AS IM$(11), 2 AS IM$(12), 2 AS
IM$(13), 2 AS IM$(14), 2 AS IM$(15), 2 AS IM$(16)

IF imagesize < 0 OR imagesize > 16 THEN GOTO BEGPROG
xdisp = imagesize * 256
```

```

                                ' INITIALIZATION
OPEN "\DEV\IEEEOUT" FOR OUTPUT AS #1 ' OF
IOCTL #1, "BREAK" 'IEEE 488 INTERFACE
PRINT #1, "RESET" ' FOR
OPEN "\DEV\IEEEIN" FOR INPUT AS #2 ' OUTPUT
                                ' AND
PRINT #1, "FILL ERROR" ' INPUT
                                '-----

reterr = Al.Initialize 'INITIALIZATION
                                ' OF
                                ' A/D INTERFACE

reterr = Al.Select.Board(1) ' SELECT BOARD 1

reterr = Al.Reset ' RESET INTERFACE

reterr = Al.Get.Configuration(Configuration) ' CHECK FOR BOARD
maxchannel = Configuration.channelcount - 1 ' CONFIGURATION AND NUMBER
                                ' OF CHANNELS

'following part not in use
' reterr = Al.Declare.Buffer(0, buffer(0), 2000) 'SET A/D
' reterr = Al.Link.Buffer(0) 'BUFFER
' reterr = Al.Setup.Adc(0, 1, c(0), g(0)) 'SET CHANNELS AND GAINS
' reterr = Al.Set.Frequency(40000) 'SET FREQUENCY OF A/D

SCREEN 12 'vga GRAPHIC SCREEN

ox$ = "OUTPUT XA;" 'ox$ BECOMES THE OUTPUT ORDER FOR X-TABLE
oy$ = "OUTPUT YA;" 'oy$ BECOMES THE OUTPUT ORDER FOR Y-TABLE

PRINT #1, ox$, "A" ' INITIAL CONDITIONS
PRINT #1, ox$, "R 253" ' OF X-AXIS"
PRINT #1, ox$, "S 2" ' (CONTINUOUS MOTION)
PRINT #1, ox$, "F 20" '

PRINT #1, oy$, "A" ' INITIAL CONDITIONS
PRINT #1, oy$, "R 253" ' OF Y-AXIS
PRINT #1, oy$, "S 2" ' (INCREMENTAL MOTION)
PRINT #1, oy$, "F 20" '
PRINT #1, "ENTER 06" 'CHECK X-TABLE POSITION
INPUT #2, SX$ 'FOR LATER DATA COMPUTATION
PRINT #1, "ENTER 07" 'CHECK X-TABLE POSITION
INPUT #2, SY$ 'FOR LATER DATA COMPUTATION

PRINT #1, ox$, "+" ' + DIRECTION FOR X DISPLACEMENT
PRINT #1, ox$, "V 0"
PRINT #1, ox$, "N"; xdisp ' DEFINE NUMBER OF STEPS FOR X DISPLACEMENT

itrigger = 8000 'itrigger: VALUE MEASURED ON THR 17TH PIN
                ' OF THE KLINGER CONTROLLER AND
                ' USED AS A/D TRIGGER

```

```

n = 0                'b: COUNTER FOR D/A ACQUISITION

PRINT #1, ox$; "G"   'STARTS X-MOTION

    WHILE itrigger > 2800 'SUBROUTINE CHECKING IF
                        'X-TABLE IN MOTION
        n = n + 1
        retrerr = Al.Adc.Value(0, 1, itrigger) ' PERFORM DATA ACQUISITION
                                                ' WHILE X-TABLE IN MOTION
                                                ' I.E. ITRIGGER>2500
        PRINT #1, "ENTER 06" 'CHECK X-TABLE POSITION
        INPUT #2, A$         'FOR LATER DATA COMPUTATION
        xpos(n) = VAL(A$)

    WEND

PRINT #1, ox$; "-"   'REVERSE X DISPLACEMENT
PRINT #1, ox$; "N"; xdisp 'DEFINE THE NUMBER OF X STEPS
PRINT #1, ox$; "G"   'STARTS X-MOTION

    FOR i = 2 TO n - 1 'SUBROUTINE FOR
                      'REMOVAL OF 0 VALUES
                      'DURING CHECKING
                      'X-TABLE POSITION
st00:
        IF xpos(index) = 0 THEN
            index = index + 1
            GOTO st00
        ELSE
            z1 = xpos(i - 1)
            z2 = xpos(index)
            zxpos = z1 + (z2 - z1) / (index - i + 1)
            xpos(i) = zxpos
        END IF
    END IF

    NEXT i

    xpos(0) = 0

' START REAL DATA ACQUISITION
'-----

FOR J = 1 TO 256      ' J=NUMBER OF SCANNED LINES
                    '-----
PRINT #1, ox$; "+"   '+ DIRECTION FOR X DISPLACEMENT
PRINT #1, ox$; "N"; xdisp ' DEFINE NUMBER OF STEPS FOR X DISPLACEMENT

itrigger = 8000      'itrigger: VALUE MEASURED ON THR 17TH PIN
                    ' OF THE KLINGER CONTROLLER AND
                    ' USED AS A/D TRIGGER

b = 0                'b: COUNTER FOR D/A ACQUISITION

```

```

PRINT #1, ox$; "G"          'STARTS X-MOTION

      WHILE itrigger > 2800    'SUBROUTINE CHECKING IF
        b = b + 1            'X-TABLE IN MOTION

        retrerr = Al.Adc.Value(1, 1, value(b)) ' PERFORM DATA ACQUISITION
                                ' WHILE X-TABLE IN MOTION
                                ' DATA STORED IN value ARRAY

        retrerr = Al.Adc.Value(0, 1, itrigger) ' PERFORM DATA ACQUISITION
                                ' WHILE X-TABLE IN MOTION
                                ' I.E. ITRIGGER>2800

      WEND

PRINT #1, ox$; "-"          'REVERSE X DISPLACEMENT
PRINT #1, ox$; "N"; xdisp '+ 15 'DEFINE THE NUMBER OF X STEPS
PRINT #1, ox$; "G"          'STARTS X-MOTION

FOR K = 2 TO b - 1          'COMPUTATION OF THE LOCATION OF
  zb = b                    'b D/A VALUES
  zn = n
  zk = K
  zk = zk * zn / zb
  i = CINT(zk)
  zi = i
  z1 = xpos(i)
  z2 = xpos(i + 1)
  xpk = z1 + (z2 - z1) * (zk - zi)
  dist(K) = xpk

NEXT K

      dist(1) = xpos(0)
      dist(b) = xpos(n)
      index0 = 1
      V(1) = value(1)
      V(256) = value(b)

FOR K = 2 TO 255            ' COMPUTATIONS FOR
  zdmax = dist(b)          ' 256 EQUIDISTANT VALUES
  zdistk = K
  zdistk = zdistk * zdmax / 256

st01:
  IF dist(index0) < zdistk THEN
    index0 = index0 + 1
    GOTO st01
  ELSE
    index0 = index0 - 1
    zvi1 = value(index0)

```

```

        zvi2 = value(index0 + 1)
        zdi1 = dist(index0)
        zdi2 = dist(index0 + 1)
        zvalk = zvi1 + (zvi2 - zvi1) * (zdistk - zdi1) / (zdi2 - zdi1)
        V(K) = zvalk
    ENDIF
NEXT K

    PRINT #1, ox$; "+"          'REVERSE X DISPLACEMENT
    ' PRINT #1, ox$; "N"; 15    'DEFINE THE NUMBER OF X STEPS
    ' PRINT #1, ox$; "G"      'STARTS X-MOTION

    FOR K = 1 TO 256
        zk = V(K)
        zk = 15 * zk / 4095
        PSET (K + 160, J + 50), (zk MOD 14) + 1 'SIMPLE PLOTTING
    NEXT K
    PRINT #1, oy$; "+"          'PLUS Y DISPLACEMENT
    PRINT #1, oy$; "N"; imagesize 'DEFINE NUMBER OF STEPS FOT Y MOTION
    PRINT #1, oy$; "G"          'START Y MOTION
    LOCATE 1, 1: PRINT "NUMBER OF DATA: "; b

FOR i = 1 TO 16                'SAVE DATA ON A FILE

    FOR K = 1 TO 16
        RECORDINDEX = (i - 1) * 16 + K
        LSET IM$(K) = MKI$(V(RECORDINDEX))
    NEXT K

    FILEINDEX = (J - 1) * 16 + i
    PUT #3, FILEINDEX
NEXT i
NEXT J
PRINT #1, ox$; "P"; VAL(SX$)
PRINT #1, oy$; "P"; VAL(SY$)

PRINT #1, "OUTPUT 06;0" 'RESET X-TABLE
PRINT #1, "LOCAL 06" 'X-TABLE BECOMES LOCAL (enable KLINGER front pannel)

PRINT #1, "OUTPUT 07;0" 'RESET Y-TABLE
PRINT #1, "LOCAL 07" 'Y-TABLE BECOMES LOCAL (enable KLINGER front pannel)

CLOSE
COLOR 15
LOCATE 23, 5: PRINT "IMAGE DONE";

A$ = ""          ' CLOSE LOOP
WHILE A$ = ""    ' FOR DELAY:
A$ = INKEY$     ' HIT ANY KEY TO CONTINUE
WEND            '

    END

```

Program 2:

PROGRAM LISTING OF SCAN2.BAS

```

$include "leeeIO.BAS"
DEFINT A-X
DEFDBLZ
BUFFERSIZE = 2000
DIM value(30000), V(256), k(5000), xpos(1000), dist(3000)
DIM S(16), R(16), F(16)
DIM IM$(256)
CLOSE
BEGPROG:

CLS
color 11
print : print "IMAGE SIZE  5 - 18"; : INPUT imagesize
color 14
print : input "File Name [E:\{file name}];IMAGE$

IF imagesize < 5 OR imagesize > 18 THEN GOTO BEGPROG
xdisp = imagesize * 256
cls
          ***** GPIB Interface initialization *

Buf$=Space$(10)
call leeeOpen
call leeeWrite("LOCAL XA")
call leeeWrite("LOCAL YA")
call leeeWrite("RESET")
call leeeWrite("FILL ERROR")
call leeeWrite("ERROR OFF")
call leeeWrite("RESET")
call leeeWrite("CLEAR")

out (&h210),0
out (&h211),0
out (&h210),&h19
out (&h211),0
out (&h212),2

OPEN "R", #3, "E:\" + IMAGE$ + ".DAT", 32
FIELD #3, 2 AS IM$(1), 2 AS IM$(2), 2 AS IM$(3), 2 AS IM$(4), 2 AS IM$(5), 2 AS IM$(6), 2
AS IM$(7), 2 AS IM$(8), 2 AS IM$(9), 2 AS IM$(10), 2 AS IM$(11), 2 AS IM$(12), 2 AS
IM$(13), 2 AS IM$(14), 2 AS IM$(15), 2 AS IM$(16)

SCREEN 12

          ***** XY-Table initialization *****
call leeeWrite("OUTPUT XA;A")
call leeeWrite("OUTPUT XA;R 249")

```

```

call leeeWrite("OUTPUT XA;S 2")
call leeeWrite("OUTPUT XA;F 20")
call leeeWrite("OUTPUT YA;A")
call leeeWrite("OUTPUT YA;R 251")
call leeeWrite("OUTPUT YA;S 2")
call leeeWrite("OUTPUT YA;F 20")
call leeeWrite("OUTPUT XA;V 0")

```

```

call leeeWrite("ENTER YA")
SY$ = FNleeeRead$
call leeeWrite("ENTER XA")
SX$ = FNleeeRead$
IMAGE$=ucase$(IMAGE$)
locate 23,5:print "> ";IMAGE$+".DAT"
line (161,101) - (416,356),2,b

```

***** X-Table motion characteristics ****

```

itrigger = 1000
n = 0
call leeeWrite("OUTPUT XA;-")
call leeeWrite("OUTPUT XA;N"+str$(xdisp))
call leeeWrite("OUTPUT XA;G")
'delay 0.1
call leeeWrite("ENTER YA")
tp$ = FNleeeRead$

WHILE itrigger > 200
  incr n
  out (&h210),&h19
  out (&h211),0
  while (inp(&h210) and &h01)=0
  wend
  itrigger=(inp(&h213)*&h100)+inp(&h212)
  if (inp(&h211) and &h80)=0 then call er

  call leeeWrite("ENTER XA")
  A$ = FNleeeRead$
  xpos(n) = abs(VAL(A$))
WEND
call leeeWrite("OUTPUT XA;+")
call leeeWrite("OUTPUT XA;N"+str$(xdisp))
call leeeWrite("OUTPUT XA;G")
delay 2

```

***** Zero correction ****

```

for i = 2 to n-1
  if xpos(i) = 0 then
    index = i+1
  hb1:
    if xpos(index) = 0 then
      index = index + 1
      goto hb1
  else

```

```

    z1 = xpos(i - 1)
    z2 = xpos(index)
    zxpos = z1 + (z2 - z1) / (index - i + 1)
    xpos(i) = zxpos
  end if
end if
next i

          ***** START REAL DATA ACQUISITION
          '-----
FOR J = 1 TO 256

  if inkey$ = " " then goto final
  for i = 1 to b + 200
    value(i) = 0
  next i

  delay 1.2
  itrigger = 1000
  b = 0
  ptr = 0
  sr = 0
  iw = 0
  ic = 0
  call lxxxWrite("OUTPUT XA;-")
  call lxxxWrite("OUTPUT XA;N"+str$(xdisp))
  call lxxxWrite("OUTPUT XA;G")

call lxxxWrite("ENTER YA")
tp$ = FNlxxxRead$

  WHILE itrigger > 180
    b = b + 1
    out (&h210),&h19
    out (&h211),1
    while (inp(&h210) and &h01)=0
    wend
    value(b)=(inp(&h213)*&h100)+inp(&h212)
    if (inp(&h211) and &h80)=0 then call er

    out (&h210),&h19
    out (&h211),0
    while (inp(&h210) and &h01)=0
    wend
    itrigger=(inp(&h213)*&h100)+inp(&h212)
    if (inp(&h211) and &h80)=0 then call er
  WEND
  call lxxxWrite("OUTPUT XA;+")
  call lxxxWrite("OUTPUT XA;N"+str$(xdisp))
  call lxxxWrite("OUTPUT XA;G")
  call lxxxWrite("OUTPUT YA;+")
  call lxxxWrite("OUTPUT YA;N"+str$(imagesize))
  call lxxxWrite("OUTPUT YA;G")
          ***** Find max A/D values

```

```

    icmax=5
    for ic=1 to 20
        if value(ic)>icmax then
            icmax=value(ic)
            ptr=ic
        end if
    next ic
    k(0)=value(ptr)
    sr=0
deb1:
    icmax=5
    incr sr
    ic=ptr+12
    if ic>b then goto fin1
        for iw = ic to ic+6
            if value(iw)>icmax then
                icmax=value(iw)
                k=iw
            end if
        next iw
        ptr=k
        k(sr)=value(ptr)
    goto deb1
fin1:
for k = 2 to sr - 1
    zsr = sr
    zn = n
    zk = k
    zk = zk * zn / zsr
    i = CINT(zk)
    zi = i
    z1 = xpos(i)
    z2 = xpos(i + 1)
    xpk = z1 + (z2 - z1) * (zk - zi)
    dist(k) = xpk
next k
dist(1) = xpos(0)
dist(sr) = xpos(n)

index0 = 1
V(1) = k(1)
V(256) = k(sr)

for k = 2 to 255
    zdmax = dist(sr)
    zdistk = k
    zdistk = zdistk * zdmax / 256
st1:
    if dist(index0) < zdistk then
        index0 = index0 + 1
        goto st1
    else
        index0 = index0 - 1
        zvi1 = k(index0)

```

```

        zvi2 = k(index0 + 1)
        zdi1 = dist(index0)
        zdi2 = dist(index0 + 1)
        zvalk = zvi1 + (zvi2 - zvi1) * (zdistk - zdi1) / (zdi2 - zdi1)
        V(k) = zvalk
    end if
next k

fin2:
        ***** plot pixels
    FOR K = 1 TO 256
        zk = V(K)
        zk = 15 * zk / 2047
        PSET (K + 160, J + 100), (zk MOD 14) + 1
    NEXT K

        ***** save data on file
    FOR i = 1 TO 16
        FOR K = 1 TO 16
            RCINDEX = (i - 1) * 16 + K
            LSET IM$(K) = MKI$(V(RCINDEX))
        NEXT K
        FLINDEX = (J - 1) * 16 + i
        PUT #3, FLINDEX
    NEXT i

        locate 1, 1: print "NUMBER OF DATA: "; sr,b
        locate 1, 50: print "LINES MORE TO GO: ";256 - J
NEXT J
final:
    call lxxxWrite("OUTPUT XA;P"+str$(VAL(SX$)))
    call lxxxWrite("OUTPUT YA;P"+str$(VAL(SY$)))
    call lxxxWrite("OUTPUT 06;0")
    call lxxxWrite("LOCAL 06")
    call lxxxWrite("OUTPUT 07;0")
    call lxxxWrite("LOCAL 07")

CLOSE
COLOR 15
LOCATE 23, 5: PRINT "IMAGE DONE ";
call lxxxClose

A$ = ""
WHILE A$ = ""
A$ = INKEY$
WEND

sub er
shared ibase
out(&h211),(inp(&h211) and &hf7)
end sub
END

```

Program 3:

PROGRAM LISTING OF SCAN3.BAS

This is only the data acquisition section of the SCAN3.BAS experimental program, because the other parts are similar to the previous program SCAN2.BAS

```
out (&h210),0
out (&h211),0

out (&h210),&h19
out (&h211),0
out (&h212),2

while inkey$ = ""

    out (&h210),&h1A
    out (&h211),0
    while (inp(&h210) and &h01)=1

        wend
locate 10,35: print (inp(&h213)*&h100)+inp(&h212)

    if (inp(&h211) and &h80)=0 then call er

wend

end
```

Appendix D:

Description of stepper motor controller
movement characteristics

Also, it is possible to load an entire program with a single byte count value. To do this, issue the E command with a data count value of zero, followed by the first command character of the program. Instead of following this character by the normal data count, use a count equal to the remaining total characters of the program, up to, and including the 0 command. Do not include the Q command in the count. The Q command should then be issued separately, ending the program entry mode and reverting to command mode. When this method of program loading is used, the 0 command must have a binary value of zero, not the ASCII character "0". The program may also be loaded as separate commands, with a normal data count for each command. This is the procedure used for command mode operation as well.

6.5 STEP RATE CONTROL

The CC-1 allows you to define the step rate and acceleration rates in very fine increments (10 microsecond changes). This is easily done through the rate, slope and factor (R, S, and F) commands. By proper choice of the R, S, and F parameters, it is possible to control the starting rate, the number of steps from the starting rate to the slew rate, and the final slew rate.

<p>CC-1 Rate Equation</p> $\text{Steps per second} = \frac{10^6}{(256-r) \cdot (80) + z \cdot (10) + 75 \pm 7.5}$
--

The equation and this discussion use several variables which are defined as follows:

- r = Rate parameter as set by the R command
- s = Slope parameter as set by the S command
- f = Factor parameter as set by the F command
- y = Integer (255-f) / s
- z = Internal factor value

The variable y represents the number of steps required to ramp up from the starting rate to the slew rate, and the number of steps to ramp down again before stopping.

The internal factor, z, changes in value for each step while ramping. When accelerating, $z = 255 - n \cdot s$, where n is the step number from the start of motion, beginning with $n = 1$. When $z = f$ (slew speed) the maximum step rate for any particular value of r and f has been reached. While decelerating, $z = f + n \cdot s$, where n is the step number from the start of deceleration.

From the above discussion, we can deduce the starting step rate equation and the final (slew) step rate equation:

Starting Step Rate

$$\text{Steps per second} = \frac{10^6}{(256-r) \cdot 80 + (255-s) \cdot 10 + 75 \pm 7.5}$$

Slew Step Rate

$$\text{Steps per second} = \frac{10^6}{(256-r) \cdot 80 + f \cdot 10 + 75 \pm 7.5}$$

The rate equation applies as specified when $1 \leq r \leq 254$. In the case where $r = 255$, the rate will not follow the equation, but will differ, depending on the direction of motion

The rate for the + direction is $10^6 / (218 + z \cdot 10)$.

The rate for the - direction is $10^6 / (232 + z \cdot 10)$.

The ± 7.5 term in the rate equations represents an uncertainty between the exact instant the step time expires and the point at which it is detected. For any given setting of the parameters, the step rate will be a constant within the \pm range specified. The CC-1 will not exhibit a jitter from step to step and the exact step rate is repeatable with the same input parameters.

Table 6.4 is a listing of the range of possible slew rates for a given setting of r. The slowest step rate in each range uses the value f = 255, and the fastest rate is obtained when f = 1.

Table 6.4

Rate Table

Rate r	Steps/second	
	f = 255	f = 1
1	43	48
25	47	53
50	52	60
75	58	68
100	66	79
125	76	94
150	90	116
175	109	152
200	140	219
205	149	240
210	158	265
215	169	297
220	181	337
225	195	389
230	212	461
235	232	566
240	256	732
245	285	1036
250	322	1769
251	330	2061
252	339	2469
253	349	3076
254	359	4081

Note that the CC-1 is capable of outputting step rates much greater than 2000Hz. However, for UE30 and UE72 motor types, operation is not guaranteed above 2000Hz.

6.5.1 RAMPING MODE OF OPERATION

The maximum step rate is defined by a combination of the rate and factor parameters, as indicated in the step rate equation. For step rates greater than 400Hz, the initial step rate will not be at the maximum rate, but will ramp up to this rate from a slower value. The slope, or number of steps required to attain the maximum rate, is defined by the slope parameter. When stepping begins, an internal factor value (z) is set to 255. The value of the slope parameter is then subtracted from this internal factor once per step, increasing the step rate as the factor decreases (see the equation). Note that the rate parameter is not changed by this process, only the internal factor. When the internal factor becomes less than or equal to the value specified by the factor command (f), the maximum rate has been reached, and the internal factor is set so the specified rate is maintained. The CC-1 will continue slewing until it is time to ramp down to hit the target position. The point at which this occurs is determined automatically and the value of the slope parameter is added to the internal factor once per step, producing a slower step rate until the target position is reached, or the slowest rate is attained (internal factor $z = 255$).

IMPORTANT

If the number of steps to travel is less than the number required to reach the maximum step rate and then ramp down again, the CC-1 will not ramp. Instead it will just step to the target position at a step rate determined by the value of the R parameter and f equals 255.

The number of steps needed to accelerate is given by $(255 - f) / s$. This same number of steps is necessary to decelerate. If the number of steps to reach the target position is less than twice the value given by $(255 - f) / s$, the CC-1 will not ramp at all. It will use the R parameter given, ignore the F parameter given and instead set it to 255. It will then use the slew rate equation to determine the stepping rate. For example, if the following program was entered:

```
"R 253!"; "S 1!"; "F 20!"; "N 460!"; "G!"
```

The number of steps necessary to accelerate and then decelerate is equal to:

$$2 \cdot [(255 - f) / s] = 2 \cdot [(255 - 20) / 1] = 470$$

Since our target position is less than 470 steps away, the CC-1 will not ramp. It will step to the target position at a rate determined by:

$$\text{steps/sec} = 10^6 / (256 - r) \cdot 80 + 10 \cdot f + 75 \pm 7.5$$

The CC-1 will set $f = 255$ and use the r parameter given.

$$\text{steps/sec} = 10^6 / (256 - 253) \cdot 80 + 10 \cdot (255) + 75 \pm 7.5 = 348$$

It is recommended that a rate parameter of 253 or higher be chosen for slewing. This minimizes the time it takes to reach the maximum speed.

Depending on the motor used, the load, and the final speed, a fast acceleration ramp ($s = 7, 8$, etc.) or a slow ramp ($s = 1, 2$, etc.) may be used. Note that since the slope parameter changes the instantaneous step rate once per step (not at a constant rate) the acceleration is not linear. The effective acceleration rate is higher for higher step rates. For speeds below 400Hz (or higher if your application permits) where ramping is not required, use a value of 255 for the slope (s) parameter.

IMPORTANT

Note that the factor command must always be entered after the slope command. If the slope is changed, the factor command must be repeated after the new slope, to insure proper ramping operation. This is because the variable y is calculated only when a factor value is entered, not when a slope value is entered or before a motion is executed. A new set of parameters is not entered for each motion, but may be entered to change the step rate.

6.6 APPLICATION HINTS AND TECHNIQUES

Programming the CC-1 is straightforward. However, you may encounter some problems setting the optimal step and acceleration rates. In this section we first present a functional grouping of the CC-1 commands and second, we present a discussion for setting the rate, slope and factor parameters for optimal performance.

6.6.1 FUNCTIONAL GROUPING OF CC-1 COMMANDS

Relative Indexing

Relative indexing makes use of the N, +, -, and G instructions.

N specifies the number of steps in the motion (not a final position).

+ or - is used to set the direction.

G is the command to make the motion.

Motions of equal length may be performed without re-entering the N parameter.

Absolute Indexing

For absolute indexing, the A instruction is used to establish the zero position.

The P instruction is then used to move to a specified positive position.

Although all positions must be positive (with respect to the zero position), the direction of motion depends upon the starting and end positions of a move. For example, if the position before the execution of a "P 5000!" command is 10000, the direction of the move is negative. If the position before the execution of the command is 1000, the direction is positive. Note that this zero position does not necessarily correspond to the zero position of the display

Positive and negative relative indexing may be intermixed with absolute indexing provided that any negative relative motion does not move the stage past the established zero position. If this occurs, the position defined by the A command is lost and all subsequent P commands will execute incorrectly.

When mixing absolute and relative indexing you must keep track of the last direction of travel. This is because there is a single direction register for both indexing modes. For example, if a relative move is desired immediately after a negative direction P command is executed, the motion will be in the negative direction, even though you may have outputted a "+" command previously. The example below will make this clear.

```
"A!"  
"N 1000!"  
"+!"           :direction register = +  
"G!"  
"P 2000!"     .direction register = +  
"P 0!"        :direction register = -  
"G!"          :relative motion will be in negative direction
```

Wait Instructions

The X instruction may be executed during command mode or program execution mode to perform a timing function. It takes a numerical argument which is the time in multiples of 1.83 msec.

The U and W instructions are used only in program execution mode to poll the wait input line (pin #15, G.P. I/O connector). If the line is in the wait state, program execution is halted until it changes state.

Loop Instructions

These instructions are used only in program execution mode.

The L instruction takes two arguments. The first argument is the loop counter. The second is the location of the instruction which begins the loop (zero marks the first instruction entered after an E command).

The J instruction simply performs the jump function of the L instruction without having a loop counter. Its single argument is equivalent to the second argument of the L instruction. It can also be used to start stored program execution at any desired location.

The T instruction will cause the program to loop back to location zero as long as the loop input is low.

The D instruction is normally given in command mode to start execution of a stored program. If it is also included in a stored program, the program will loop back to location zero indefinitely. Program execution can be stopped by resetting the system or by inputting an I instruction or a Q instruction. The Q instruction will halt the execution and return the system to command mode. The I instruction will do the same and, in addition, erase the stored program.

Programmable Output

The B and C instructions are used to set and clear a programmable output line (pin 16 on the General Purpose I/O connector). This line is initialized in the high state.

Rate Control

The R, S, and F instructions are used to define the step rate and acceleration rates in very fine increments ($10 \mu\text{sec}$ changes). By proper choice of the rate, slope, and factor parameters, it is possible to control the starting rate, the number of steps from the starting rate to the slew rate, and the final slew rate

6.6.2 DETERMINING OPTIMAL R, S, F PARAMETERS

The optimal values of the R, S, F parameters will vary depending on the load, the desired stepping rate and the mechanical properties of the positioning stage. By optimal, we mean achieving the desired stepping rate with the quickest acceleration without stalling the stepping motor.

The determination of the parameters is best done by trial and error when your system is set up. The trial and error method involves varying one parameter while keeping the other two constant.

The equation for steps per second is

$$\text{steps/sec} = 10^6 / (256 - r) \cdot 80 + 10 \cdot z + 75 \pm 7.5$$

The variable z is equal to $255 - n \cdot s$ and changes in value for each step while ramping. The variable n is the step number from start of low speed motion beginning with $n = 1$. This implies that the starting low speed is given by.

$$\text{steps/sec (low speed)} = 10^6 / (256 - r) \cdot 80 + (255 - s) \cdot 10 + 75 \pm 7.5$$

The CC-1 will start the stepping at the low speed rate and accelerate towards the high speed rate. For each step taken while ramping, the variable z will decrease. The CC-1 will stop accelerating when z is less than or equal to f. This then is the slew rate. Using the fact that $z = 255 - n \cdot s$ ($n = 1$) in low speed and $z = f$ in high speed, we can determine the number of steps needed to accelerate. This is handy because it tells you how much travel distance is needed to ramp up to high speed.

$$z = 255 - n \cdot s = f$$

Solving for n, we get $n = \frac{255 - f}{s}$. n = number of steps in ramp

Using the fact that $z = f$ in high speed we deduce the slew rate equation:

$$\text{steps/sec (slew rate)} = 10^6 / (256 - r) \cdot 80 + 10 \cdot f + 75 \pm 7.5$$

Studying the equations and considering the properties of a positioning stage with its load the following are apparent:

1. The highest low speed is attained with the largest r and s parameters, regardless of the f parameter.
2. The highest slew rate is attained with the largest r parameter and the smallest f parameter.
3. The quickest acceleration is attained with a large f and a large s. However, a large f will reduce the slew rate. This would imply that we should keep f small and make s larger to compensate. However, we do not get good resolution when we change the value of the s parameter. A numerical example should make this point clear.

For example, let's assign $f = 15$, and $s = 2$ in one instance and $s = 3$ in another instance. From the equation:

$$n = \frac{255-f}{s} \text{ we get:}$$

$$\text{for } s=2; n = \frac{255-15}{2} = \frac{240}{2} = 120$$

$$\text{for } s=3; n = \frac{255-15}{3} = \frac{240}{3} = 80$$

We see that for a small change in s (the smallest possible) we get a drastic difference in the number of steps needed to accelerate. Here you may find that 120 steps is too long an acceleration and 80 steps is too short (it stalls the stepping motor).

To get better resolution so that the number of steps to accelerate is somewhere between 80 and 120 steps we can do one of two things:

1. with $s=2$, increase f, or
2. with $s=3$ decrease f

If we choose alternative 1 and increase f, the number of steps to accelerate will go down from 120 but the slew rate will also decrease.

If we choose instead to decrease f, the number of steps to accelerate will go up from 80 but the slew rate will increase. However, even though the number of steps to accelerate has increased, it may still be too quick because the slew rate has also increased.

Point 3 outlines the compromise that you must deal with. The best way to arrive at a solution is through trial and error. As a convenience, the following BASIC program is presented, which allows you to quickly change the value of parameters, prints the starting speed, final speed and the number of steps to accelerate, then outputs the parameters to the CC-1 and initiates a movement. Depending on the result of the movement, you can change the value of the parameters to meet your needs.

The program is written using the IEEE-488 and BASIC commands of the PET Commodore microcomputer. The device address is assumed to be 6. Refer to section VII for explanation of IEEE-488 programming.